1991

Electrocatalysis of anodic, oxygen-transfer reactions at noble metal electrodes

Joseph Edward Vitt
Iowa State University

Order Number 9202404

Electrocatalysis of anodic, oxygen-transfer reactions at noble metal electrodes

Vitt, Joseph Edward, Ph.D.

Iowa State University, 1991

U·M·I
300 N. Zeeb Rd.
Ann Arbor, MI 48106

Electrocatalysis of anodic, oxygen-transfer reactions at noble metal electrodes

by

Joseph Edward Vitt

A Dissertation Submitted to the
Graduate Faculty in Partial Fulfillment of the
Requirements for the Degree of
DOCTOR OF PHILOSOPHY

Department: Chemistry
Major: Analytical Chemistry

Approved:

Signature was redacted for privacy.

In Charge of Major Work

Signature was redacted for privacy.

For the Major Department

Signature was redacted for privacy.

For the Graduate College

Iowa State University
Ames, Iowa

1991

TABLE OF CONTENTS

LIST OF ABBREVIATIONS

CE	electron transfer preceded by a homogeneous chemical reaction
ECE	two electron transfer steps separated by a homogeneous chemical reaction
ECL	electrogenerated chemiluminescence
GC	glassy carbon
I_{ECL}	ECL intensity
i-E	current potential curve, voltammetric data
i-t	chronoamperometric data
ox	species corresponding to the higher oxidation state in oxidation-reduction reactions
red	species corresponding to the lower oxidation state in oxidation-reduction reactions
RDE	rotated disk electrode
RRDE	rotated ring-disk electrode
SCE	saturated calomel electrode, E^{o} = 0.241 V
SHE	standard hydrogen electrode, E^{o} = 0.0 V

LIST OF SYMBOLS

Symbol	Definition	Units
A	electrode area	cm^2
C^b	bulk concentration	mol cm^{-3}
C^s	surface concentration	mol cm^{-3}
D	diffusion coefficient	cm^2 sec^{-1}
E	electrode potential	V
E^o	thermodynamic potential	V
$E^{o'}$	E^o adjusted for pH	V
$E_{1/2}$	E where $i = i_{lim}/2$	V
F	Faraday constant, 96485	coul eq^{-1}
i	electrode current	A
i_{lim}	mass-transport limited current	A
i_o	exchange current	A
k^o	standard heterogeneous rate constant	cm sec^{-1}
k_{app}	apparent electrochemical rate constant	cm sec^{-1}
N	number of moles	mol
n	number of electrons transferred	eq mol^{-1}
n_{app}	apparent value of n	eq mol^{-1}
Q	charge	coul
R	molar gas constant, 8.31	J mol^{-1} K^{-1}
T	temperature	K
t	time	sec
v	kinematic viscosity	cm^2 sec^{-1}
w	electrode rotation rate	rad sec^{-1}

Symbol	Definition	Units
X_R	reaction layer thickness	cm
α_a	anodic transfer coefficient	
α_c	cathodic transfer coefficient	
δ	diffusion layer thickness	cm

SECTION I.

GENERAL INTRODUCTION

EXPLANATION OF DISSERTATION FORMAT

This dissertation follows the alternate format as described in the Graduate College Thesis Manual--1990. This includes a general introduction (Section I) which gives background information about the electrochemical techniques described in this dissertation. Also included is a brief statement of the goals of this research.

The research described in this dissertation was performed under the direction of Prof. Dennis Johnson beginning in June 1988. Section II includes the results of competitive adsorption studies for several anodic oxygen-transfer reactions at Au electrodes. This work was performed with the additional guidance and assistance of Dr. Larry Larew. Section III includes kinetic studies of the oxidation and electrogenerated chemiluminescence of luminol at several electrode materials. Additional data were obtained with the assistance of Prof. Royce Engstrom during a one-week visit to the University of South Dakota-Vermillion. Anodic oxygen-transfer reactions catalyzed by O_2 evolution are described in Section IV. Section V includes preliminary results of the use of Kel-F composite electrodes to improve the current efficiency of anodic oxygen-transfer reactions. A brief conclusion to the dissertation is included in Section VI.

ELECTROCHEMICAL KINETICS

Electrochemistry is particularly well-suited to kinetic studies, since the electrode current provides a direct measure of the overall rate of the electrochemical reaction. This relationship becomes apparent from differentiating Faraday's law with respect to time (1).

$$Q = nFN \quad [1]$$

$$dQ/dt = i = nF(dN/dt) \quad [2]$$

Eqn. [2] illustrates the difference between electrochemical kinetics, where the rate of a reaction is given as the number of moles reacted per unit time (dN/dt), and homogeneous solution kinetics, where the rate is often expressed as a change in concentration per unit time (dC/dt). The current is proportional to the electrode area and, therefore, the rate is usually normalized by the electrode area.

$$\text{rate} = dN/Adt = i/nFA = k_{app}C^{s} \quad [3]$$

Eqn. [3] is based on the assumption that the net rate of the reaction can be approximated by an elementary reaction involving the transfer of n electrons in a single step. The apparent heterogeneous rate constant, k_{app}, is the forward rate constant for this hypothetical one-step reaction, and is used as an empirical measure of the kinetics of the electrode

reaction. The equivalence between electrode current and the rate of the reaction makes the application of steady-state methods very desirable. Rotated-disk electrodes (RDE) can be used to provide a constant flux of reactant and, therefore, the current is independent of time (or potential in voltammetry).

A concentration gradient between the surface of the electrode and the bulk solution often develops as the reactant is consumed by the electrochemical reaction, resulting in diffusion to the electrode. Nernst estimated that the concentration gradient could be approximated by a linear relationship, where the diffusion layer thickness (δ) is the distance from the electrode surface where the concentration is approximately equal to the bulk concentration (C^b). In this case, the rate is equal to the flux of reactant due to diffusion (Eqn. [4]) (2).

$$i/nFA = (D/\delta)(C^b - C^s) \qquad [4]$$

By comparison with Eqn. [3], it is apparent that the term D/δ can be thought of as a rate constant for mass transport, and has the same units (cm sec^{-1}) as does k_{app}. For a reaction that is completely mass-transport limited, C^s can be assumed to be essentially zero. The diffusion layer thickness, δ, has been solved for two experimental situations which will be of

interest here: a planar electrode in unstirred solution, and a rotated-disk electrode.

The diffusion layer thickness is equal to $(\pi Dt)^{1/2}$ for a planar, disk electrode in an unstirred solution where diffusion is restricted to the direction normal to the plane of the electrode surface. This value is substituted into Eqn. [4] to yield the Cottrell equation (Eqn. [5]) (3). This

$$i_{lim} = nFAD^{1/2}C^{b}/(\pi t)^{1/2} \qquad [5]$$

equation is based on the assumption that at t = 0, the potential of the electrode is stepped from a value where no reaction occurs to a value where the reaction occurs at a mass-transport limited rate. This implies that C^{S} is essentially zero for t > 0. Also, the disk electrode must be uniformly accessible to the reactant, that is, the current must be equal at all points on the electrode surface.

The current at a stationary disk electrode varies with the inverse square root of time ($t^{-1/2}$), as shown in Eqn. [5]. It is much more useful to choose conditions where the current does not vary with time. This is the case at a rotated-disk electrode (RDE), where convection supplies a constant flux of reactant to the electrode surface. With this experimental configuration, the current is constant if the bulk concentration of the electroactive species can be assumed to be constant for the duration of the experiment.

The diffusion layer thickness at a rotated-disk electrode was solved by Levich (Eqn. [6]) and, when combined with Eqn. [4], gives the Levich equation (Eqn. [7]) (4). A correction

$$\delta = 1.61D^{1/3}\nu^{1/6}\omega^{-1/2} \quad [6]$$

$$i_{lim} = 0.62nFAD^{2/3}\nu^{-1/6}Cb\omega^{1/2} \quad [7]$$

to the constant term 0.62 in Eqn. [7] has been given (Eqn. [8]) (5). This constant reduces to 0.62 when D is much

$$\text{constant} = 0.554/(0.8934 + 0.316(D/\nu)^{0.36}) \quad [8]$$

smaller than ν. Like the Cottrell equation, the Levich equation is based on the assumption that the current is equal at all points on the electrode surface and that the current is limited only by mass transport. The diffusion layer thickness is the distance at which convection maintains the concentration of the electroactive species approximately equal to the bulk concentration. At distances $< \delta$, mass transport of the electroactive species in the direction normal to the electrode surface occurs mainly by diffusion.

Measurement of the current for a mass-transport limited reaction can give useful information about the net reaction, such as the value of n or D. However, kinetic information is necessarily absent from current measurements that are limited only by mass-transport of the electroactive species to the electrode. Kinetic information is present only under

conditions when the current is less than the mass-transport limited values predicted by Eqns. [5] and [7].

The equation for conditions of mixed control by mass transport and kinetic processes is obtained by solving Eqn. [3] for C^s and substituting this result into Eqn [4]. This equation can be rearranged to give Eqn. [9]. When the

$$i = nFADC^b/(\delta + D/k_{app}) \qquad [9]$$

kinetics are fast with respect to mass transport ($D/k_{app} << \delta$), this equation reduces to Eqn. [4] where $C^s = 0$, <u>i.e.</u>, the equation for mass-transport controlled reactions. When kinetics are slow compared to the rate of mass transport ($D/k_{app} >> \delta$), this equation reduces to Eqn. [3] where $C^s = C^b$, <u>i.e.</u>, the equation for irreversible reactions in the absence of mass-transfer effects.

The equation for reactions under mixed control at a stationary disk electrode (Eqn. [10]) is obtained by substituting the diffusion layer thickness from the Cottrell equation (Eqn. [5]) into Eqn. [9]. Note that at long times,

$$i = nFADC^b/((\pi Dt)^{1/2} + D/k_{app}) \qquad [10]$$

the current approaches the current for the purely mass-transport limited case. Therefore, in theory, Cottrell data at long times can be used to determine useful information

about the net reaction such as n and D, even when there are kinetic limitations on the current at short times.

The equation for the RDE can be obtained in an analogous manner by substituting Eqn. [6] into Eqn. [9]. This equation is commonly called the Koutecky-Levich equation (4).

$$i^{-1} = (nFAk_{app}C^b)^{-1} + (0.62nFAD^{2/3}\nu^{-1/6}C^b w^{1/2})^{-1} \qquad [11]$$

This equation is written in the inverse form so that the effects of mass transport can be separated from the effects of kinetics. Based on Eqn. [11], a plot of i^{-1} vs. $w^{-1/2}$ gives a slope dependent on the mass transport characteristics of the net reaction, and an intercept dependent on the kinetics.

The current-potential (i-E) characteristics for a reaction at the RDE can be obtained by solving k_{app} for the specific mechanism and substituting the result into Eqn. [11]. For example, the i-E curve for an irreversible electron-transfer oxidation can be obtained by substituting k_{app} for an anodic electron-transfer reaction into Eqn. [11]. The apparent rate constant, k_{app}, varies with potential according to Eqn. [12]. The results are plotted in Figure 1 according to Eqn. [13] for three different values of k^o. Note that at

$$k_{app} = k^o \exp\{\alpha_a nF(E-E^{o'})/RT\} \qquad [12]$$

$$i = nFADC^b/(1.61D^{1/3}\nu^{1/6}w^{-1/2} + D/k^o\exp\{\alpha_a nF(E-E^{o'})/RT\}) \qquad [13]$$

large overpotentials, the current reaches the mass-transport

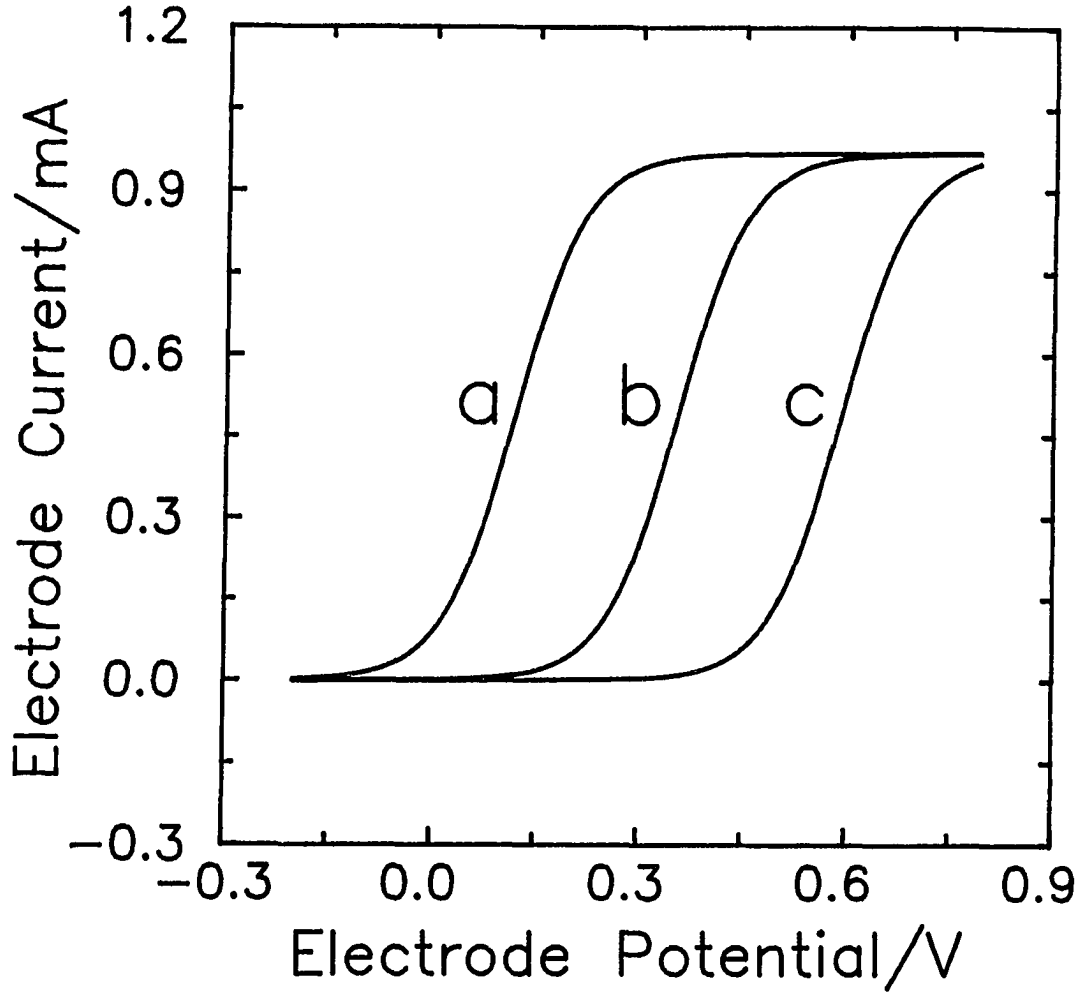

Figure 1. Voltammetric curves plotted according to Eqn. [13] for various values of the heterogenous rate constant.

Conditions: $C^{b}_{red} = 1$ mM, $C^{b}_{ox} = 0$ mM, $\alpha_a = 0.5$, $D = 10^{-5}$ cm^2/sec, $w = 2500$ rev/min, $n = 1$ eq/mol, $v = 0.01$ cm^2/sec, $E^{o'} = 0.0$ V, $A = 1$ cm^2.

Curves: (a) $k^o = 10^{-3}$ cm/sec, (b) $k^o = 10^{-5}$ cm/sec, (c) $k^o = 10^{-7}$ cm/sec.

limited value regardless of k^o. Thus, a plot of i^{-1} *vs.* $w^{-1/2}$ for a simple electron-transfer process yields no kinetic information, and corresponds to the mass-transport limited response predicted by the Levich equation (Eqn. [7]). However, the anodic wave is shifted to more positive potentials as k^o decreases. The half-wave potential ($E_{1/2}$) can be solved by setting Eqn. [13] equal to one-half of the mass-transport limited current given by Eqn. [7] (6).

$$E_{1/2} = E^{o'} + (RT/\alpha_a nF)\ \ln(D/(1.61D^{1/3}\nu^{1/6}w^{-1/2}k^o)) \quad [14]$$

Thus, i-E data at the RDE can be used to obtain both the kinetic and mass-transport characteristics of simple electron-transfer reactions.

For real electrochemical systems, the mass-transport limited current predicted by Eqn. [7] is rarely achieved. However, i-E curves often show large regions where the current is independent of potential, indicating that some other step besides electron transfer is rate limiting.

The apparent rate constant has been solved for several possible mechanisms where electron transfer is not rate limiting. Consider an electrochemical reaction where the electron transfer is preceded by a chemical step, as represented by Eqns. [15] and [16]. This is commonly referred to as a CE mechanism. When $E >> E^{o'}$, the apparent rate constant is given by Eqn. [17] (7).

$$A \underset{k_r}{\overset{k_f}{\rightleftharpoons}} B \qquad [15]$$

$$B \xrightarrow{k_a} C + ne^- \qquad [16]$$

$$k_{app} = DK_{eq}/X_R \qquad [17]$$

$$\text{where } X_R = (D/(k_f + k_r))^{1/2}$$

The limiting currents were calculated from Eqns. [11] and [17] for various rotation rates of the electrode. These results are plotted in Figure 2, along with the results from Eqn. [7] for the mass-transport limited reaction. For the CE mechanism, the limiting currents are much smaller than the mass-transport limited values. This difference becomes larger at larger rotation rates (smaller δ). The rate constants were deliberately chosen so that at high overpotentials, D/k_{app} would be about the same size as δ. For much larger values of D/k_{app} (slower kinetics), the limiting current is independent of rotation rate. For much smaller values of D/k_{app} (faster kinetics), the limiting current would correspond to the mass-transport limited value predicted by the Levich equation.

The data in Figure 2 are plotted as i^{-1} *vs.* $w^{-1/2}$ in Figure 3. The slope calculated from i^{-1} *vs.* $w^{-1/2}$ data is unchanged by kinetic limitations on the current, and can be used to calculate the number of electrons transferred in the net electrochemical reaction, provided a value of D is

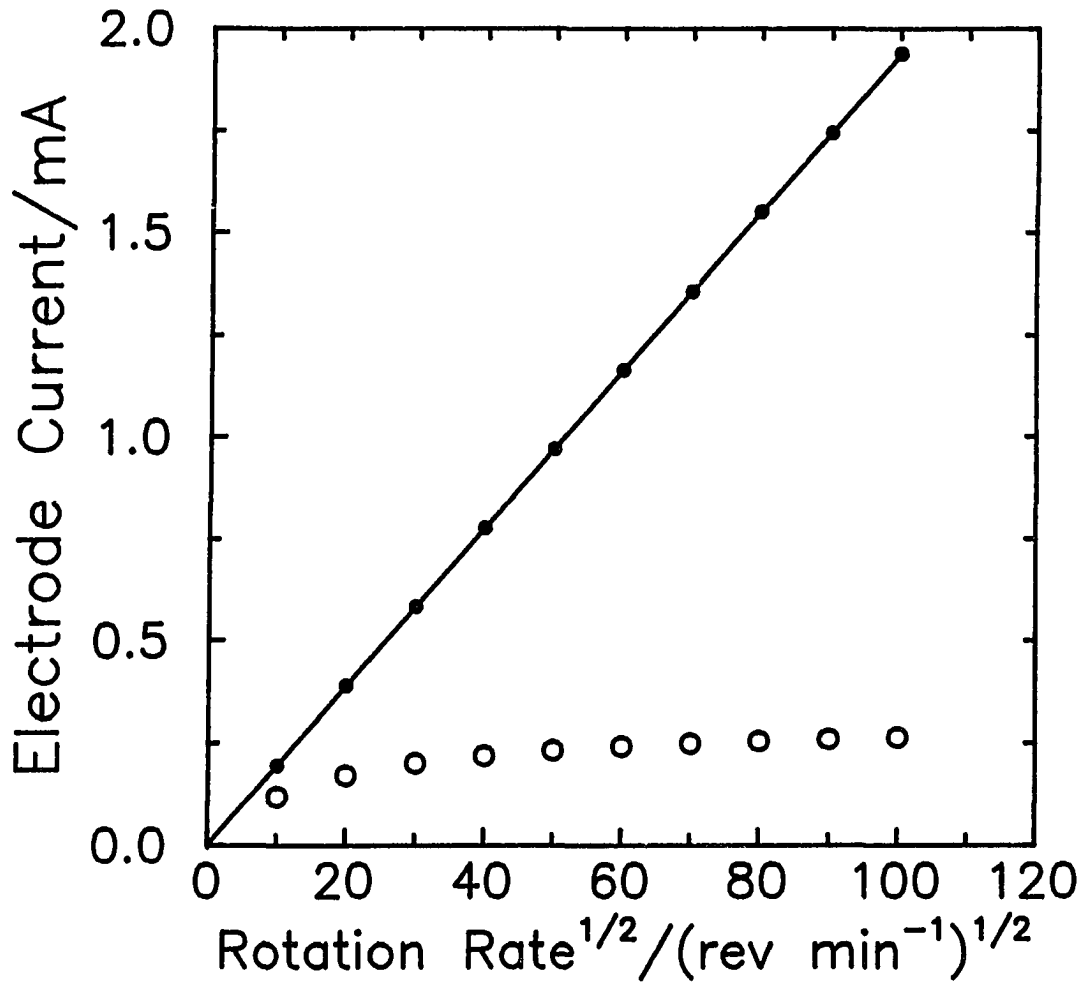

Figure 2. Current as a function of rotation rate$^{1/2}$ for a CE mechanism compared to the mass-transport limited values.

Conditions: same as Figure 1.

Curves: closed circles-- Eqn. [7],
open circles--CE mechanism, Eqns. [11] and [17], k_f = 100 sec^{-1}, k_r = 10000 sec^{-1}.

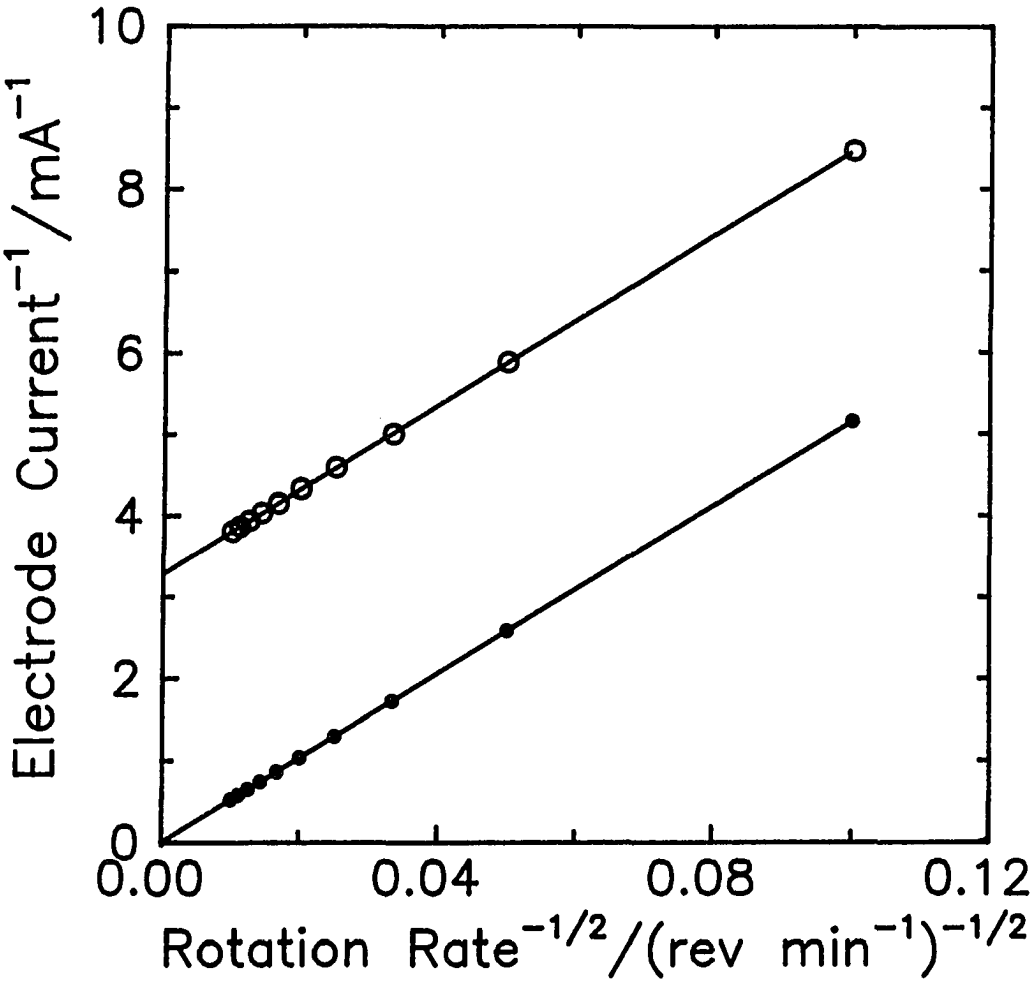

Figure 3. Current^{-1} as a function of rotation rate$^{-1/2}$ for a CE mechanism compared to the mass-transport limited values.

Conditions: same as Figure 2.

available. The value of k_{app} calculated from the intercept can be used to calculate rate constants, provided k_{app} can be solved based on the mechanism of the reaction. This is possible for only a few simple mechanisms, including the CE mechanism described here. It is much more common to simply use the value of k_{app} as an empirical measure of the rate of the electrochemical reaction.

Voltammetric data often resemble the data shown in Figures 2 and 3 for the simple CE model. For example, the anodic, oxygen-transfer reactions discussed in this dissertation are almost always irreversible, with $E_{1/2}$ values that are much greater than their $E^{o'}$ values. Also, the limiting current rarely approaches the mass-transport limited value predicted by the Levich equation. This implies that a step other than electron transfer is rate limiting for these reactions. The slow chemical step might correspond to any combination of the following: deprotonation, oxygen transfer, adsorption of reactants, a change in the surface characteristics of the electrode, or a change in conformation of a reactant or an intermediate species.

The value of k_{app} in Eqn. [17] for the CE mechanism was calculated using the reaction layer approach based on the assumption that the homogeneous reactions are rapid so that the hypothetical reaction layer (X_R) is much smaller than the diffusion layer (δ). Digital simulation can be used to

provide a more exact solution for electrochemical problems which can only be solved directly by making numerous assumptions (8-9). Finite difference and orthogonal collocation methods have been used to calculate the disk current at the RDE for various mechanisms (10-13). These methods also have been used to calculate the current at the disk and ring electrodes of an RRDE (14-19). Recently, the Hale transformation was used to calculate the chronoamperometric response at the RDE for a wide variety of possible mechanisms (20). These results confirmed the qualitative behavior predicted by the reaction layer concept. For the CE mechanism discussed previously, it was argued that digital simulation and the reaction layer model are actually complementary techniques, where the results calculated using the reaction layer model were equivalent to those calculated with digital simulation when the chemical steps are fast (21). The computation time becomes prohibitive as the rate constants for the chemical steps are increased, therefore, the reaction layer approach was deemed more useful for fast solution kinetics.

Digital simulation methods are used not only to quantitatively predict the effect of homogeneous chemical reactions on the voltammetric response, but also to distinguish between various mechanisms based on the qualitative electrochemical response. Consider the ECE

mechanism, which consists of two electron transfer steps separated by a chemical reaction in solution. Mechanisms of the ECE type have been solved using digital simulation (17, 22) and steady-state approximations (23, 24). Both methods concluded that the apparent value of n (n_{app}) varies with the rotation rate of the electrode. At high rotation rates, n_{app} approaches the value corresponding to the first electron transfer step, whereas, at low rotation rates, n_{app} approaches the value corresponding to the net electrochemical reaction. When n_{app} varies in this manner, significant curvature of Koutecky-Levich plots (Eqn. [11]) is observed. Therefore, ECE-type mechanisms can be identified based on simple rotation rate studies at the RDE. Curvature in Koutecky-Levich plots also can be observed when the requirement of uniform accessibility is no longer fulfilled at the RDE. However, experimental situations where the current density is not uniformly distributed across the electrode surface can usually be distinguished from ECE-type mechanisms by other techniques.

NONUNIFORM CURRENT DENSITY

There are many experimental situations when a disk electrode exhibits nonuniform current density. This situation can arise because of electrode fouling by impurities or reaction products. Also, many electrochemical reactions are either catalyzed or inhibited by the presence of small amounts of oxide on the electrode surface. Spatial heterogeneity can be intentionally introduced, as is the case for electrodes doped with catalytic sites, such as Bi-doped PbO_2 film electrodes. This is also true of composite electrodes, where conducting particles are suspended in a nonconducting matrix. Examples of this type of electrode include the carbon-paste electrode, and composite electrodes fabricated from mixtures of conducting particles and Kel-F polymer (polychlorotrifluoroethylene) (Section V).

The electrochemical response of the RDE is extremely difficult to calculate under conditions of nonuniform current density, since mass transport by convection and diffusion is no longer limited to the direction normal to the plane of the electrode. These calculations are much simpler if convection is eliminated. Therefore, chronoamperometry in quiescent solution is often used to characterize the dimensions of the active sites at spatially heterogeneous disk electrodes.

The chronoamperometric response at microelectrode ensembles is discussed here, although the results are also

applicable to other examples of nonuniform current density. First, consider the chronoamperometric response at an individual microelectrode. At short times, the current at an inlaid microdisk electrode is given by Eqn. [18] (25), where P is the circumference of the electrode. The first term is the

$$i_{lim} = nFDC^{b}(A/(\pi Dt)^{1/2} + P/2) \qquad [18]$$

where $P = 2\pi r$

familiar Cottrell equation where diffusion is restricted to the direction normal to the electrode surface. The second term reflects the contribution to the total current from enhanced diffusion to the edge of the electrode. This term is insignificant at a conventional disk electrode, but is the source of the higher current densities that are observed at single microelectrodes and microelectrode ensembles. At long times, the current is given by Eqn. [19], and is equal to that at a hemispherical electrode with a radius of $2r/\pi$ for $t \longrightarrow \infty$ (25,26,27).

$$i_{lim} = 4nFC^{b}Dr \qquad [19]$$

Equation [19] can be solved for the steady-state diffusion layer thickness (Eqn. [20]) (28). The equivalence between the

$$\delta = \pi r/4 \qquad [20]$$

limiting currents at an inlaid microelectrode and at a

hemisperical electrode demonstrate that the current is independent of the shape of the microelectrode when the diffusion layer is $\geq$ the dimensions of the electrode. For an inlaid microelectrode, short times (Eqn. [18]) correspond to $t << r^2/D$, whereas long times (Eqns. [19] and [20]) correspond to $t >> r^2/D$ (25).

Equations [18]-[20] were derived for an isolated microelectrode, but also apply to a microelectrode ensemble where there is no overlap of the diffusion layers for adjacent active sites. In this case, the total current is just the sum of the currents at each individual microelectrode, i.e., Eqns. [18] or [19] multiplied by the number of microelectrode elements. From Eqn. [20], one might expect that there would be no overlap of diffusion layers when the spacing between elements is larger than their diameter. However, it has been recommended that the elements be separated by at least 6 diameters to avoid diffusion layer overlap (29). In the experimental limit that diffusion layer overlap is complete, the current is given by Eqn. [18], but the area term refers to the geometric area of the disk. This means that at long times, the microelectrode ensemble behaves as if the whole surface is active. The current at times intermediate between zero diffusion layer overlap and total diffusion layer overlap can be solved by digital simulations, and an empirical solution has been given (30). Recently, an analytical

solution was derived which was accurate within 5% of experimental data (31).

Chronoamperometric data at short times (Eqn. [18]) can be used to calculate the fractional active area and the total perimeter for a composite electrode. From inspection of Eqn. [18], higher current densities are expected for microelectrode ensembles that have a larger perimeter to area ratio. Thus, for electrodes with the same fractional active area, higher current densities are expected for the electrode with a larger number of smaller active sites.

Chronoamperometry is useful for determining active site sizes and separations, but mass-transport properties are important since practical applications certainly involve convective conditions. The earliest solution for the current at a partially blocked RDE (32,33) predicted that curvature in both Levich plots (i-$w^{1/2}$) and Koutecky-Levich plots (i^{-1}-$w^{-1/2}$) would be observed when the distance between the active sites was comparable to the diffusion layer thickness.

This treatment was criticized (34) because it was based on a uniform diffusion layer thickness across the electrode surface. Alternate treatments have neglected mass-transport by radial diffusion (34,35), and concluded that the rotation rate dependence of the current would be equal to that of a uniformly accessible RDE of smaller geometric area. The response was characterized by an attenuation factor (ρ), which

is the ratio of the current at a partially blocked RDE to the current at a uniformly accessible RDE of the same geometric area. It was concluded that ρ is independent of rotation rate when radial diffusion is negligible. Therefore, a linear relationship was predicted for both Levich plots (i-$w^{1/2}$) and Koutecky-Levich plots (i^{-1}-$w^{-1/2}$).

Experimental results demonstrated that curvature can be observed for both Levich and Koutecky-Levich plots at an electrode poisoned by chemisorbed substances (36-37). Recently, digital simulation was used to calculate the current at a partially blocked RDE as a function of rotation rate and fractional active area (38). This calculation included terms for radial mass transport by both diffusion and convection, as well as diffusion and convection in the direction normal to the electrode surface. These calculations support the conclusion that the attenuation factor (ρ) is a function of rotation rate, i.e., both i-$w^{1/2}$ and i^{-1}-$w^{-1/2}$ plots show significant deviations from linearity. These calculations also demonstrate that for electrodes with equal fractional active areas, the current density was higher for a RDE with a larger number of smaller active sites.

Qualitative results for disk electrodes under both stationary and convective (RDE) conditions demonstrate that a greater enhancement in current density is observed by maximizing the edge effect, i.e., for a larger number of

smaller active sites. These results are given for electrodes with macroscopic inhomogeneities (active sites with r $\simeq$ um). It is interesting to speculate whether these trends can be extended to electrodes with microscopic inhomogeneities. Under these conditions, the electrode response may be equal to the response at a uniformly active electrode (ρ = 1) for extremely short times in chronoamperometry, or for all accessible rotation rates at a RDE. This situation would result in an extremely large signal-to-background current enhancement if the background current was mainly due to the active sites.

RESEARCH GOALS

The aims of this research include the determination of the effects of nonuniform current density on anodic oxygen-transfer reactions. Previous research in this group has demonstrated that these reactions almost always exhibit extremely slow kinetics. The effects of nonuniform current density are important because the electrocatalysis of a wide variety of oxygen-transfer oxidations has been achieved by doping PbO_2 with various catalysts (39-44). The electrogenerated chemiluminescence of luminol was investigated to determine if the light emitted could be used to map nonuniform current density for spatially heterogeneous electrodes, especially doped PbO_2 electrodes. This was also an interesting mechanistic study since the oxidation of luminol involved an ECE-type mechanism and the transfer of two oxygen atoms.

In addition, the effects of nonuniform current density were studied by intentionally introducing spatial heterogeneity into electrode surfaces, i.e., composite electrodes fabricated from mixtures of KEL-F, graphite, and noble metals. Noble metals, especially Pt and Au, have been investigated for their electrocatalytic properties with respect to oxygen-transfer oxidations (45-49). Composite electrodes based on noble metal active sites were investigated as a practical alternative to pure noble metal electrodes.

These electrodes are not only less expensive, but also exhibit higher current densities than solid electrodes. Higher current densities are important since many oxygen-transfer oxidations occur with low current efficiencies due to the simultaneous evolution of O_2. The premise that adsorbed hydroxyl radicals present during O_2 evolution are involved in oxygen-transfer oxidations was tested at Au, Pt, Pd, Ir, and glassy carbon electrodes using the oxidation of I^- as the model reaction.

REFERENCES

1. Bard, A. J.; Faulkner, L. R., Electrochemical Methods; Wiley: New York, NY, 1980; p 19.
2. Brett, C. M. A.; Brett, A. M. C. F. O. Comprehensive Chemical Kinetics; C. H. Bamford, R. G. Compton, Eds.; Elsevier: New York, NY, 1986; Chapter 5, p 358.
3. Cottrell, F. G. Z. Physik. Chem. **1902**, 42, 385.
4. Levich, V. G., Physicochemical Hydrodynamics; Prentice Hall: Englewood Cliffs, NJ, 1962; p 75.
5. Gregory, D. P.; Riddiford, A. C. J. Chem. Soc. **1956**, 3756-3764.
6. Rieger, P. H. Electrochemistry; Prentice Hall: Englewood Cliffs, NJ, 1987; p 300.
7. Ref. (1), p 466.
8. Britz, D. Digital Simulation in Electrochemistry; Springer-Verlag: New York, NY, 1981.
9. Feldberg, S. W. Electroanalytical Chemistry; A. J. Bard, Ed.; Marcel Dekker: New York, NY, 1969; Vol. 3, pp 199-296.
10. Eddowes, M. J. J. Electroanal. Chem., **1983**, 159, 1-22.
11. Pons, S.; Speiser, B.; McAleer, J. F. Electrochim. Acta, **1982**, 27, 1177-1179.
12. Adanuvor, P. K.; White, R. E.; Lorimer, S. E. J. Electrochem. Soc., **1987**, 134, 625-631.
13. Feldberg, S. W.; J. Electroanal. Chem., **1980**, 109, 69-82.

14. Feldberg, S. W.; Bowers, M. L.; Anson, F. C. J. Electroanal. Chem., 1986, 215, 11-28.

15. Prater, K. B.; Bard, A. J. J. Electrochem. Soc., 1970, 117, 207-213.

16. Prater, K. B.; Bard, A. J. J. Electrochem. Soc., 1970, 117, 335-340.

17. Prater, K. B.; Bard, A. J. J. Electrochem. Soc., 1970, 117, 1517-1520.

18. Puglisi, V. J.; Bard, A. J. J. Electrochem. Soc., 1972, 119, 833-837.

19. Maloy, J. T.; Prater, K. B.; Bard, A. J. J. Am. Chem. Soc., 1971, 93, 5959-5968.

20. Compton, R. G.; Laing, M. E.; Mason, D.; Northing, R. J.; Unwin, P. R. Proc. R. Soc. Lond. A, 1988, 418, 113-154.

21. Ref. (20), pp 147-148.

22. Compton, R.G.; Harland, R.G.; Unwin, P.R.; Waller, A.M. J. Chem. Soc. Faraday Trans. 1, 1987, 83, 1261-1268.

23. Malachesky, P. A.; Marcoux, L. S.; Adams, R. N. J. Phys. Chem., 1966, 70, 4068-4070.

24. Karp, S. J. Phys. Chem., 1968, 72, 1082.

25. Oldham, K. B. J. Electroanal. Chem. 1981, 122, 1-17.

26. Newman, J. J. Electroanal. Chem. 1966, 113, 501.

27. Aoki, K.; Osteryoung, J. J. Electroanal. Chem. 1981, 122, 19-35.

28. Sleszynski, N.; Osteryoung, J.; Carter, M. Anal. Chem. 1984, 56, 130-135.

29. Caudill, W. L.; Howell, J. O.; Wightman, R. M. Anal. Chem., 1982, 54, 2532-2535.

30. Shoup, D.; Szabo, A. J. Electroanal. Chem. 1984, 160, 19-26.

31. Scharifker, B. R. J. Electroanal. Chem. 1988, 240, 61-76.

32. Landsberg, R.; Thiele, R. Electrochim. Acta 1966, 11, 1243-1259.

33. Scheller, F.; Muller, S.; Landsberg, R.; Spitzer, H.-J. J. Electroanal. Chem. 1968, 19, 187-198.

34. Filinovsky, V. Yu. Electrochim. Acta 1980, 25, 309-314.

35. Contamin, O.; Levart, E. J. Electroanal. Chem. 1982, 136, 259-270.

36. Trukhan, A. M.; Povarov, Yu. M.; Lukovtsev, P. D. Elektrokhimiya 1970, 6, 425-429.

37. Povarov, Yu. M.; Lukovtsev, P. D. Electrochim. Acta 1973, 18, 13-18.

38. Levart, E. J. Electroanal. Chem. 1985, 187, 247-263.

39. Yeo, I.-H.; Johnson, D. C. J. Electrochem. Soc., 1987, 134, 1973-1977.

40. Hsiao, Y.-L.; Johnson, D. C. J. Electrochem. Soc., 1989, 136, 3704-3711.

41. LaCourse, W. R.; Hsiao, Y.-L.; Johnson, D. C.; Weber, W. H. J. Electrochem. Soc., 1989, 136, 3714-3719.

42. Feng, J.; Johnson, D. C. J. Electrochem. Soc., 1990, 137, 507-510.

43. Chang, H.; Johnson, D. C. J. Electrochem. Soc., 1990, 137, 2452-2457.

44. Yeo, I.-H.; Kim, S.; Jacobson, R.; Johnson, D. C. J. Electrochem. Soc., 1989, 136, 1395-1401.

45. Cabelka, T. D.; Austin, D. S.; Johnson, D. C. J. Electrochem. Soc., 1984, 131, 1595-1602.

46. Austin, D. S.; Polta, J. A.; Polta, T. Z.; Tang, A. P.-C.; Cabelka, T. D.; Johnson, D. C. J. Electroanal. Chem., 1984, 168, 227-248.

47. Larew, L. A.; Johnson, D. C. J. Electroanal. Chem., 1989, 262, 167-182.

48. Cabelka, T. D.; Austin, D. S.; Johnson, D. C. J. Electrochem. Soc., 1985, 132, 359-364.

49. Wels, B.; Johnson, D. C. J. Electrochem. Soc., 1990, 137, 2785-2791.

SECTION II.

THE IMPORTANCE OF ADSORPTION IN ANODIC SURFACE-CATALYZED OXYGEN-TRANSFER REACTIONS AT GOLD ELECTRODES[1]

---

[1] Published in Vitt, J. E.; Larew, L. A.; Johnson, D. C. Electroanalysis 1990, 2, 21-30.

ABSTRACT

A large number of anodic oxygen-transfer reactions were studied at Au electrodes in both acidic and alkaline media. Results of competitive adsorption studies are interpreted to support the conclusion that adsorption is a prerequisite to subsequent oxygen- and electron-transfer steps. Many of these oxidation reactions gave the voltammetric appearance of reversible waves, even though the observed half-wave potential values were shifted hundreds of millivolts positive of the thermodynamic potentials. A catalytic mechanism is proposed in which adsorbed hydroxyl radicals (AuOH) participate in the oxygen-transfer step. The absence of pH effects on half-wave potentials for several inorganic compounds suggests that the electron transfer precedes the deprotonation step for these reactants.

INTRODUCTION

The voltammetric response (i-E) recorded for any given electroactive compound is expected to be a complex function of the various thermodynamic, kinetic and mass-transport parameters which are characteristic of the corresponding redox process. As a result, the interpretation of voltammetric response patterns can be somewhat complicated, especially when the electrode surface participates catalytically within the reaction mechanisms. In cases of so-called "surface-controlled" mechanisms, the observed i-E response can be dictated more by the potential dependence of the electrode surface state than by the reversible redox potential of the reactant, provided the minimum thermodynamic criterion of reactivity is satisfied, i.e., $E_{applied} > E_{reversible}$. We report here on a voltammetric study of numerous reactants at Au electrodes in alkaline and acidic media which are characterized by similar values of half-wave potential ($E_{1/2}$) in spite of a large divergence of standard potentials. Evidence is given that the electrode surface state involved in many oxygen-transfer oxidations on Au electrodes is the adsorbed hydroxyl radical (AuOH).

The presence of adsorbed hydroxyl radicals on Pt electrodes (PtOH) in acidic and alkaline solutions is well established. The involvement of PtOH has been proposed for many anodic electrocatalytic reactions in both acidic and

alkaline electrolytes. Included among these reactions are the oxidations of HCOOH (1), CH_3OH (2,3), ethanol (4), ethylene glycol (5), several aldehydes (6), and H_3AsO_3 (7,8). Electrocatalytic mechanisms also have been proposed for oxidations on Au electrodes in acidic and alkaline solutions which involve adsorbed hydroxyl radicals (AuOH). The aldehydes studied on Pt were also determined to be oxidized at Au electrodes and an identical mechanism was proposed for both electrode materials (6). Other anodic reactions involving AuOH include oxidations of ethylene glycol (9) and H_3AsO_3 (10). A study of the oxidation of several saturated, oxygenated, organic compounds on Au electrodes stressed the importance of a submonolayer of adsorbed hydroxyl radicals in electrocatalytic mechanisms in alkaline solutions (11). However, mechanisms involving AuOH, especially in acidic media, have frequently been criticized because of the lack of conclusive proof that adsorbed hydroxyl radicals are present at the low values of applied potential where these oxidations are observed to occur.

More recent studies of the oxidation of Au surfaces have provided direct evidence for the existence of AuOH in acidic and alkaline solutions. Spectroscopic studies of single crystal Au electrodes have clearly demonstrated the existence of adsorbed hydroxyl radicals (AuOH) in alkaline solutions at potential values considerably below the onset of anodic

formation of the "normal" phase oxide on Au surfaces (AuO) (12). The anodic formation of AuO on Au electrodes in acidic solutions also has been shown to proceed via a AuOH intermediate (13,14,15). Voltammetric evidence for formation of AuOH is usually concluded to be a shoulder on the anodic wave for AuO formation during the positive scan (16). However, voltammetric studies, concurrent with determination of mass change using the quartz crystal microbalance, do not explicitly rule out the formation of some AuOH at less positive potentials (13). It seems reasonable to propose that there is a low surface coverage of AuOH (i.e., < 10% of a monolayer) even in acidic solutions at potentials where anodic electrocatalytic phenomena have been observed. The adsorbed hydroxyl radicals might be present initially at unusual surface micro-structures, such as Au adatoms, grain boundaries, or steps in a surface plane.

As demonstrated here by cyclic voltammetry, a great many anodic oxygen-transfer reactions of organic and inorganic compounds occur at Au electrodes with virtually identical values of half-wave potential ($E_{1/2}$). Results from competitive adsorption studies are presented which are concluded to be consistent with mechanisms involving oxygen transfer via AuOH sites on the Au surface.

EXPERIMENTAL

Equipment. Voltammetric data (i-E) were obtained using an RDE3 potentiostat and Au rotated disk electrode (RDE, 0.196 cm^2) in an ASR rotator from Pine Instrument Co. (Grove City, PA), and recorded by a Model 100 X-Y recorder from Houston Instruments Co. (Austin, TX). Potential control was maintained vs. a saturated calomel electrode and potentials are reported vs. the SCE. The counter electrode was a coiled Pt wire. The electrochemical cell was made of Pyrex with porous glass disks separating the working, reference, and counter electrode compartments.

Reagents. Except for formaldehyde, all chemicals were Reagent Grade from Baker Chemical Co. (Phillipsburg, NJ) or Fisher Scientific Co. (Fair Lawn, NJ). A 37% solution of formaldehyde, containing 10-15% methanol as a preservative, was from Fisher Scientific Co. No voltammetric response for methanol was obtained in the formaldehyde solutions at the concentration used (0.4 mM). Water was purified in a Milli-Q system from Millipore (Bedford, MA) after distillation. Where indicated, solutions were kept free of dissolved O_2 by purging with dispersed N_2 and then maintaining a N_2 atmosphere over solutions.

Procedures. Current-potential (i-E) curves were recorded in 0.1 M H_2SO_4 and 0.1 M NaOH at room temperature (25 $\pm$ 2 C). The Au RDE was polished with 0.05-micron alumina in H_2O on

microcloth (Buehler Ltd.; Lake Bluff, IL), rinsed with deionized H_2O, and the electrode potential cycled in the supporting electrolyte between the values for onset of O_2 and H_2 evolution until the i-E curves were reproducible.

RESULTS AND DISCUSSION

Alcohols and aldehydes in alkaline solutions. Shown in Figure 1 are cyclic voltammograms (i-E) of 0.2 mM glucose (Curve b), 0.4 mM formaldehyde (Curve c), and 0.75 mM benzaldehyde (Curve d) in 0.1 M NaOH, in comparison to the residual response for the Au electrode (Curve a). As shown in Table 1, the $E_{1/2}$ values for oxidation of these compounds were hundreds of millivolts positive of their $E^{o'}$ values. Despite the large overpotentials required for these oxidations, the currents for each compound rapidly reached constant values during the positive scan, giving the appearance of reversible, transport-limited waves. This behavior is consistent with an electrocatalytic mechanism, to be proposed later, in which a common rate controlling step exists for these various reactions. The anodic currents decreased rapidly for these compounds with onset of formation of AuO (E > ca. 0.2 V) during the positive potential scan and oxidation resumed on the negative scan only after the cathodic peak was obtained for stripping of the AuO (E < ca. 0.1 V).

The residual voltammetric response of the Au electrode in 0.1 M NaOH was recorded using a large current sensitivity. A voltammetric wave was quite apparent ($E_{1/2}$ = ca. -0.48 V, Figure 2) on the positive scan which we conclude corresponds to anodic formation of AuOH. The presence of AuOH at Au surfaces at these potential values in alkaline solution has

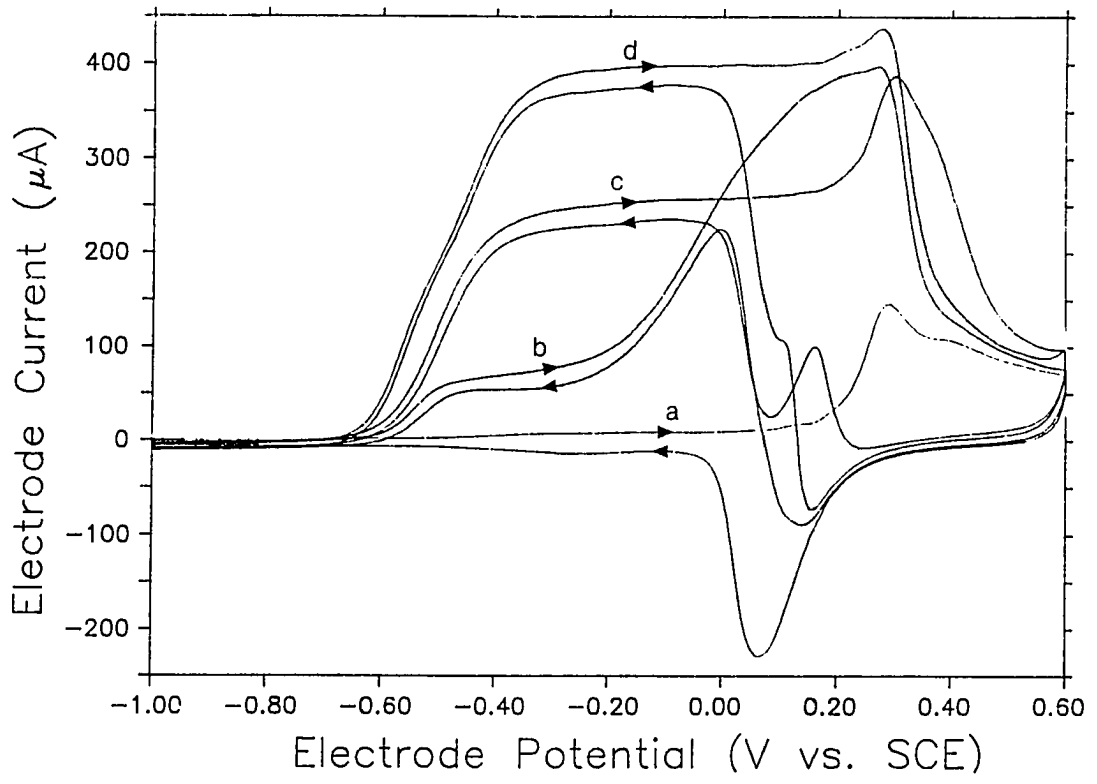

Figure 1. Voltammetric response of glucose, formaldehyde, and benzaldehyde at a Au RDE in alkaline solution.

Conditions: 0.1 M NaOH, 6.0 V min^{-1}, 900 rev min^{-1} (94.2 rad sec^{-1}), O_2 removed.

Curves: (a) residual response,
(b) 0.20 mM glucose,
(c) 0.40 mM formaldehyde,
(d) 0.75 mM benzaldehyde.

Table 1 Values of $E^{o'}$ and $E_{1/2}$ in acidic and alkaline solutions.

Reactant	Product	pH 1		pH 13	
		$E^{o'}$[a]	$E_{1/2}$[b]	$E^{o'}$[a]	$E_{1/2}$
glucose	gluconic acid	-0.212	1.0	-0.912	-0.55
HCHO	HCOOH, CO_2	-0.272	1.0	-1.227	-0.51
benzaldehyde	benzoic acid				-0.49
CH_3OH	HCHO, HCOOH, CO_2	-0.101		-0.778	0.10
benzyl alcohol	benzoic acid		0.90		-0.32
glycerol			1.07		-0.04
1-propanol	propionic acid		0.96		0.07
phenol	hydroquinone		0.89		0.27
Au	AuOH		0.40[c]		-0.48
Au, AuOH	AuO, Au_2O_3		1.07		0.23
EDA[d]					0.09
SO_3^{2-}	SO_4^{2-}	-0.188	0.40	-1.113	0.29
$S_2O_3^{2-}$	SO_4^{2-}, $S_2O_4^{2-}$	-0.162	0.50	-0.724	0.39
$S_2O_4^{2-}$	SO_4^{2-}	-0.314	0.37	-1.24	0.39
NO_2^-	NO_3^-	0.603	0.80	-0.175	0.75
N_2H_4	N_2	-0.304	0.37	-1.332	-0.47

[a] Calculated from data in (20, 21).

[b] The lowest value of $E_{1/2}$ is given.

[c] Estimated from $E_{1/2}$ for SO_3^{2-}.

[d] Ethylenediamine.

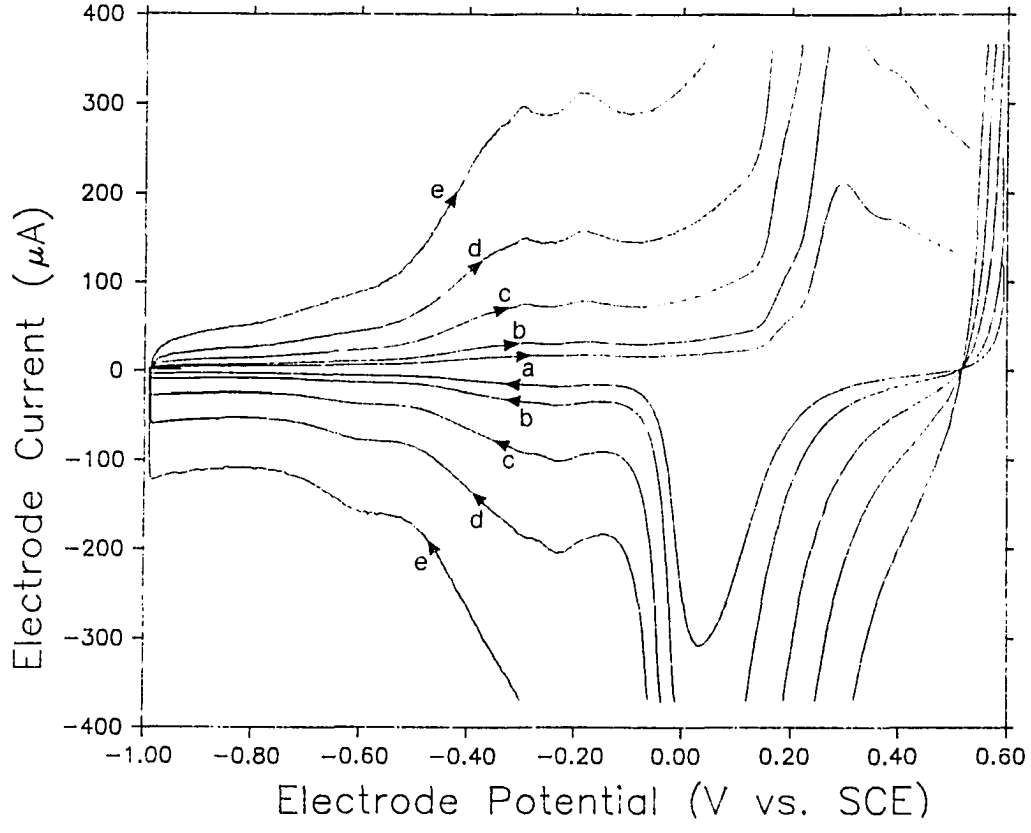

Figure 2. Residual voltammetric response for 0.1 M NaOH as a function of increased current sensitivity of the X-Y recorder.

Conditions: 400 rev min^{-1} (41.9 rad sec^{-1}), 10 V min^{-1}, O_2 removed.

Current sensitivity: (a) scale, (b) scale/2, (c) scale/5, (d) scale/10, (e) scale/20.

been proposed on the basis of spectroscopic evidence (12). The value of $E_{1/2}$ for the anodic formation of AuOH was virtually identical to the $E_{1/2}$ values for oxidation of glucose, benzaldehyde and formaldehyde (Table 1), as well as various other aldehydes (6). These facts are indicative of a surface-catalyzed oxidation mechanism in which AuOH is a participant.

Also studied were the oxidations of several alcohols on Au electrodes in alkaline solutions. The voltammetric responses for benzyl alcohol, glycerol, 1-propanol, and methanol, are shown in Figure 3. The $E_{1/2}$ values for oxidation of these alcohols were positive of the potential at which the AuOH was formed, and the anodic signals decreased sharply with the formation of AuO. Very large concentrations (i.e., C^b > 5 mM) were required to produce an observable anodic wave for 1-propanol and methanol. The values of $E^{o'}$ and $E_{1/2}$ for the alcohols are listed in Table 1. The potentials at which current peaks were obtained for oxidation of the alcohols correspond fairly well to the potential at which the large current peak was observed for glucose in Figure 1.

A mechanism has been proposed for the oxidation of the alcohol functionalities of glucose which necessitates the prior anodic generation of AuOH on the Au electrode (17). It is interesting to note that the $E_{1/2}$ value observed for glycerol oxidation was nearly identical to the potential at

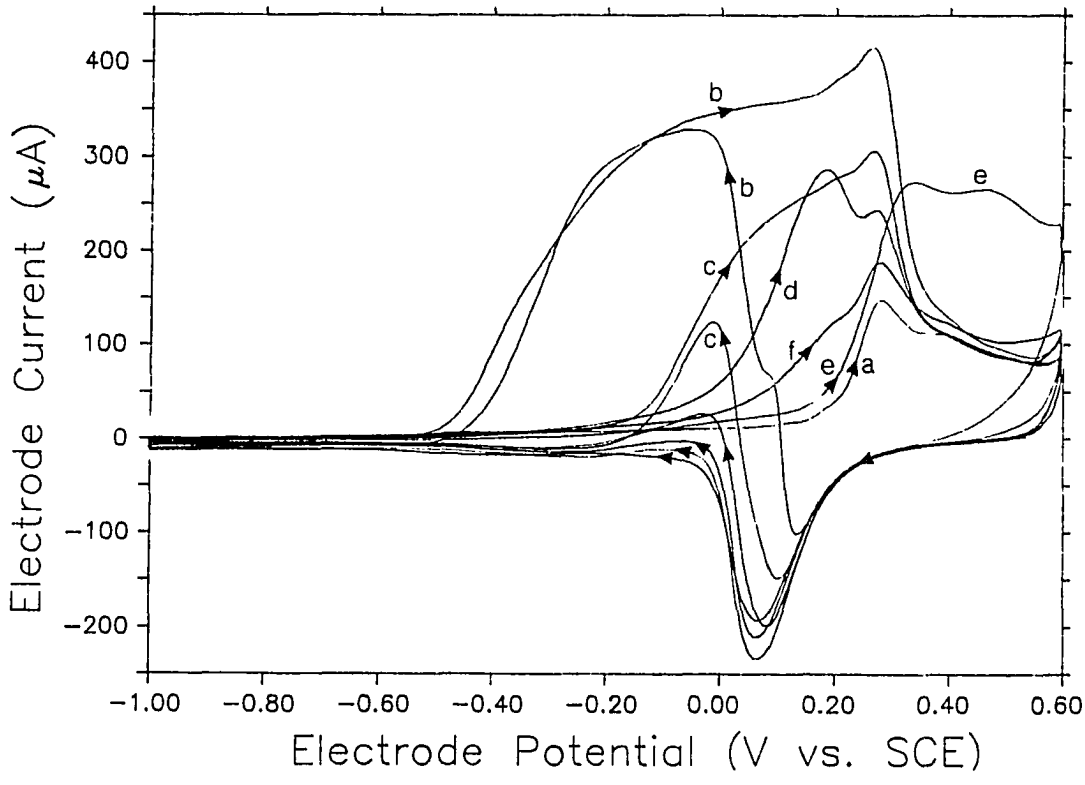

Figure 3. Voltammetric response of alcohols at a Au RDE in alkaline solution.

Conditions: 0.1 M NaOH, 6.0 V min^{-1}, 900 rev min^{-1} (94.2 rad sec^{-1}), O_2 removed.

Curves: (a) residual, (b) 0.40 mM benzyl alcohol, (c) 0.20 mM glycerol, (d) 0.027 M n-propanol, (e) 1.0 mM phenol, (f) 0.99 M methanol.

which the anodic signal for glucose rapidly increases ($E_{1/2}$ = -0.08 V), which is attributed to oxidation of the alcohol groups. As will be demonstrated, adsorption is necessary for the oxidation of these compounds. It is possible that the onset of oxidation is dictated in part by the relative strength of adsorption of each compound on Au. This could help explain the oxidation of methanol and 1-propanol at slightly more positive potentials than benzyl alcohol and glycerol.

The voltammetric response of phenol (Figure 3, Curve e) was substantially different than that for the alcohols tested, revealing an anodic wave on the positive scan concurrently with AuO formation. The oxidation of phenol did not appear to be inhibited by the further oxidation of the Au surface. We conclude that the oxidation of phenol is catalyzed by the simultaneous formation of the higher oxide (AuO).

Alcohols and aldehydes in acidic solutions. The voltammetric behavior of alcohols and aldehydes at Au in acidic solution was markedly different than the corresponding behavior in alkaline solution. Their oxidations were less facile in the acidic solutions and required much higher concentrations to produce an observable voltammetric response. Also, the resulting anodic waves appeared much less reversible. Essentially no anodic current was seen for 1 M methanol in 0.1 M H_2SO_4 within the selected potential limits

(1.4 V and -0.2 V). Also, no signal for benzaldehyde was obtained under the same conditions, but the reduced solubility in 0.1 M H_2SO_4 restricted testing at high concentrations. The voltammetric response for the remaining analytes in 0.1M H_2SO_4 is shown in Figure 4A & B. Caution is recommended in interpretation of these voltammograms because of the extremely high concentrations required. For glucose, a much larger response was seen on the first scan, but the current decreased on subsequent scans. Increased values of the potential scan limits did not alter this continual decline in sensitivity. Only potential cycling in glucose-free solution with more extreme scan limits (e.g., 2.0 V and -1.0 V) resulted in renewed electrode activity for glucose. This behavior is concluded to be the result of increased fouling of the electrode surface at high concentrations by adsorption of glucose and/or its oxidation products. The anodic response for phenol also decreased rapidly with repeated cycling, but this behavior was observed at far lower concentrations than for glucose. Electrode fouling during phenol oxidation is probably due to polymerization of the intermediate phenoxy radicals on the electrode surface (18).

Unlike the observations in alkaline solutions, the formation of the phase oxide in acidic solutions did not shut off the oxidation of the alcohols and aldehydes tested. Refer to Table 1 for $E_{1/2}$ values for the aldehydes, alcohols, and

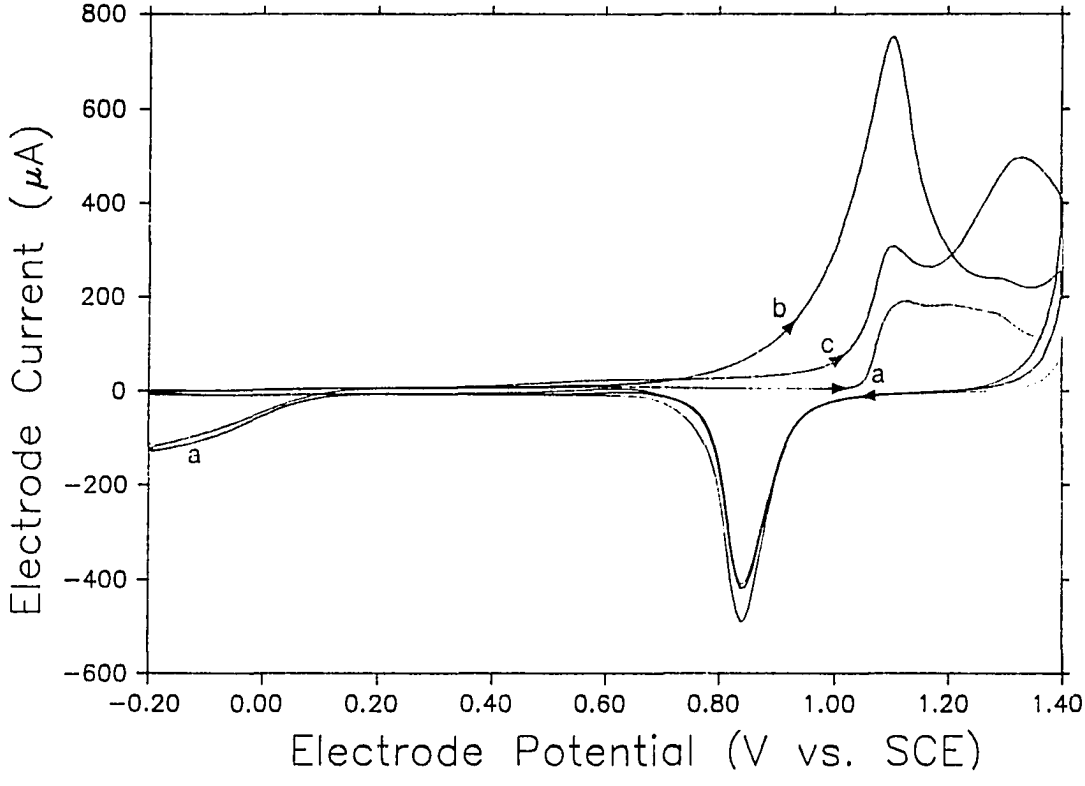

Figure 4A. Voltammetric response of glucose and formaldehyde at a Au RDE in acidic solution.

Conditions: 0.1 M H_2SO_4, 6.0 V min^{-1}, 900 rev min^{-1} (94.2 rad sec^{-1}).

Curves: (a) residual, O_2 present;
(b) 0.25 M formaldehyde, O_2 removed;
(c) 1.0 M glucose, O_2 removed.

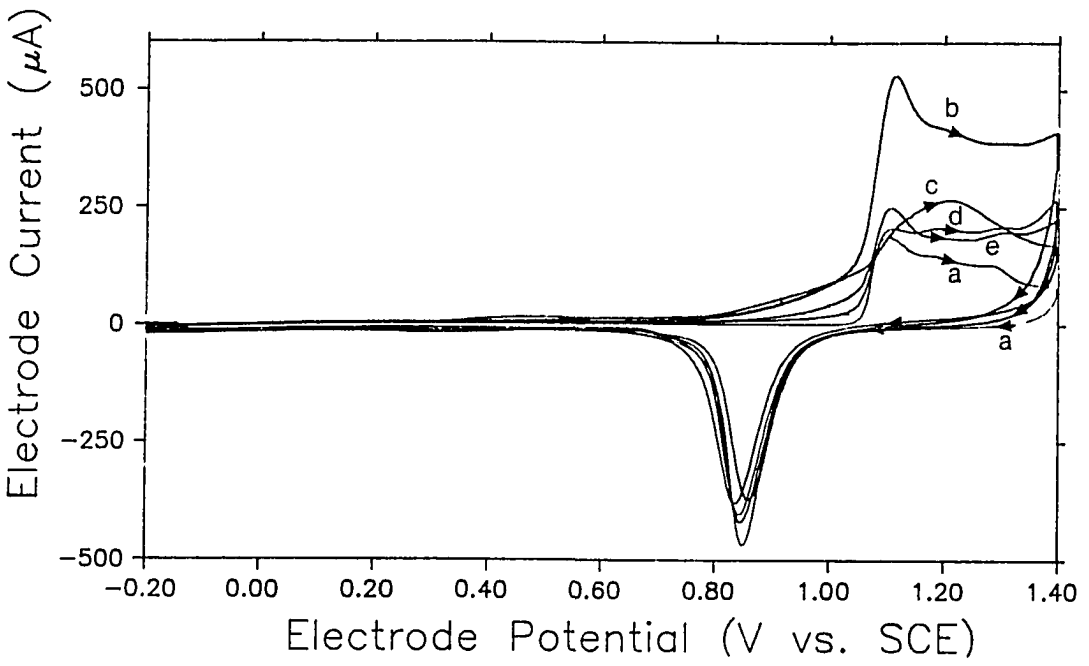

Figure 4B. Voltammetric response of alcohols at a Au RDE in acidic solution.

Conditions: 0.1 M H_2SO_4, 900 rev min^{-1}, O_2 removed, 6.0 V min^{-1}.

Curves: (a) residual
(b) 0.096 M benzyl alcohol
(c) 0.40 mM phenol
(d) 1.5 M glycerol
(e) 2.2 M n-propanol

AuO in acidic solution. For glycerol, the $E_{1/2}$ value was the same as the $E_{1/2}$ value for AuO, and oxidation continued at a small but seemingly constant rate until the potential scan was reversed. For benzyl alcohol, phenol, 1-propanol, and glucose, the $E_{1/2}$ values were negative of the $E_{1/2}$ value for AuO, but oxidation continued after the formation of AuO on the positive scan. In contrast, the anodic current corresponding to the oxidation of formaldehyde increased rapidly at potentials negative of oxide formation and decreased sharply when oxide formation begins. This behavior was similar to the voltammetric behavior of alcohols and aldehydes in basic solution. However, the magnitude of the response was much less in the acidic solution.

The much more irreversible nature of alcohol and aldehyde oxidations observed in acidic solution is not necessarily due to the absence of catalytic AuOH sites. Their oxidation mechanisms include dehydrogenation reactions involving consumption of solution OH^- (17,19), which can become the rate limiting step in acidic solutions. Thus, a small anodic current was obtained for oxidation of alcohols and aldehydes on the AuOH surface in acidic solutions. Oxidation continued at a slow rate on the AuO, which was also the observation in alkaline media.

Ethylenediamine in alkaline solutions. The voltammetric behavior of ethylenediamine in 0.1 M NaOH is shown in Figure

5. An anodic wave ($E_{1/2}$ = 0.09 V, see Table 1) was obtained prior to AuO formation on the positive scan and continued until the potential scan was reversed. The cathodic peak for oxide stripping on the negative scan was decreased and broadened due to the effect of adsorbed ethylenediamine on the formation and stripping of the AuO. The anodic response for ethylenediamine showed essentially no dependence on electrode rotation speed; however, the anodic peak current did increase with increased concentration. The anodic current also increased with increased scan rates. These effects were also exhibited for the wave prior to AuO formation, indicating the anodic current is under surface control and is the result of oxidation of adsorbed ethylenediamine.

Inorganic sulfur compounds. The effect of pH on the $E_{1/2}$ values for oxidation of SO_3^{2-}, $S_2O_3^{2-}$, and $S_2O_4^{2-}$ is illustrated in Figure 6A-C. In 0.1 M NaOH, oxidation coincided with the onset of AuO formation but was quickly attenuated by the further oxidation of the surface. This resulted in sharp anodic peaks at ca. 0.3 V for SO_3^{2-} (Figure 6A), and 0.5 V for $S_2O_3^{2-}$ (Figure 6B) and $S_2O_4^{2-}$ (Figure 6C). The $E_{1/2}$ values for these compounds in 0.1 M H_2SO_4 were within about 100 mV of their $E_{1/2}$ values in alkaline solutions. Refer to Table 1 for the values of $E^{O'}$ and $E_{1/2}$ for these compounds in 0.1 M H_2SO_4 and 0.1 M NaOH. For $S_2O_3^{2-}$ and $S_2O_4^{2-}$, the anodic current was quite small until the AuO was

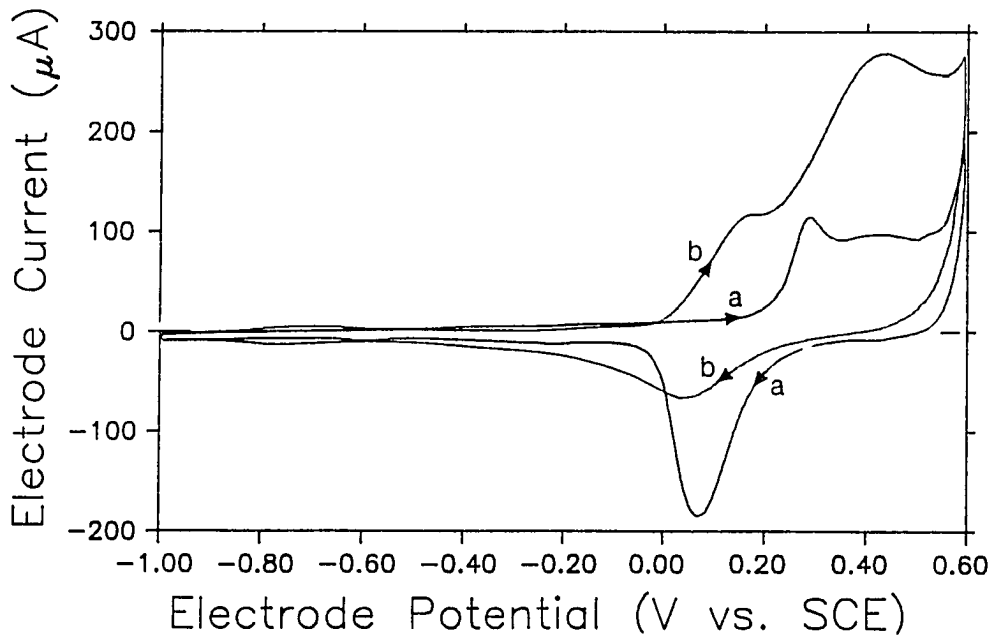

Figure 5. Voltammetric response of ethylenediamine at a Au RDE in alkaline solution.

Conditions: 0.1 M NaOH, 900 rev min^{-1}, 5 V min^{-1}, O_2 removed.

Curves: (a) residual
(b) 1.0 mM ethylenediamine.

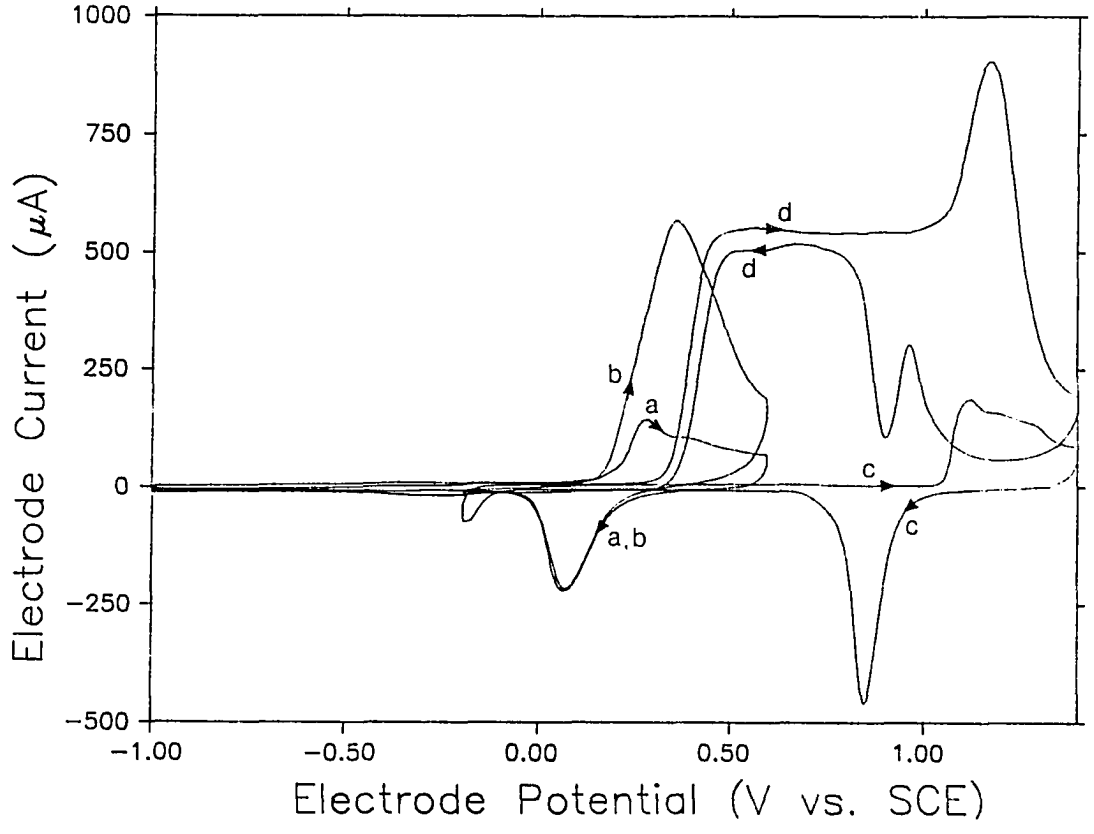

Figure 6A. Voltammetric response of sulfite as a function of pH at a Au RDE.

Conditions: 900 rev min^{-1}, 6.0 V min^{-1}, O_2 removed.

Curves: (a) residual in 0.1 M NaOH
(b) 0.99 mM $NaHSO_3$ in 0.1 M NaOH
(c) residual in 0.1 M H_2SO_4
(d) 0.99 mM $NaHSO_3$ in 0.1 M H_2SO_4

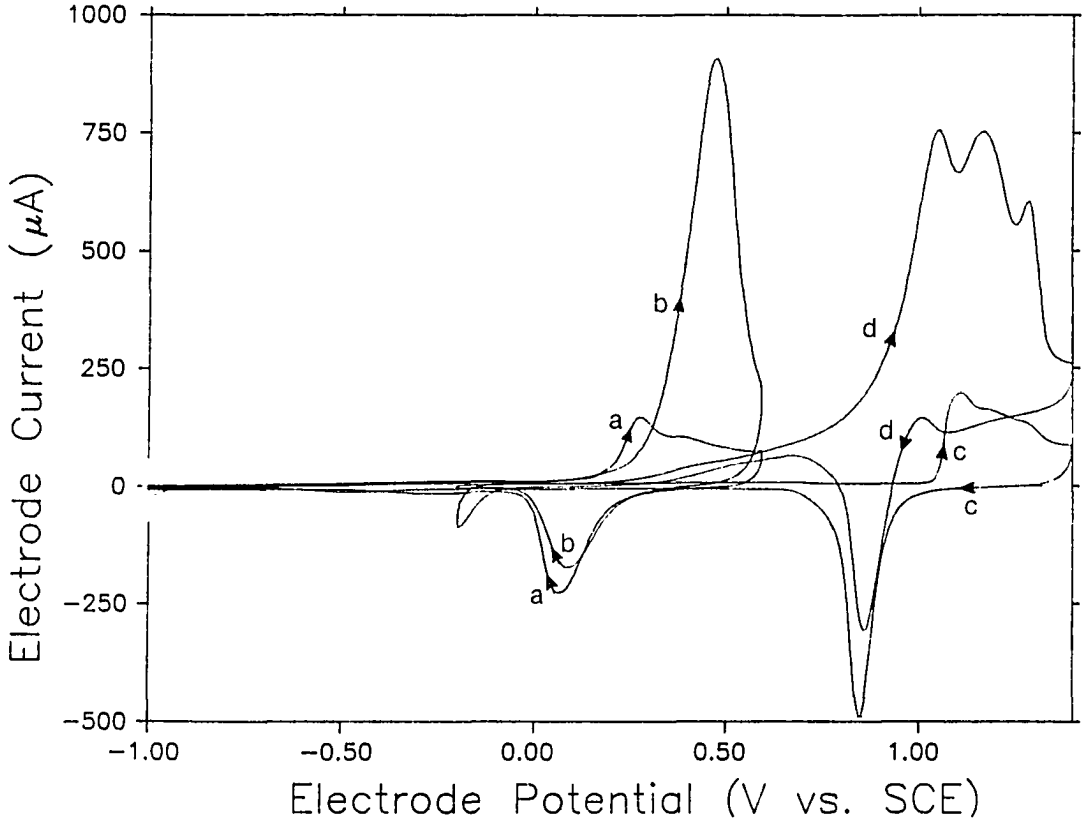

Figure 6B. Voltammetric response of thiosulfate as a function of pH at a Au RDE.

Conditions: 900 rev min^{-1}, 6.0 V min^{-1}, O_2 removed.

Curves: (a) residual in 0.1 M NaOH
(b) 0.20 mM $Na_2S_2O_3$ in 0.1 M NaOH
(c) residual in 0.1 M H_2SO_4
(d) 0.10 mM $Na_2S_2O_3$ in 0.1 M H_2SO_4

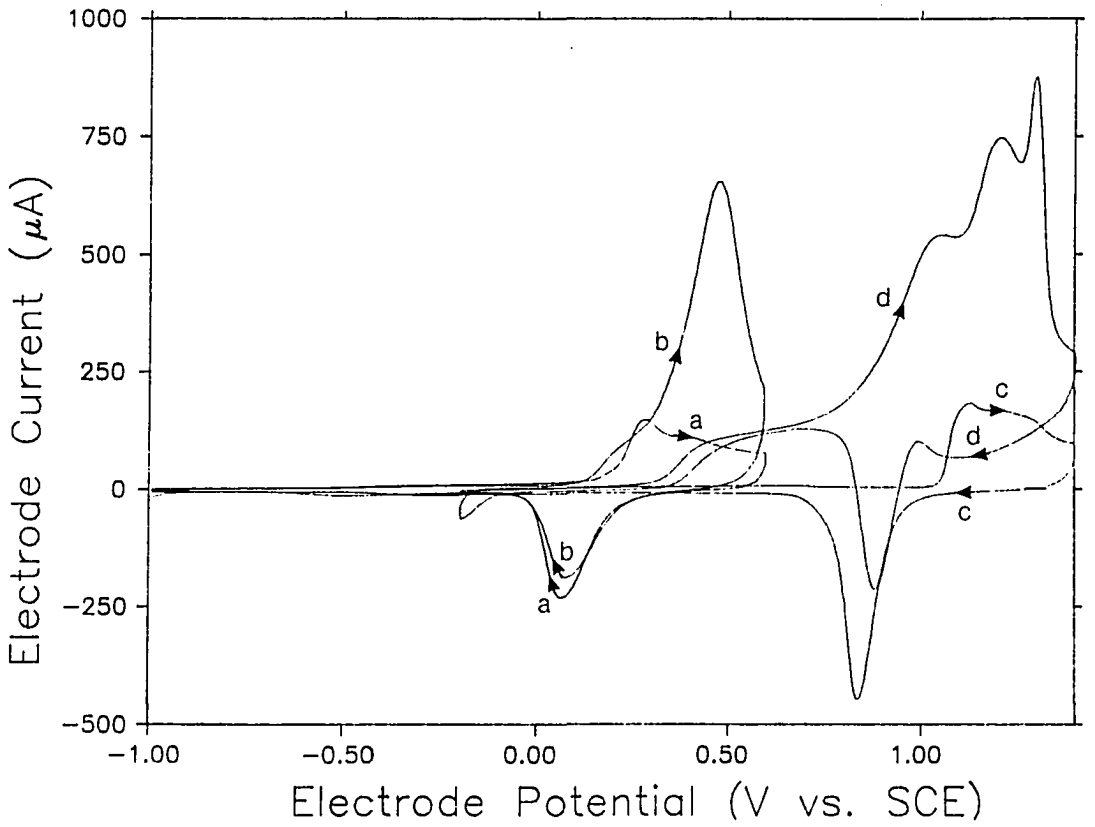

Figure 6C. Voltammetric response of hydrosulfite as a function of pH at a Au RDE.

Conditions: 900 rev min^{-1}, 6.0 V min^{-1}, O_2 removed.

Curves: (a) residual in 0.1 M NaOH
(b) 0.20 mM $Na_2S_2O_4$ in 0.1 M NaOH
(c) residual in 0.1 M H_2SO_4
(d) 0.20 mM $Na_2S_2O_4$ in 0.1 M H_2SO_4

formed, at which point a large increase was seen with two or three current peaks. For SO_3^{2-}, a current plateau region was observed about 650 mV prior to the peak coinciding with the AuO formation wave. For all three analytes, further oxidation of the Au surface greatly decreased the activity of the electrode.

Oxidation of each of these molecules began at about the same potential value in both acidic and alkaline solutions (Table 1), even though their respective net oxidations to SO_4^{2-} indicate H^+ consumption. The lack of pH dependence is tentatively concluded to be the result of deprotonation occurring after the rate-limiting electron-transfer steps.

Nitrite. As shown in Figure 7, NO_2^- did not undergo oxidation until ca. 0.8 V on the positive scan. In 0.1 M H_2SO_4, the anodic current reached a constant value very rapidly and was only slightly inhibited by the formation of AuO. The $E_{1/2}$ values for nitrite showed the same relative lack of pH dependence as observed for the sulfur compounds, which precluded the appearance of any significant anodic current in 0.1 M NaOH until oxygen evolution because of the large positive potentials required for NO_2^- oxidation. Table 1 lists the values of $E^{o'}$ and $E_{1/2}$ for NO_2^- in acidic and alkaline solutions. A mechanism directly analogous to that for SO_3^{2-} can be expected to apply for NO_2^- which includes

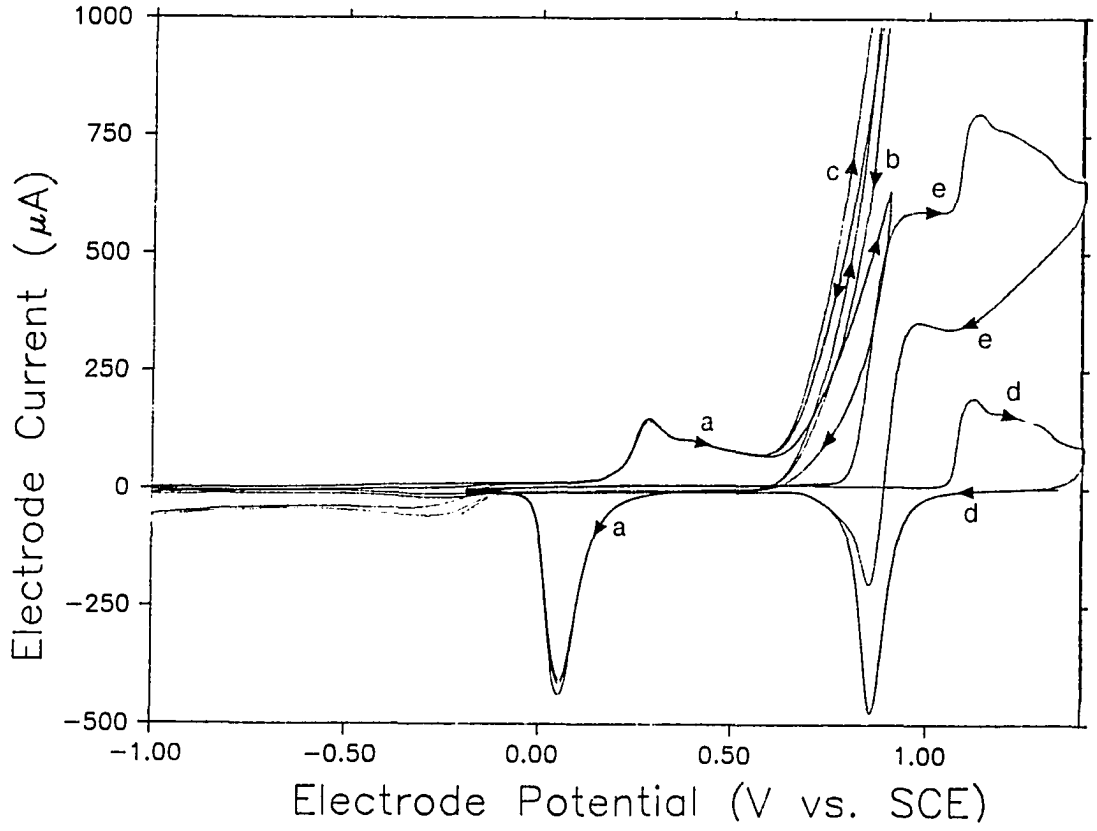

Figure 7. Voltammetric response of nitrite as a function of pH at a Au RDE.

Conditions: 6.0 V min^{-1}, O_2 removed.

Curves: (a) residual in 0.1 M NaOH,
(b) 0.99 mM $NaNO_2$ in 0.1 M NaOH (900 rev/min),
(c) 0.99 mM $NaNO_2$ in 0.1 M NaOH (3600 rev/min),
(d) residual in 0.1 M H_2SO_4,
(e) 0.99 mM $NaNO_2$ in 0.1 M H_2SO_4 (900 rev/min).

deprotonation after the rate-controlling, electron-transfer step.

Hydrazine. A typical cyclic voltammogram for N_2H_4 in 0.1 M NaOH is shown by Curve b in Figure 8. The $E_{1/2}$ value for oxidation of N_2H_4 (Table 1) was similar to the $E_{1/2}$ values for aldehyde oxidations. The anodic current rapidly attained a constant value on the positive scan and was not affected by the formation of AuO. On the negative scan, the oxidation continued at a near constant rate, providing the voltammogram was corrected for the residual current. Once again, oxidation of N_2H_4 was observed to occur a few hundred millivolts positive of its thermodynamic potential ($E^{O'}$ = -1.33 V, $E_{1/2}$ = -0.47 V) and had the appearance of a reversible wave. The oxidation of $N_2H_5^+$ in acidic solution showed a similar anodic wave (data not shown) whose $E^{O'}$ and $E_{1/2}$ values are given in Table 1.

Adsorption hierarchy. Despite the noted similarities in the voltammetric behavior of hydrazine and aldehydes in basic solution, a completely different mechanism of oxidation is operating in both cases, as demonstrated by Curves c-e of Figure 8. These curves correspond to additions of 0.2, 1.0, and 2.0 mM sulfite to the solution containing hydrazine, whose response is shown by Curve b. On the positive potential scan, the onset of oxidation occurred about 70 mV more positive than in the absence of sulfite. As the positive scan continued, an

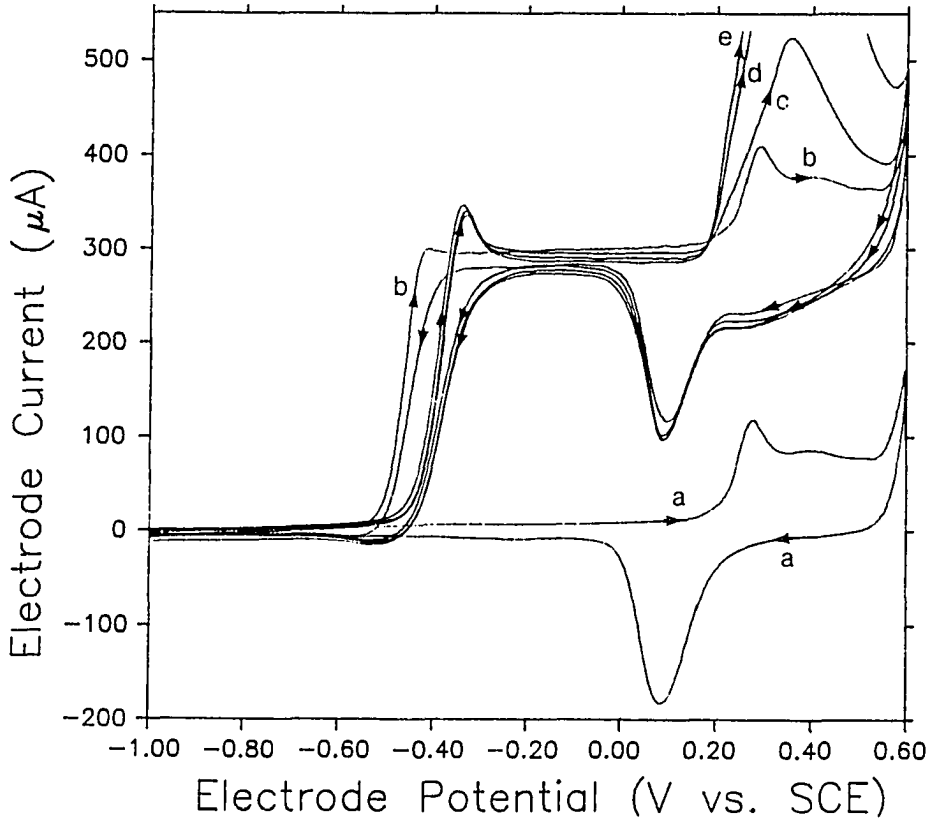

Figure 8. Voltammetric response of hydrazine as a function of sulfite concentration at a Au RDE in alkaline solution.

Conditions: 900 rev min^{-1}, 5.0 V min^{-1}, O_2 removed.

Curves: (a) residual in 0.1 M NaOH,
(b) 0.20 mM hydrazine,
(c) 0.20 mM hydrazine/0.20 mM sulfite,
(d) 0.20 mM hydrazine/1.0 mM sulfite,
(e) 0.20 mM hydrazine/2.0 mM sulfite.

anodic current was obtained which was equivalent to the mass transport limited value for oxidation of hydrazine. The anodic current increased in the potential region where sulfite is oxidized corresponding to the sum of the current due to sulfite and hydrazine oxidation. The response observed during the negative scan was identical to the voltammogram when sulfite was absent, except that the oxidation of hydrazine shut off about 70 mV more positive when sulfite was present. Even if a complete monolayer of adsorbed sulfite was not present, the electrochemical potential gradient in the double layer would be modified by the adsorbed anion with the effect of shifting the oxidation wave by ca. 70 mV. Other than this effect, hydrazine oxidation continued as if sulfite were not present. Hydrazine oxidation is concluded to occur without a prior adsorption step, which is in sharp contrast to the behavior of other analytes studied.

Similar experiments, in which the effect of added sulfite on hydrazine oxidation was observed, were carried out in order to establish the relative strength of adsorption on Au. Hydrazine was used as an example of a compound that does not require preadsorption for oxidation. For all the other analytes tested, the evidence strongly indicated that adsorption was necessary for oxidation. One example is the effect of sulfite on glucose oxidation, as shown in Figure 9. Curve b corresponds to the oxidation of 0.5 mM glucose in

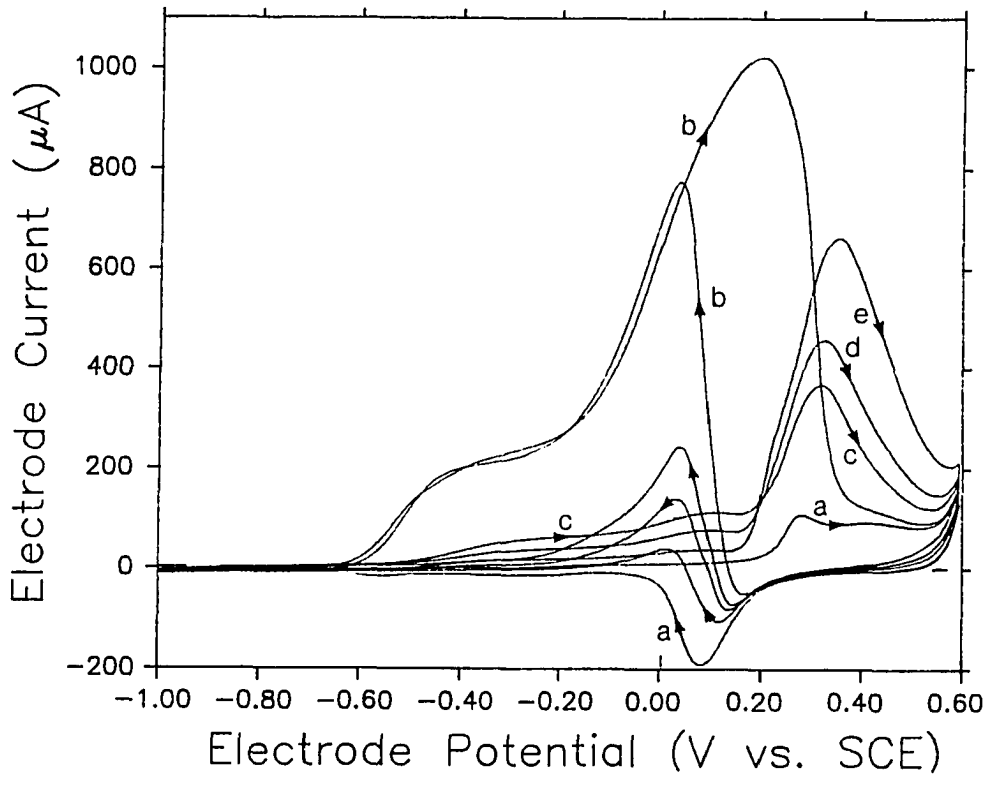

Figure 9. Voltammetric response of glucose as a function of sulfite concentration at a Au RDE in alkaline solution.

Conditions: 1600 rev min^{-1}, 5.0 V min^{-1}, O_2 removed.

Curves: (a) residual in 0.1 M NaOH,
(b) 0.50 mM glucose,
(c) 0.50 mM glucose/0.20 mM sulfite,
(d) 0.50 mM glucose/0.40 mM sulfite,
(e) 0.50 mM glucose/1.0 mM sulfite.

sulfite-free solution. Curves c-e correspond to 0.5 mM glucose oxidation in the presence of 0.2 mM, 0.4 mM, and 1.0 mM sulfite, respectively. The anodic wave for glucose was not merely shifted in a positive direction, as was the case for hydrazine, but it was effectively eliminated when the concentration of sulfite was about the same as that of glucose. Even when the sulfite concentration was only 40% that of glucose (curve c), the current due to oxidation of glucose was decreased by greater than 90% of its peak value. Based on these results, it is concluded that glucose must be adsorbed in order to undergo oxidation, and that sulfite is more strongly adsorbed on Au than glucose under these conditions.

Experiments were performed to establish an adsorption hierarchy for the other functional groups tested. Since sulfite blocked both the aldehyde and alcohol functionalities of glucose, glycerol and formaldehyde were chosen as models of easily oxidized alcohols and aldehydes, respectively. The effect of sulfite on their oxidations is shown in Figures 10 and 11. Curve b in Figure 10 shows the anodic response for 0.4 mM glycerol in sulfite free solution. One can see that the presence of half as much sulfite as glycerol completely blocked glycerol oxidation (Curve c). The effect of sulfite on the anodic wave for formaldehyde was not so dramatic. As shown in Figure 11, even in the presence of sulfite at a

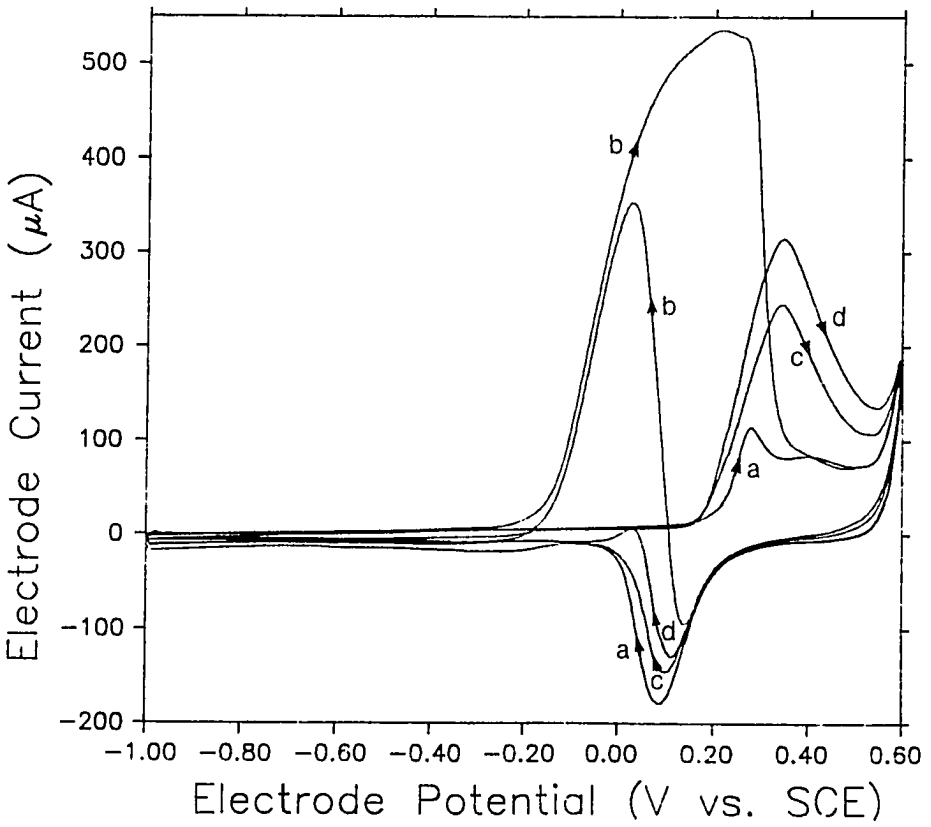

Figure 10. Voltammetric response of glycerol as a function of sulfite concentration at a Au RDE in alkaline solution.

Conditions: 900 rev min^{-1}, 5.0 V min^{-1}, O_2 removed.

Curves: (a) residual in 0.1 M NaOH,
(b) 0.40 mM glycerol,
(c) 0.40 mM glycerol/0.20 mM sulfite,
(d) 0.40 mM glycerol/0.40 mM sulfite.

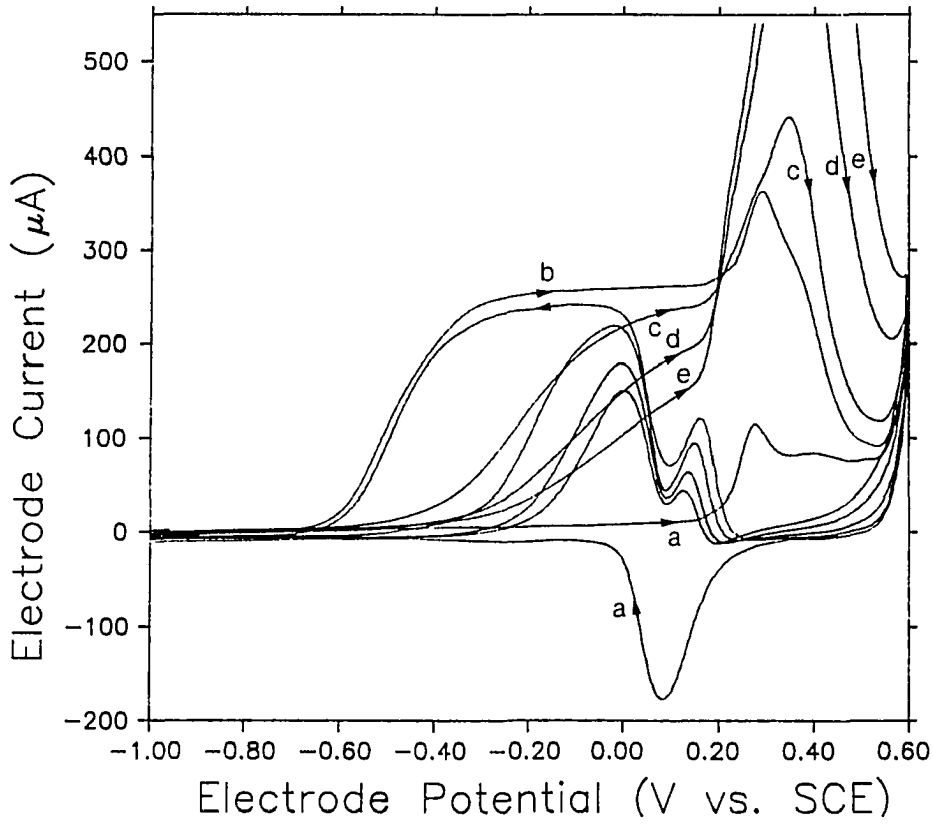

Figure 11. Voltammetric response of formaldehyde as a function of sulfite concentration at a Au RDE in alkaline solution.

Conditions: 900 rev min^{-1}, 5.0 V min^{-1}, O_2 removed.

Curves: (a) residual in 0.1 M NaOH,
(b) 0.40 mM HCHO,
(c) 0.40 mM HCHO/0.20 mM sulfite,
(d) 0.40 mM HCHO/1.0 mM sulfite,
(e) 0.40 mM HCHO/2.0 mM sulfite.

concentration 5 times that of formaldehyde, the oxidation of formaldehyde was still not completely shut off. However, the effect was not similar to that of sulfite on hydrazine, so it is concluded that formaldehyde must be adsorbed as a prerequisite to oxidation. The decreased ability of sulfite to block the formaldehyde oxidation, as compared to glycerol, would seem to indicate that aldehydes are more strongly adsorbed than alcohols. Evidence of sulfite blocking of the ethylenediamine response is more tenuous since their oxidations occur near the same potential. However, as shown in Figure 12, oxidation of ethylenediamine should occur at less positive potentials than sulfite. This first shoulder for ethylenediamine oxidation was completely absent in the presence of sulfite.

These competitive adsorption studies show that sulfite is capable of blocking the anodic reactions of all other compounds chosen, with the exception of hydrazine, and ,thus, sulfite is concluded to be adsorbed most strongly on Au. The effect seems to be general for the three sulfur compounds chosen. Glucose oxidation was blocked by both $S_2O_3^{2-}$ and $S_2O_4^{2-}$, as shown in Figures 13 and 14, respectively. If anything, these two sulfur compounds seem to be even more effective than sulfite in blocking oxidation of the aldehyde functionality in glucose.

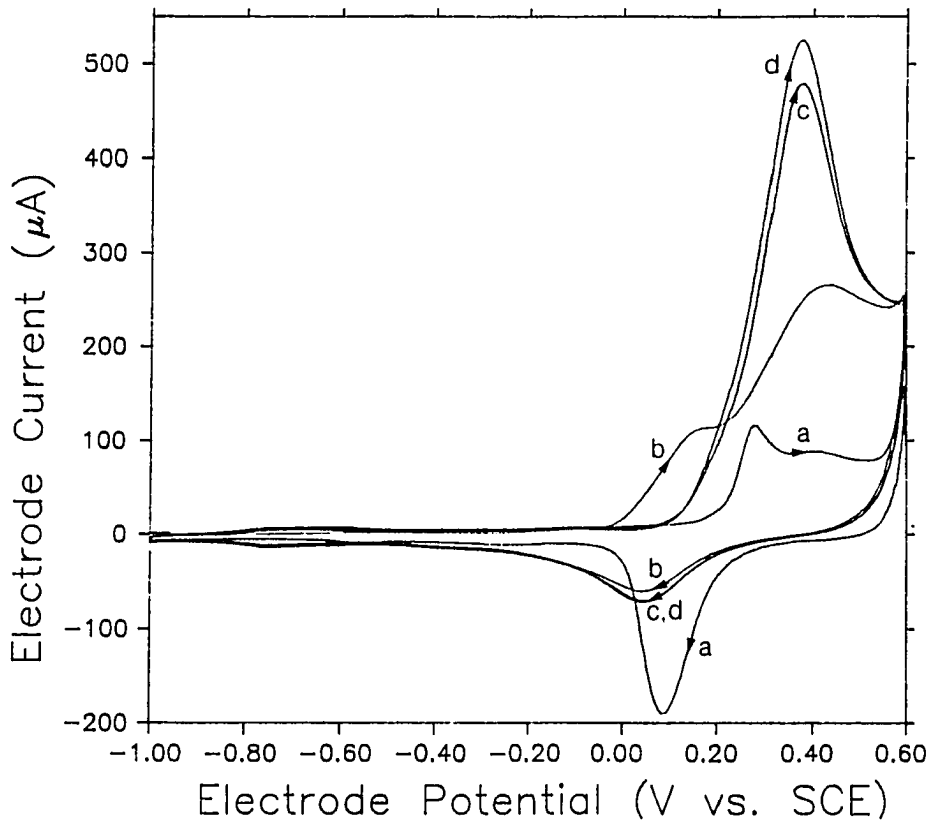

Figure 12. Voltammetric response of ethylenediamine as a function of sulfite concentration at a Au RDE in alkaline solution.

Conditions: 1600 rev min^{-1}, 5.0 V min^{-1}, O_2 removed.

Curves: (a) residual in 0.1 M NaOH,
(b) 1.0 mM ethylenediamine (EDA),
(c) 1.0 mM EDA/0.20 mM SO_3^{2-},
(d) 1.0 mM EDA /0.40 mM SO_3^{2-}.

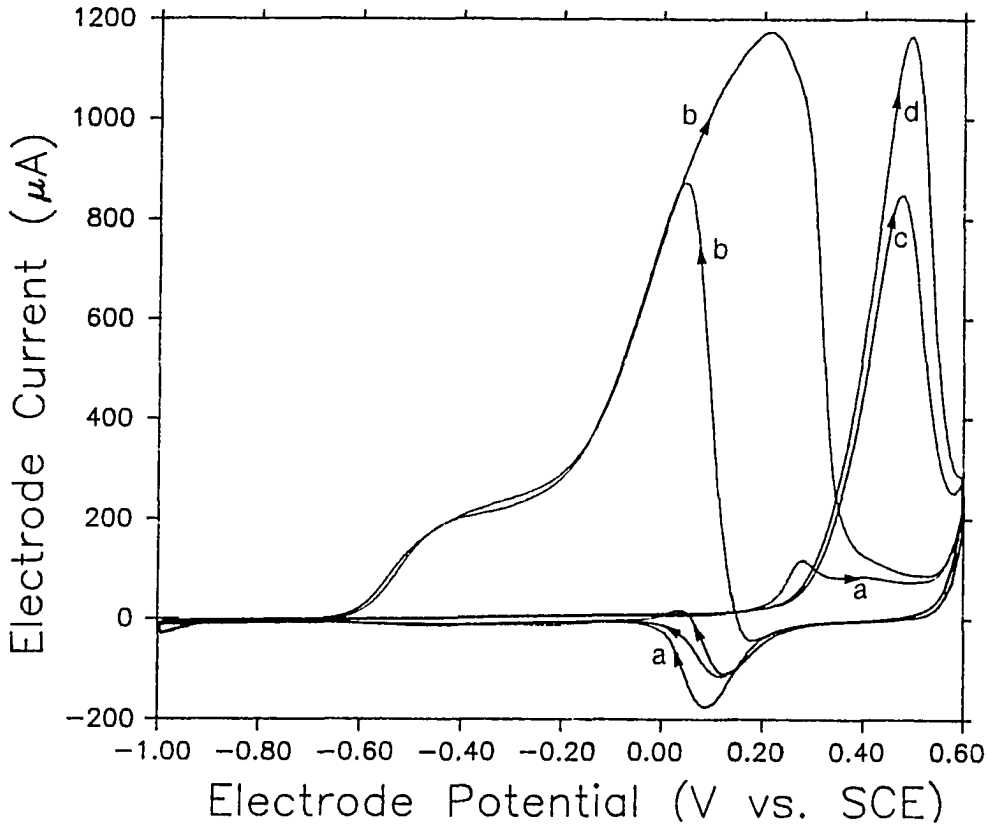

Figure 13. Voltammetric response of glucose as a function of thiosulfate concentration at a Au RDE in alkaline solution.

Conditions: 1600 rev min^{-1}, 5.0 V min^{-1}, O_2 removed.

Curves: (a) residual in 0.1 M NaOH,
(b) 0.50 mM glucose,
(c) 0.50 mM glucose/0.20 mM $S_2O_3^{2-}$,
(d) 0.50 mM glucose/0.40 mM $S_2O_3^{2-}$.

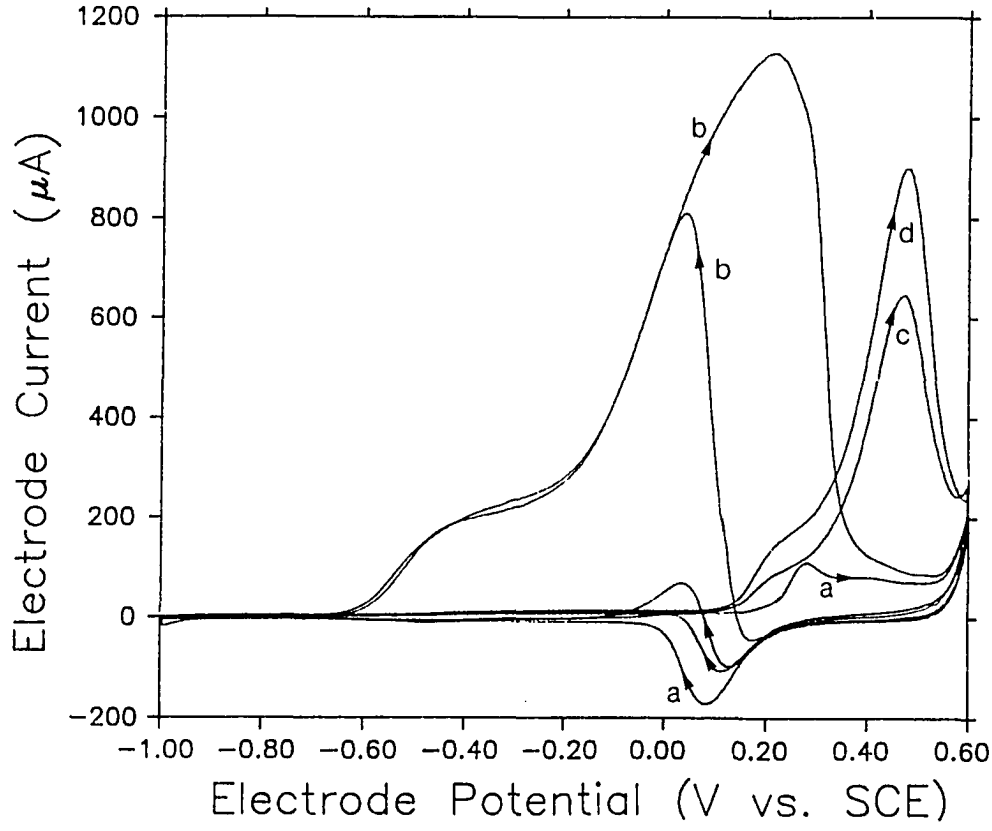

Figure 14. Voltammetric response of glucose as a function of hydrosulfite concentration at a Au RDE in alkaline solution.

Conditions: 1600 rev min^{-1}, 5.0 V min^{-1}, O_2 removed.

Curves: (a) residual in 0.1 M NaOH,
(b) 0.50 mM glucose,
(c) 0.50 mM glucose/0.20 mM $S_2O_4^{2-}$,
(d) 0.50 mM glucose/0.40 mM $S_2O_4^{2-}$.

The next most strongly adsorbed compound appears to be ethylenediamine (EDA). This compound was able to block glucose, glycerol, and formaldehyde from being adsorbed and oxidized. The effect on formaldehyde oxidation is shown in Figure 15. It appears that EDA was more effective than sulfite (Figure 11) in blocking formaldehyde oxidation. The presence of 1.0 mM ethylenediamine (Figure 15, Curve e) nearly eliminated the anodic wave for oxidation of 0.4 mM formaldehyde (Figure 15, Curve b). Voltammetric curves showing the loss of glucose and glycerol response with added EDA are not shown here.

One interesting aspect of these experiments arose when chloride was tested for possible adsorption. The presence of chloride had almost no effect on glucose oxidation on Au. The oxidation of 0.5 mM glucose (Figure 16, Curve b) was virtually uninhibited by 1 mM NaCl (Figure 16, Curve c). The presence of NaCl at 30 times the glucose concentration (15 mM) (Figure 16, Curve e) decreased the peak current by less than 10%. Chloride also did not interfere with sulfite oxidation, indicating it was less strongly adsorbed than any of the analytes chosen. There seems to be a possibility for useful analytical applications of competitive adsorption. For instance glucose can be detected in the presence of chloride. Also, since sulfite blocks almost everything, it may be detectable without separation in a messy sample. Furthermore,

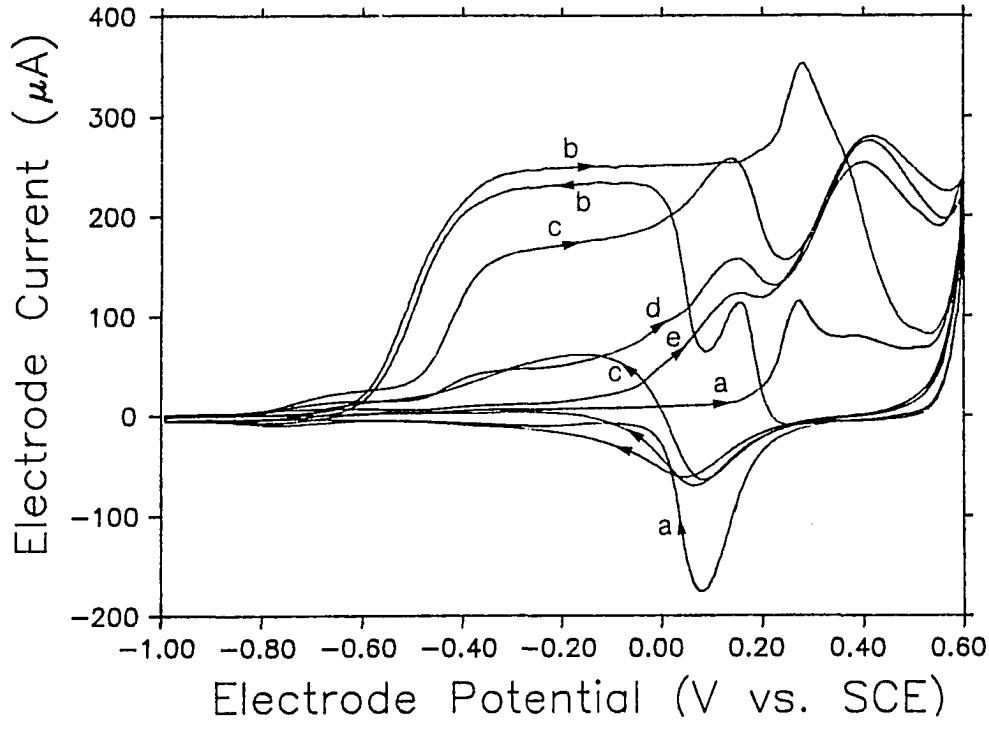

Figure 15. Voltammetric response of formaldehyde as a function of ethylenediamine concentration at a Au RDE in alkaline solution.

Conditions: 900 rev min^{-1}, 5.0 V min^{-1}, O_2 removed.

Curves: (a) residual in 0.1 M NaOH,
(b) 0.40 mM HCHO,
(c) 0.40 mM HCHO/0.20 mM EDA,
(d) 0.40 mM HCHO/0.40 mM EDA,
(e) 0.40 mM HCHO/1.0 mM EDA.

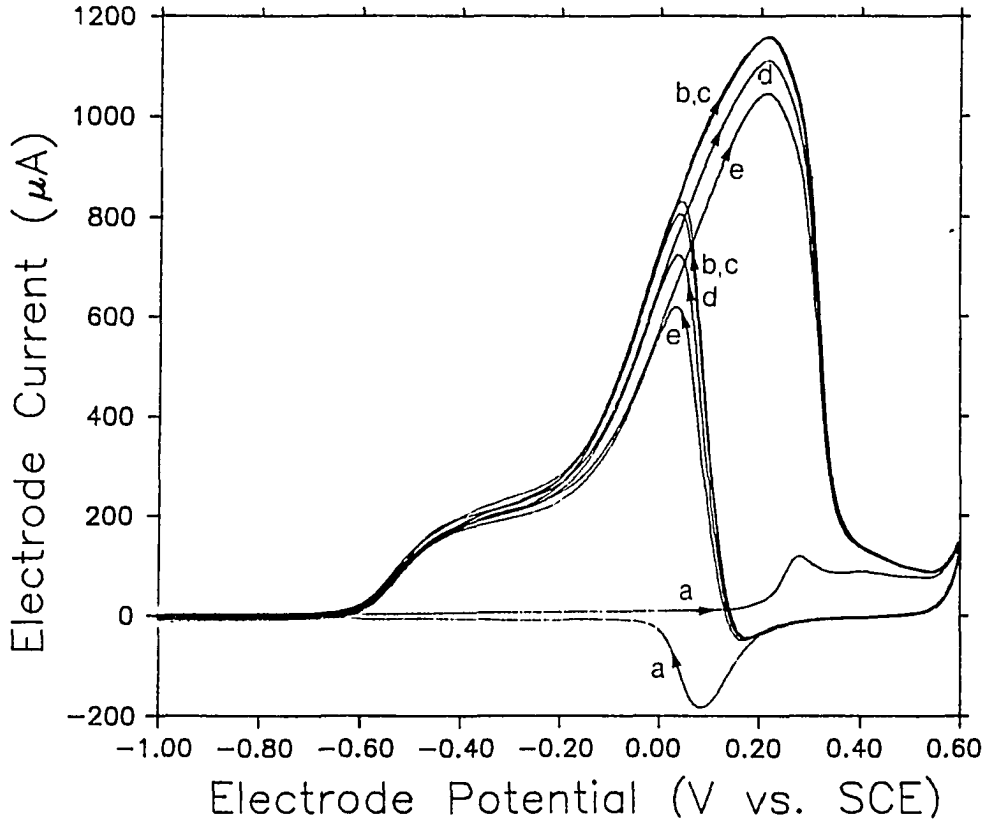

Figure 16. Voltammetric response of glucose as a function of chloride concentration at a Au RDE in alkaline solution.

Conditions: 1600 rev min^{-1}, 5.0 V min^{-1}, O_2 removed.

Curves: (a) residual in 0.1 M NaOH,
(b) 0.50 mM glucose,
(c) 0.50 mM glucose/1.0 mM NaCl,
(d) 0.50 mM glucose/5.0 mM NaCl,
(e) 0.50 mM glucose/15 mM NaCl.

the post-column addition of various surface active (blocking) reagents in liquid chromatography with amperometric detection might aid in making qualitative judgements as to the identity of sample components producing the detection peaks.

Based on these results, an adsorption hierarchy for the functionalities tested is deduced to be that shown below.

$$SO_3^{2-},\ S_2O_3^{2-},\ S_2O_4^{2-} \ >\ EDA \ >\ RCHO,\ ROH$$

strongly adsorbed <————————> weakly adsorbed

Absent from this list are hydrazine, which does not need to be adsorbed to be oxidized, and chloride, which showed no anodic current in 0.1 M NaOH in the potential range used. Although it seems that aldehydes may be more strongly adsorbed than alcohols, they are tentatively put at the same level because the data was somewhat inconclusive. For instance, the voltammogram for formaldehyde and glycerol appeared to be the simple sum of their respective anodic currents, similar to the oxidation of glucose. However, glucose response at high concentrations appeared to be just that of the aldehyde group (17).

CONCLUSIONS

With the exception of hydrazine, all compounds tested are concluded to be oxidized by mechanisms with adsorption as a prerequisite to oxidation. The product of hydrazine oxidation is N_2 both in 0.1 M H_2SO_4 and 0.1 M NaOH. Hence, the hydrazine oxidation does not involve an oxygen-transfer reaction. It is proposed that adsorption is necessary for all compounds whose oxidation is accompanied by the transfer of oxygen via the electrode surface. The oxygen transfer agent at Au electrodes is concluded to be adsorbed hydroxyl radicals (AuOH). In addition to acting as the oxygen transfer agent, the AuOH could enhance the adsorption of these compounds by making the electrode surface more polar. Furthermore, it appears that the oxidation of Au to AuOH follows the same pH dependence as the formation of the phase oxide (AuO). If the $E_{1/2}$ for SO_3^{2-} is used as the earliest evidence of AuOH formation during the positive scan in acidic solution, the potential difference for formation of AuOH at pH 1 and pH 13 is ca. 0.88 V. The difference in $E_{1/2}$ for formation of AuO at pH 1 and pH 13 is ca. 0.84 V (see Table 1).

Simple mechanisms can be devised for these anodic reactions which involve three fundamental processes for the various adsorbed species: i) oxygen transfer between the analyte and adsorbed hydroxyl radical (AuOH), ii) deprotonation and iii) electron transfer. The mechanisms for

the various compounds studied appear to differ only in the order of these three reactions. For the sulfur compounds and nitrite, deprotonation is proposed to follow electron transfer, as indicated by the absence of a dependence of $E_{1/2}$ on solution pH. For the organic compounds, deprotonation precedes electron transfer and a dependence of $E_{1/2}$ on pH is observed.

A simple mechanism for aldehyde oxidations is presented by reactions [1]-[8]. Adsorbed species are denoted by brackets. The first two steps involve formation of the catalytic AuOH (reaction [1]) and adsorption of the aldehyde (reaction [2]). The third step is the oxygen-transfer reaction between adsorbed intermediates (reaction [3]). A deprotonation reaction follows (reaction [4]) succeeded by transfer of the second electron (reaction [5]) and desorption and deprotonation of the product acid (reaction [6]). The electrode is already at a potential positive of the formation of AuOH, so the regeneration of the oxygen-transfer agent is shown in reaction [7]. Two points are important to note about this mechanism. First, the adsorbed hydroxyl radicals ([$^{\bullet}$OH]) could just as easily be written as adsorbed hydroxide with both electrons transferred in a single step (reaction [5]). Also, the deprotonation step (reaction [4]) could occur simultaneously with the oxygen-transfer step. It seems reasonable to propose that the inability to oxidize aldehydes

and alcohols at an appreciable rate, most notably in acidic solution, is not due to the lack of AuOH, but to the slowness of the deprotonation step (reaction [4]). A more complete mechanism for oxidation of the aldehyde portion of glucose has been given (17).

$$OH^- \longrightarrow [\cdot OH] + e \quad [1]$$

$$RCHO \longrightarrow [RCHO] \quad [2]$$

$$[RCHO] + [\cdot OH] \longrightarrow [\cdot RCHOOH] \quad [3]$$

$$[\cdot RCHOOH] + OH^- \longrightarrow [\cdot RCOOH^-] + H_2O \quad [4]$$

$$[\cdot RCOOH^-] \longrightarrow [RCOOH] + e \quad [5]$$

$$OH^- + [RCOOH] \longrightarrow RCOO^- + H_2O \quad [6]$$

$$OH^- \longrightarrow [\cdot OH] + e \quad [7]$$

$$\text{net:} \quad RCHO + 3OH^- \longrightarrow RCOO^- + 2H_2O + 2e \quad [8]$$

A mechanism for the sulfur compounds and nitrite can be devised in a similar manner to that above, as illustrated for sulfite in alkaline solutions by reactions [9]-[15]. The

$$OH^- \longrightarrow [\cdot OH] + e \quad [9]$$

$$SO_3^{2-} \longrightarrow [SO_3^{2-}] \quad [10]$$

$$[SO_3^{2-}] + [\cdot OH] \longrightarrow [\cdot HSO_4^{2-}] \quad [11]$$

$$[\cdot HSO_4^{2-}] \longrightarrow [HSO_4^-] + e \quad [12]$$

$$[HSO_4^-] + OH^- \longrightarrow SO_4^{2-} + H_2O \quad [13]$$

$$OH^- \longrightarrow [\cdot OH] + e \quad [14]$$

$$\text{net:} \quad SO_3^{2-} + 2OH^- \longrightarrow SO_4^{2-} + H_2O + 2e \quad [15]$$

three steps (reactions [9]-[11]) are identical to those for aldehydes (reactions [1]-[3]). The electron transfer step follows (reaction [12]). The next step is desorption and deprotonation of sulfate. Similarly to the mechanism given for aldehydes, regeneration of the catalytic AuOH is shown as the final step (reaction [14]). The formation of the catalytic AuOH is written as the first and last step of the mechanism to stress that the pH dependence of the formation of AuOH does not determine the pH dependence of the oxidation of the analyte. The potential at which AuOH is formed only determines the lowest value of applied potential at which these oxygen-transfer oxidations can occur. The $E_{1/2}$ of a compound probably also depends upon how strongly it is adsorbed at Au. It is well known that a strongly adsorbed compound can inhibit the formation of the phase oxide, so it is reasonable to expect that the formation of AuOH could also be blocked by a strongly adsorbed compound. Note that the more strongly adsorbed compounds also have more positive values of $E_{1/2}$. An analogous mechanism can be written for acidic solutions if solution OH^- in (Rxns. [9], [13] and [14]) is replaced with H_2O, and H^+ written as a product in these steps. Also, sulfite is protonated in acidic solution and adsorption involves HSO_3^- and the adsorbed radical is proposed to be [$^{\cdot}H_2SO_4^-$]. This mechanism successfully accounts for the lack of pH dependence in these oxidation reactions.

ACKNOWLEDGMENT

This work was supported by the National Science Foundation through contract CHE-8612314.

REFERENCES

1. Capon, A.; Parsons, R. J. Electroanal. Chem., 1973, 44, 239-254.
2. Bagotzky, V. S.; Vasilyev, Yu. B. Electrochim. Acta, 1964, 9, 869-882.
3. Bagotzky, V. S.; Vassilyev, Yu. B. Electrochim. Acta, 1967, 12, 1323-1343.
4. Snell, K. D.; Keenan, A. G. Electrochim. Acta, 1981, 26, 1339-1344.
5. Vijh, A. K. Can. J. Chem., 1971, 49, 78-88.
6. Sibille, S.; Moiroux, J.; Marot, J. C.; Deycard, S. J. Electroanal. Chem., 1978, 88, 105-121.
7. Cabelka, T. D.; Austin, D. S.; Johnson, D. C. J. Electrochem. Soc., 1984, 131, 1595-1602.
8. Cabelka, T. D.; Austin, D. S.; Johnson, D. C. J. Electrochem. Soc., 1985, 132, 359-364.
9. Adzic, R. R.; Avramov-Ivic, M. J. of Catalysis, 1986, 101, 532-535.
10. Cabelka, T. D. Ph.D. Dissertation, Iowa State University, 1984.
11. Beden, B.; Cetin, I.; Kahyaoglu, A.; Takky, D.; Lamy, C. J. of Catalysis, 1987, 104, 37-46.
12. Nguyen Van Huong, G.; Hinnen, C.; LeCoeur, J. J. Electroanal. Chem., 1980, 106, 185-191.

13. Bruckenstein, S.; Shay, M. J. Electroanal. Chem., 1985, 188, 131-136.

14. Angerstein-Kozlowska, H.; Conway, B. E.; Barnett, B.; Mozota, J. J. Electroanal. Chem., 1979, 100, 417-446.

15. Angerstein-Kozlowska, H.; Conway, B. E.; Hamelin, A.; Stoicoviciu, L. J. Electroanal. Chem., 1987, 228, 429-453.

16. Angerstein-Kozlowska, H.; Conway, B. E.; Hamelin, A.; Stoicoviciu, L. Electrochim. Acta, 1986, 31, 1051-1061.

17. Larew, L. A.; Johnson, D. C. J. Electroanal. Chem., 1989, 262, 167-182.

18. Koile, R. C.; Johnson, D. C. Anal. Chem., 1979, 51, 741-744.

19. Ocon, P.; Alonso, C.; Celdran, R.; Gonzalez-Velasco, J. J. Electroanal. Chem., 1986, 206, 179-196.

20. Clark, W. M. Oxidation-Reduction Potentials of Organic Systems; The Williams & Wilkins Company: Baltimore, MD, 1960; p 511.

21. Milazzo, G.; Caroli, S. Tables of Standard Electrode Potentials; Wiley: New York, NY, 1978.

SECTION III.

THE EFFECT OF ELECTRODE MATERIAL ON THE ELECTROGENERATED CHEMILUMINESCENCE OF LUMINOL[1]

---

[1] published in Vitt, J. E.; Johnson, D. C.; Engstrom, R. C. J. Electrochem. Soc., 1991, 138, 1637-1643.

ABSTRACT

The oxidation of luminol and its concomitant electrogenerated chemiluminescence (ECL) were studied at several electrode materials by voltammetry and chronoamperometry. The ECL intensity (I_{ECL}) was inversely related to the activity of the electrodes. The lowest I_{ECL} was measured when luminol was oxidized to 3-aminophthalate ($n \simeq 4$ eq mol^{-1}) at a nearly mass-transport limited rate at glassy carbon. The ECL kinetics were studied and the order of the reaction with respect to luminol was 3/2 at concentrations to ca. 1 mM when O_2 was the co-reactant. In the presence of H_2O_2, the ECL reaction was first order with respect to luminol. A reaction mechanism is proposed that is consistent with the kinetic data and the inverse relationship between electrode activity and I_{ECL}. The implications of these results are discussed with respect to imaging the spatial distribution of current density at electrode surfaces, including that of PbO_2-films activated by adsorbed Bi(V). A value of 6.6×10^{-6} cm^2 sec^{-1} was determined for the diffusion coefficient of luminol in 0.1 M NaOH.

INTRODUCTION

Electrodes formed by doping PbO_2 with various cationic and anionic species have been shown to be useful for the electrocatalysis of numerous anodic, oxygen-transfer reactions in aqueous solutions (1-5). It has been proposed that electrocatalysis occurs at specific sites that are characterized by a lower overpotential for O_2 evolution than that corresponding to the average electrode surface (2). Various oxygen-transfer reactions are believed to be coupled to the O_2 evolution reaction by a common intermediate product, adsorbed hydroxyl radicals ($^{\cdot}OH_{ads}$). If doped PbO_2 electrodes consist of active sites (dopant) in a less active matrix (PbO_2), the surface is expected to exhibit nonuniform current density during electrolysis. We are seeking means whereby the spatial heterogeneity can be determined.

Recently, the electrogenerated chemiluminescence (ECL) of luminol has been used to image spatial differences in current density across electrode surfaces. The high current density at the edge of a planar disk electrode, which results from non-linear diffusion, was directly observed using ECL (6). Also, nonuniform current density was observed for composite electrodes, e.g., an epoxy-impregnated reticulated vitreous carbon electrode and a carbon paste electrode (7). These composite electrodes represent heterogeneous surfaces because an electrochemically active (conductive) material has been

mixed with an inert (nonconductive) binder. Luminol ECL also has been used to image the kinetic heterogeneity of highly ordered pyrolytic graphite (HOPG) modified by electrochemical pretreatment or mechanical scratching (8).

Electrodes formed by electrodeposition of doped PbO_2 films also are considered to have kinetically heterogeneous surfaces. Direct evidence is sought for the expected non-uniform surface coverage by a labile oxygen species (i.e., $\cdot OH_{ads}$) available for participation in oxygen-transfer reactions. At a Bi-doped PbO_2 electrode, we expected evidence for labile oxygen linked to Bi sites. Electrodes formed by anodic adsorption of Bi(III) as Bi(V) on pure PbO_2 are catalytically active for many oxygen-transfer reactions in a manner similar to Bi-doped PbO_2 (9). The advantage of Bi-adsorbed PbO_2 electrodes is that they can be formed in-situ. Here, the ECL imaging technique is described for examination of the kinetic heterogeneity of a PbO_2-film electrode activated by adsorbed Bi(V). However, evidence of active sites linked to adsorbed Bi(V) was inconclusive because of the complex nature of the ECL reaction.

The ECL reaction results when the monobasic anion of luminol (LH^-, $pK_{a,1} = 6.2$) (10), is oxidized in the presence of O_2 or H_2O_2 in alkaline solutions. The chemiluminescence has been shown to result from the reaction of the radical product of the one-electron oxidation of LH^- ($L\cdot^-$) with the

superoxide radical ion ($O_2^{\cdot -}$) (11). The product of this reaction is 3-aminophthalate (AP^{-2}) which has been identified as the photon-emitting species (12, 13). The structures of LH^-, $L^{\cdot -}$, and AP^{-2} are shown below.

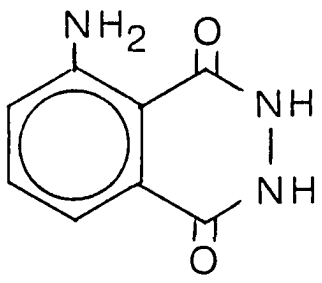

LH_2

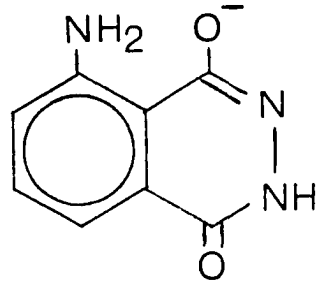

LH^-

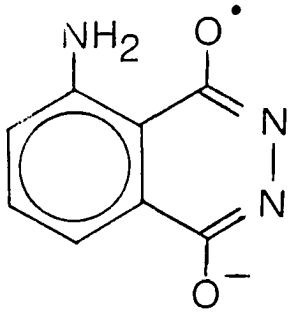

$L^{\cdot -}$

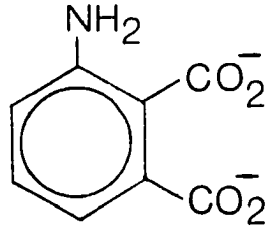

AP^{-2}

It has been a general assumption in applications of the ECL imaging technique that the bright spots observed by visual microscopy correspond to the most active sites on the electrode surfaces. However, in preliminary experiments it was observed that electrodes producing the largest anodic current for luminol yielded the smallest ECL intensity (I_{ECL}). Hence, it was deemed necessary to make a more fundamental study of the oxidation of luminol and its resulting chemiluminescence at various electrode materials. It will be shown for the electrodes examined that the chemiluminescent intensity was inversely related to electrochemical activity for oxidation of luminol, as defined by the product of n (eq mol^{-1}) and k_{app} (cm sec^{-1}) (2). A reaction mechanism is presented which is in agreement with experimental data.

EXPERIMENTAL

Equipment. The electrochemical system for operation of rotated disk and ring-disk electrodes consisted of an RDE4 potentiostat and an ASR rotator (Pine Instrument Co.). The ECL intensities were measured with the detector from a Model 100-10 spectrophotometer (Hitachi). The photomultiplier was positioned with its window facing upward and the electrochemical cell was placed directly on this opening. The electrode surface was positioned less than 1 cm from the opening to the detector. The electrochemical cell was made of Pyrex with porous glass disks separating the working, reference, and counter electrode compartments. The bottom of the cell was flat to minimize dispersion of light from the ECL process. Data were recorded using a Model 100 X-Y recorder (Houston Instruments Co.), a Model 7133A strip-chart recorder (Hewlett Packard), or an interface with an IBM PC. The interface consisted of a DAS-8PGA data acquisition board (MetraByte Corp.) and ASYST-2.0 software (ASYST Software Technologies). The ECL imaging system has been described (8).

Electrodes. The reference electrode was a saturated calomel electrode (SCE) and all electrode potentials are reported vs. the SCE. The counter electrode was a coiled Pt wire (ca. 7.6 cm^2). Rotated ring-disk electrodes (RRDE) were Model AFDT (R_1 = 0.383 cm, R_2 = 0.398 cm, R_3 = 0.422 cm; Pine Instrument Co.). Electrode materials were Au, Pt, Pd, and

glassy carbon (GC). A GC rotated disk electrode (RDE; 0.196 cm^2) was used in the determination of values for n (eq mol^{-1}) and D (cm^2 sec^{-1}). PbO_2-film electrodes were electrodeposited on the disk of the Au RRDE at 400 rev min^{-1} from 0.1M HNO_3 containing 20 mM Pb^{+2} dissolved from $Pb(NO_3)_2$. Prior to deposition, the Au disk potential was cycled for 10 min from 1.7 V to -0.2 V (5 V min^{-1}). The potential was then set at 1.5 V for 15 min for deposition of the PbO_2 films. The Bi-doped PbO_2 (Bi-PbO_2) electrodes were prepared in the same manner from solutions containing 0.2 mM Bi^{+3}, as $Bi(NO_3)_3$, with 20 mM Pb^{+2} in 0.1 M HNO_3. The resulting film contained 1% Bi (mol/mol) (1).

Reagents. Luminol (5-amino-2,3-dihydro-1,4-phthalazinedione) was obtained from Aldrich Chemical Co. or Eastman Kodak. 3-Aminophthalic acid hydrochloride was from Pfaltz & Bauer. The $Pb(NO_3)_2$ was from Fisher Scientific Co. and $Bi(NO_3)_3$ was from Alfa Products. Solutions of H_2O_2 were prepared fresh daily from a 30% stock solution (Mallinckrodt). Water was purified in a Milli-Q system (Millipore) after passing through two D-45 deionizing tanks (Culligan). Compressed mixtures of O_2 in N_2 were from Matheson.

Procedures. Voltammetric (i-E) and chronoamperometric (i-t) data were obtained at ambient room temperature (23 $\pm$ 2 C). With the exception of PbO_2 and Bi-PbO_2 films, electrodes were polished with 0.05-um alumina in H_2O on microcloth

(Buehler Ltd.), and then rinsed with deionized H_2O. The electrode potential was then cycled in supporting electrolyte between values for onset of O_2 and H_2 evolution until the residual i-E curves were reproducible.

The photometric detector was not calibrated and, therefore, the output (mV), corresponding to the intensity of the ECL process (I_{ECL}) is arbitrary. However, the configuration of the detector remained constant and values of I_{ECL} can be intercompared.

RESULTS AND DISCUSSION

ECL of luminol in the presence of O_2. Recent studies of the mechanism of LH^- ECL involved oxidation of H_2O_2 to produce $O_2^{\cdot -}$ (14, 15). However, the electrode current from oxidation of LH^- could not be measured separately from the concomitant current for H_2O_2 oxidation. Hence, the ECL reaction was studied here in the presence of O_2 rather than H_2O_2 to permit measurement of I_{ECL} as a function of the current resulting solely from LH^- oxidation.

Shown in Figure 1 is the cyclic voltammogram (i-E) for 0.39 mM LH^- (Curve b) at the disk of the Au RRDE in air-saturated 0.1 M NaOH, in comparison to the residual response (Curve a). An anodic wave with $E_{1/2}$ = ca. 0.22 V was obtained for the oxidation of LH^- on the positive potential scan simultaneously with formation of surface oxide. For the subsequent negative scan at the oxide-covered electrode, the LH^- oxidation ceased for E >> 0.22 V. On the negative scan, the $E_{1/2}$ for O_2 reduction was shifted from -0.17 V to -0.38 V by the presence of LH^-. Furthermore, the limiting current for O_2 was decreased slightly. Both effects are thought to be the result of LH^- adsorption.

The ECL intensity (I_{ECL}) was measured as a function of potential concurrently with electrode current and the results are shown in Figure 2A. The $E_{1/2}$ of the first I_{ECL} peak at 0.22V during the positive scan was identical to that of the

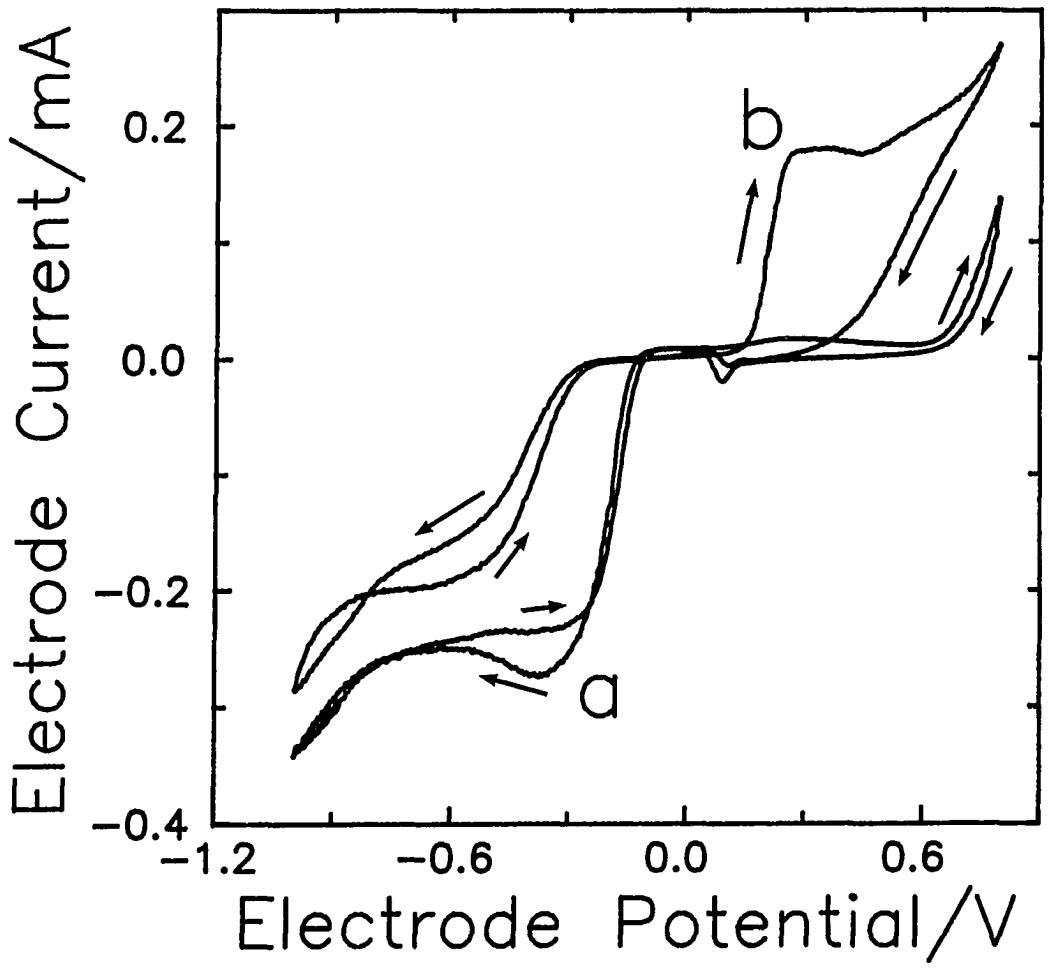

Figure 1. Voltammetric response of luminol at a Au RDE in alkaline solution.

Conditions: 0.1 M NaOH, 5 mV sec^{-1}, 900 rev min^{-1} (94.2 rad sec^{-1}), air saturated.

Curves: (a) residual response,
(b) 0.39 mM luminol

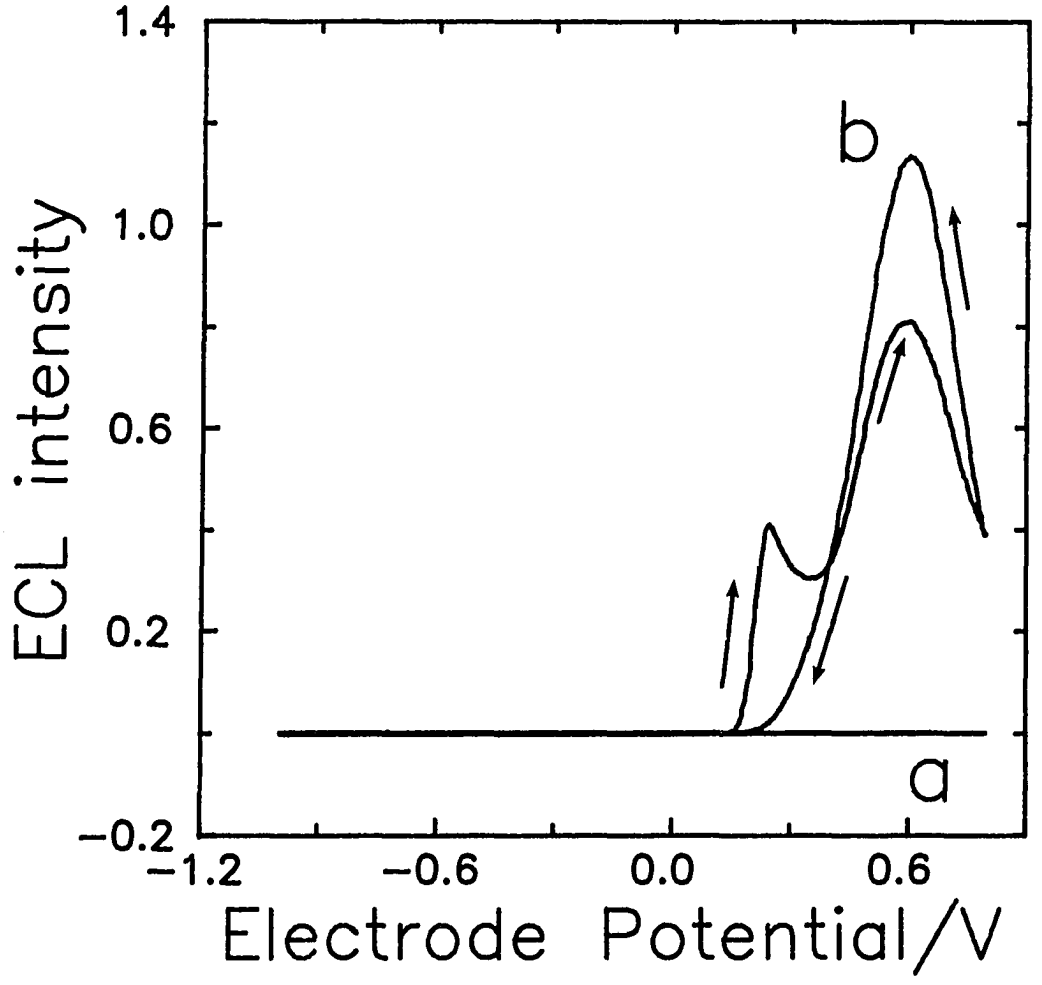

Figure 2A. ECL intensity as a function of electrode potential at a Au RDE in alkaline solution.

Conditions: same as Figure 1.

Curves: (a) residual response,
(b) 0.39 mM luminol

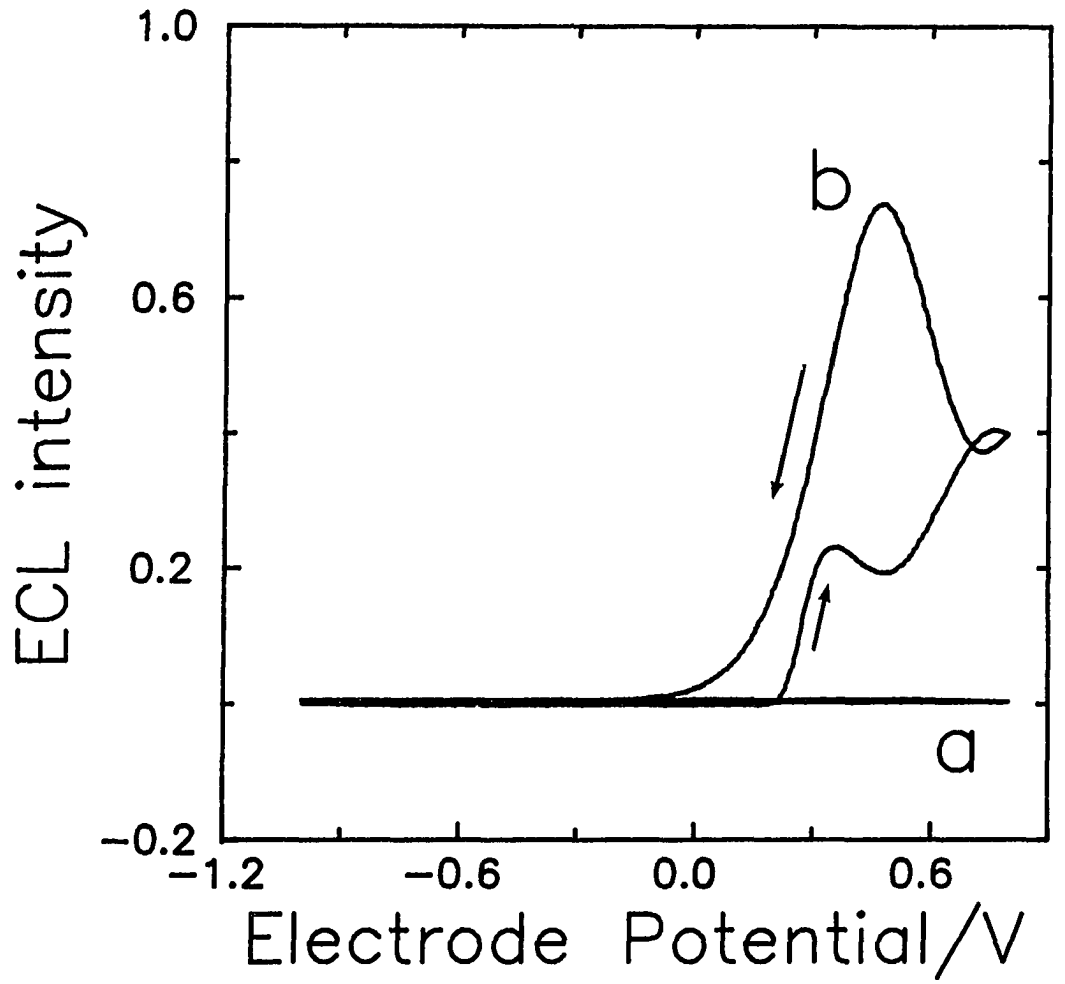

Figure 2B. ECL intensity as a function of electrode potential at a Au RDE in alkaline solution.

Conditions: 0.1 M NaOH, 900 rev min^{-1}, 200 mV sec^{-1}, air saturated.

Curves: (a) residual response,
(b) 0.39 mM luminol

first peak in the i-E curve (Fig. 1). A second, larger I_{ECL} peak was obtained on the positive scan with E_{peak} of ca. 0.6 V. During the negative scan, the E_{peak} for I_{ECL} was again 0.6 V; however, an I_{ECL} peak was absent at the less positive potentials. When ECL data were obtained by stepping the potential from 0.0 V to constant values in the range 0.0 to 0.8V, the shape of I_{ECL}-E data was identical to that obtained voltammetrically during the negative scan (Figure 2A). We conclude that the initial I_{ECL}-E peak on the positive scan was the result of a transient surface activity caused by formation of surface oxide and is not characteristic of the electrode process at constant potential on the oxide covered surface. At a faster scan rate of 200 mV sec^{-1} (Fig. 2B), the $E_{1/2}$ of the first I_{ECL} peak on the positive scan was shifted from 0.22 V to 0.28 V and E_{peak} on the negative scan was shifted from 0.6 V to 0.45 V.

Because both the anodic current and I_{ECL} were dependent on potential scan rate, subsequent measurements were obtained by stepping the potential from 0.0 V to a constant value of 0.55 V. Representative plots of current and I_{ECL} are shown in Figure 3 as a function of time. After the potential step at 5 sec, the anodic current (Curve a) increased quickly and then decayed to a constant value that increased for larger values of LH^- concentration and electrode rotation speed. At 30 sec, the potential was stepped back to 0.0 V, and after a cathodic

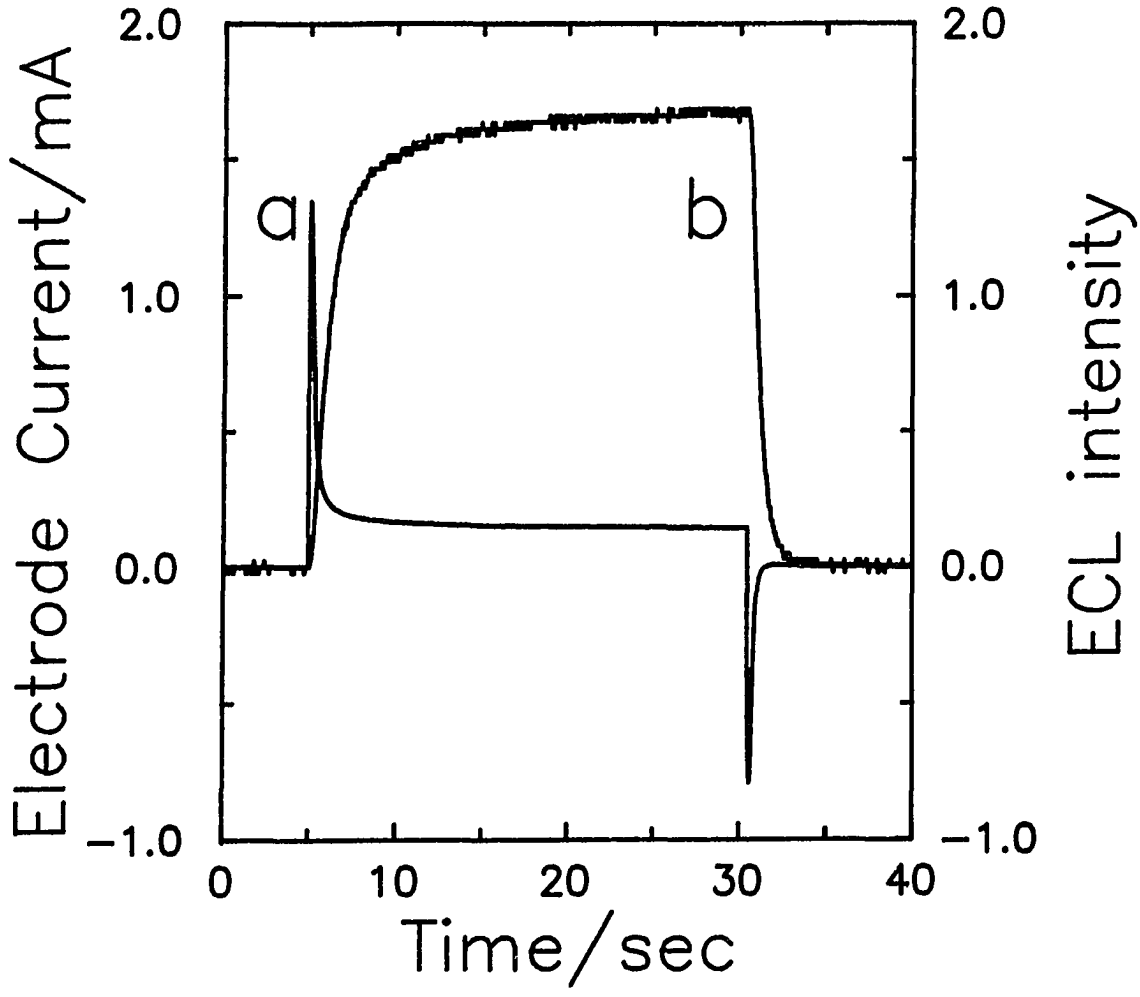

Figure 3. Electrode current and ECL intensity as a function of time after a potential step from 0.0 V to 0.55 V and then back to 0.0 V.

Conditions: 900 rev min^{-1}, 0.1 M NaOH, air saturated, 0.39mM luminol.

Curves: (a) Electrode current
(b) ECL intensity

current spike occurred for reduction of surface oxide, the current quickly decayed to a zero value. The value of I_{ECL} rose slowly to a constant value after the potential step to 0.55 V. When the potential was returned to 0.0 V, I_{ECL} decayed to zero in about 2-3 sec. The delay in onset of I_{ECL} as compared to the anodic current is consistent with a slow build-up of the intermediate products of the chemiluminescent process in the solution adjacent to the electrode.

Chemiluminescence resulted from the reaction of $L^{\cdot -}$ with $O_2^{\cdot -}$, for this case, and the $O_2^{\cdot -}$ was the product of reaction between $L^{\cdot -}$ and O_2 (16). Hence, a delay in production of light should be expected following initiation of oxidation of LH^-. A delay in onset of I_{ECL} with respect to the anodic current was less severe when the anodic oxidation of H_2O_2 was the source of $O_2^{\cdot -}$. In that case, the $O_2^{\cdot -}$ was produced directly at the electrode surface, and the concentration of $O_2^{\cdot -}$ quickly increased to a steady-state value that depended only on the electrode reaction. The chemiluminescence continued for a brief time after LH^- oxidation ceased whether O_2 or H_2O_2 was the source of $O_2^{\cdot -}$.

The O_2 concentration near the electrode surface was monitored by cathodic detection at the ring electrode of the Au RRDE to confirm that O_2 was consumed by the ECL reaction. The cathodic current for O_2 reduction as a function of time (Figure 4) was measured concurrently with the anodic current

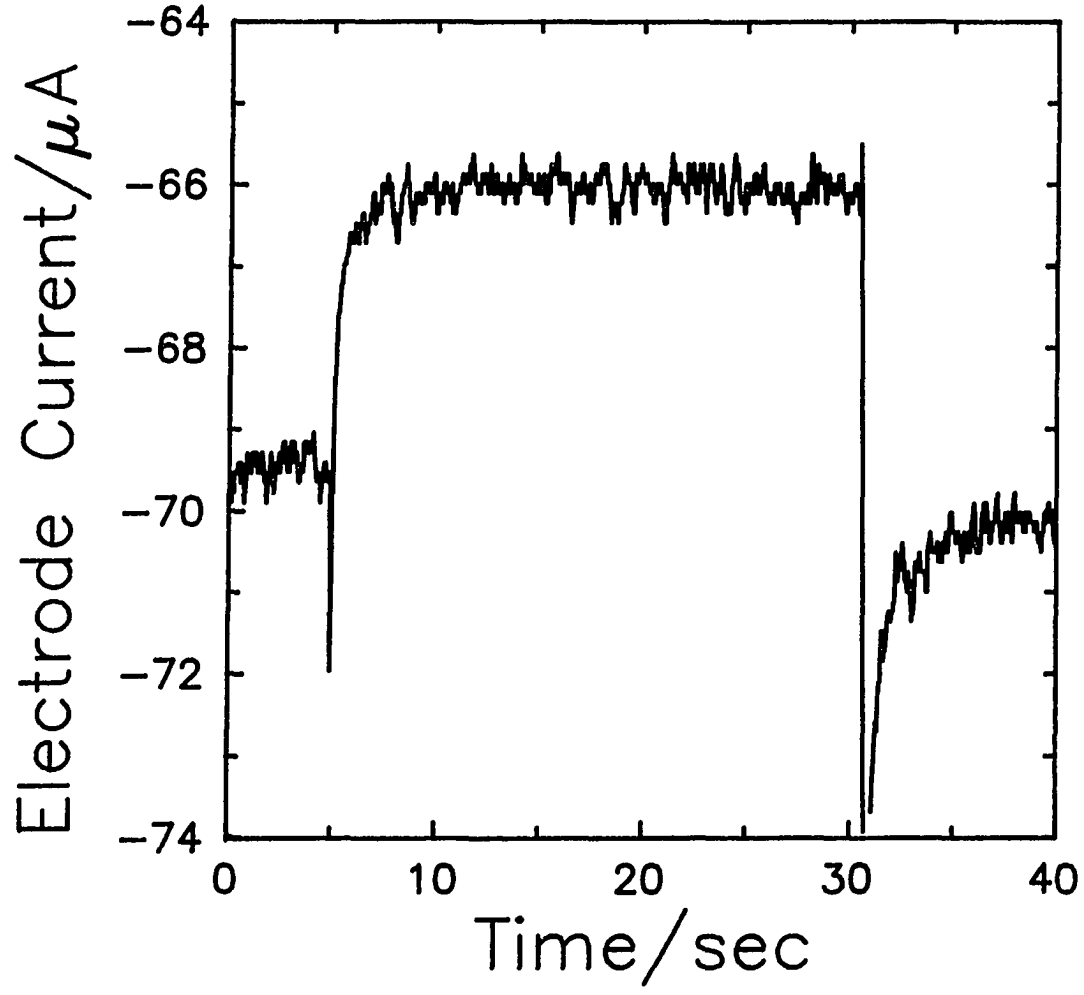

Figure 4. Electrode current for the Au ring electrode held at -0.8V as a function of time when the disk potential was stepped from 0.0 V to 0.55 V and then back to 0.0 V.

Conditions: same as Figure 3.

at the disk and I_{ECL}. When the potential of the disk electrode was stepped to 0.55 V to oxidize LH^-, the cathodic current decreased by ca. 5% (upward shift in Figure 4), which corresponded to a 5% decrease in O_2 concentration in the reaction layer. The consumption of O_2 is consistent with the reaction of $L^{\cdot -}$ with O_2 to produce the $O_2^{\cdot -}$ necessary for the chemiluminescent reaction.

Determination of n and D for luminol. The net electrochemical reaction often can be elucidated by determining the number of electrons transferred (n). The Koutecky-Levich equation (Eq. [1]) can be used to calculate the value of n in an electrochemical reaction under mixed control by kinetic and mass-transport processes at a rotated disk electrode, provided the value of the diffusion coefficient (D) is known (17).

$$\frac{1}{i} = \frac{1}{nFAk_{app}C^b} + \frac{1}{\underline{c}nFAD^{2/3}v^{-1/6}C^b w^{1/2}} \qquad [1]$$

$$\underline{c} = 0.554/(0.8934 + 0.316(D/v)^{0.36})$$

In Eq. [1], w is the rotational velocity of the electrode (rad sec^{-1}), k_{app} is an apparent rate constant (cm sec^{-1}), C^b is the bulk analyte concentration (moles cm^{-3}), v is the kinematic viscosity (cm^2 sec^{-1}), and the other terms have their usual electrochemical significance. This treatment assumes that n electrons are transferred in a single step, and

therefore k_{app} includes contributions from the rate constants for all steps involved in the transfer of n electrons. Thus, n and k_{app} can vary simultaneously, with n equal to an integer value corresponding to the net electrochemical reaction (n_{net}) only when k_{app} is very large. Conversely, for small values of k_{app}, non-integral values for $n < n_{net}$ can be expected. Epstein and Kuwana (18) assumed the value n = 3 eq mol^{-1} and calculated a value of $D = 3.0 \times 10^{-6}$ cm^2 sec^{-1} for luminol in 0.1 M NaOH. Haapakka and Kankare (15) used this value for D to analyze i^{-1}-$w^{-1/2}$ data and they calculated n = 4 eq mol^{-1} for the anodic process. Clearly, an independent determination of both n and D is needed. These values can be determined by combining the results of two independent electroanalytical measurements that depend on n and D. This strategy has been suggested by Pratt (19) to determine diffusion layer thicknesses at hydrodynamic electrodes by combining the results of a hydrodynamic experiment (e.g., rotated disk) with potential-step chronoamperometry or chronocoulometry at the stationary disk electrode in quiescent solution. When the potential of a stationary disk electrode is stepped from a value where no reaction occurs to a value where the reaction is diffusion-limited, the chronoamperometric response is predicted by the familiar Cottrell equation (Eq. [2]). Integration of this equation gives the chronocoulometric response (Eq. [3]).

$$i = nFAD^{1/2}C^{b}\pi^{-1/2}t^{-1/2} \quad [2]$$

$$Q = 2nFAD^{1/2}C^{b}\pi^{-1/2}t^{1/2} \quad [3]$$

The above method was extended to the determination of n and D for luminol. Data were plotted according to Eq. [1] and Eq. [3] and analyzed by the linear regression technique. The GC disk electrode was used for this determination because glassy carbon was determined to be the most electrochemically active material for the oxidation of LH^-. Data for both the rotated disk and stationary disk were obtained for the same solution of 1.0 mM LH^- in 0.1 M NaOH by stepping the potential from 0.0 V to 0.55 V. From five measurements at the rotated and stationary electrode, the value of n was determined to be 3.91 ± 0.11 eq mol^{-1} and D was $6.6 \pm 0.6 \times 10^{-6}$ cm^2 sec^{-1}. The uncertainties shown represent standard deviations. A value of n = 4 eq mol^{-1} corresponds to the oxidation of LH^- to AP^{-2}. No anodic current was obtained for 0.4 mM AP^{-2} in 0.1 M NaOH at the GC electrode between -1.0 V and 0.6 V, indicating that an upper limit of n = 4 eq mol^{-1} was reasonable for LH^-. The D value determined for LH^- (MW = 177) also seemed reasonable by comparison with the value 5.9×10^{-6} cm^2 sec^{-1} reported for glucose (MW = 180) having a similar size (20).

ECL as function of electrode material. The anodic current for LH^- and the resulting I_{ECL} were measured as a function of rotation rate for Au and GC electrodes, and for

pure PbO_2 and 1% (mol/mol) Bi-doped film electrodes. The experiments were performed by stepping the potential from 0.0 V to 0.55 V, as shown in Figure 3 for the Au RDE. For PbO_2 and Bi-PbO_2, however, the potential was stepped from ca. 0.15 V to 0.55 V to prevent cathodic stripping of PbO_2 at more negative potentials. The results of these experiments are plotted according to Eq. [1] in Figure 5. Larger values of the y-intercept in Figure 5 indicate lower values of k_{app} for LH^- oxidation, and a zero intercept indicates totally mass-transport limited oxidation. Larger values of slope correspond to smaller values of n. Glassy carbon (Curve d) was the most active electrode material for the oxidation of LH^- and Au (Curve a) was the least active. The Bi-PbO_2 electrode (Curve c) was ca. 1.5 times more active for the oxygen-transfer oxidation of LH^- to AP^{-2} than the pure PbO_2 electrode (Curve b).

Values calculated for n and k_{app} for the various electrode materials are listed in Table 1. Nonintegral values of $n < 4$ eq mol^{-1} indicate that the corresponding reactions are of the ece... type and that intermediate products can escape the electrode surface without being oxidized completely to AP^{-2}. Thus, as k_{app} decreased, a smaller value of n generally was observed. Conversely, for the nearly mass-transport limited oxidation observed at GC (large k_{app}), n was virtually 4 eq mol^{-1}. When the number of electrons

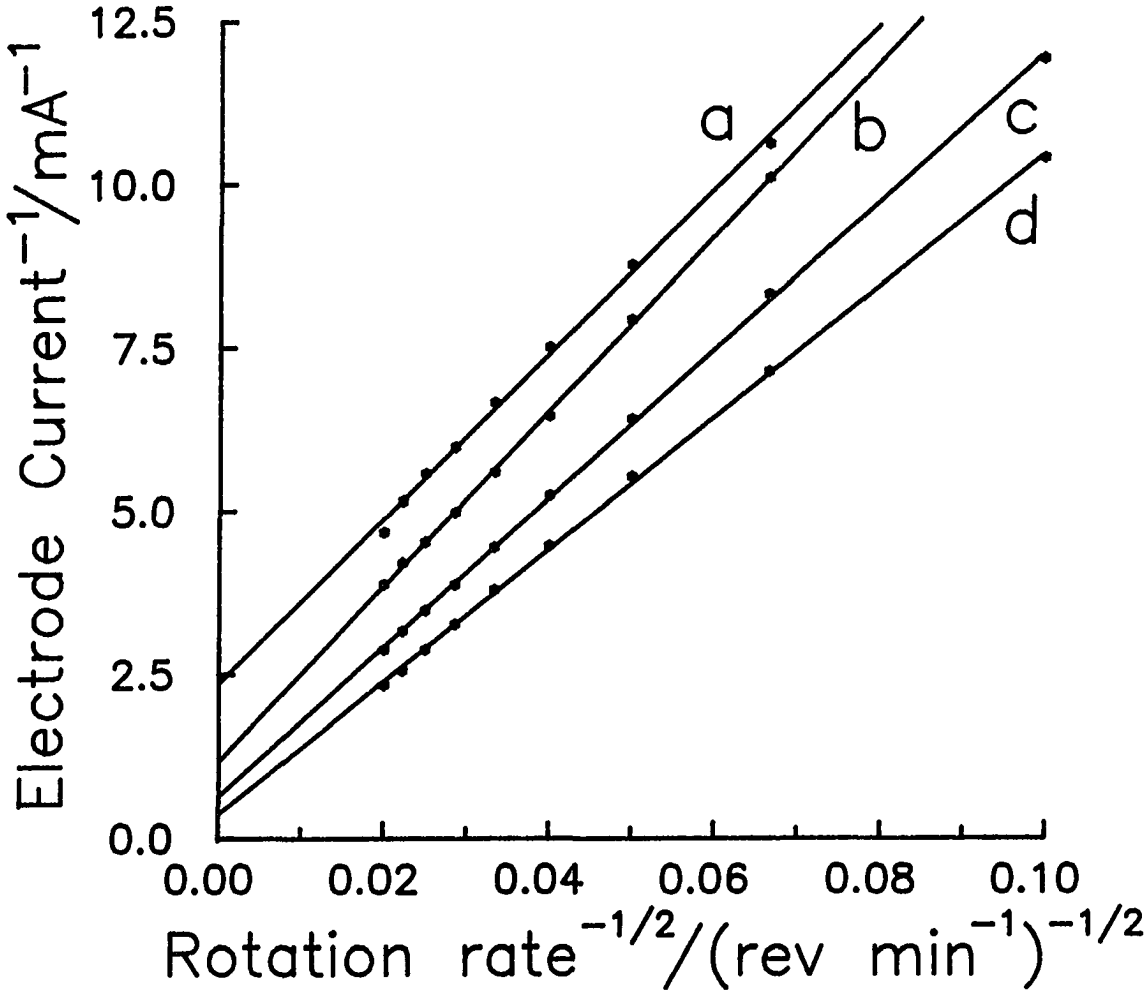

Figure 5. Electrode current^{-1} as a function of rotation rate$^{-1/2}$.

Conditions: 0.1 M NaOH, 0.55 V, air saturated, 0.39 mM luminol

Curves: (a) Au, (b) PbO_2, (c) 1% Bi-doped PbO_2, (d) glassy carbon.

Table 1. Values of n, k_{app}, and slope of I_{ECL}-$w^{1/2}$ plots for various electrode materials.

electrode material	n (eq mol^{-1})	k_{app} (cm sec^{-1})	slope [a] ($\partial I_{ECL}/\partial w^{1/2}$)
Au	3.10	0.0079	0.047
PbO_2	2.92	0.017	0.046
Bi-doped PbO_2 (Bi/Pb = 0.01)	3.44	0.026	0.031
GC	3.87	0.041	0.008
Pt	3.18	0.027	0.036
Pd	3.54	0.017	0.057

[a] From plots as shown in Fig. 6.

transferred is observed to vary in this manner, the product of n and k_{app} can be considered as being a good indication of overall electrode activity (2).

The plots of I_{ECL} as a function of $w^{1/2}$ for these electrodes are shown in Figure 6. Ranking the electrode materials in order of decreasing I_{ECL} gave Au > PbO_2 > Bi-PbO_2 > GC, which was just the opposite of the order for electrode activity. The slopes of the I_{ECL}-$w^{1/2}$ plots in the linear region at low values are shown as a function of nk_{app} in Figure 7. The I_{ECL} was observed to be inversely related to electrode activity (nk_{app}) under these conditions. It is clear

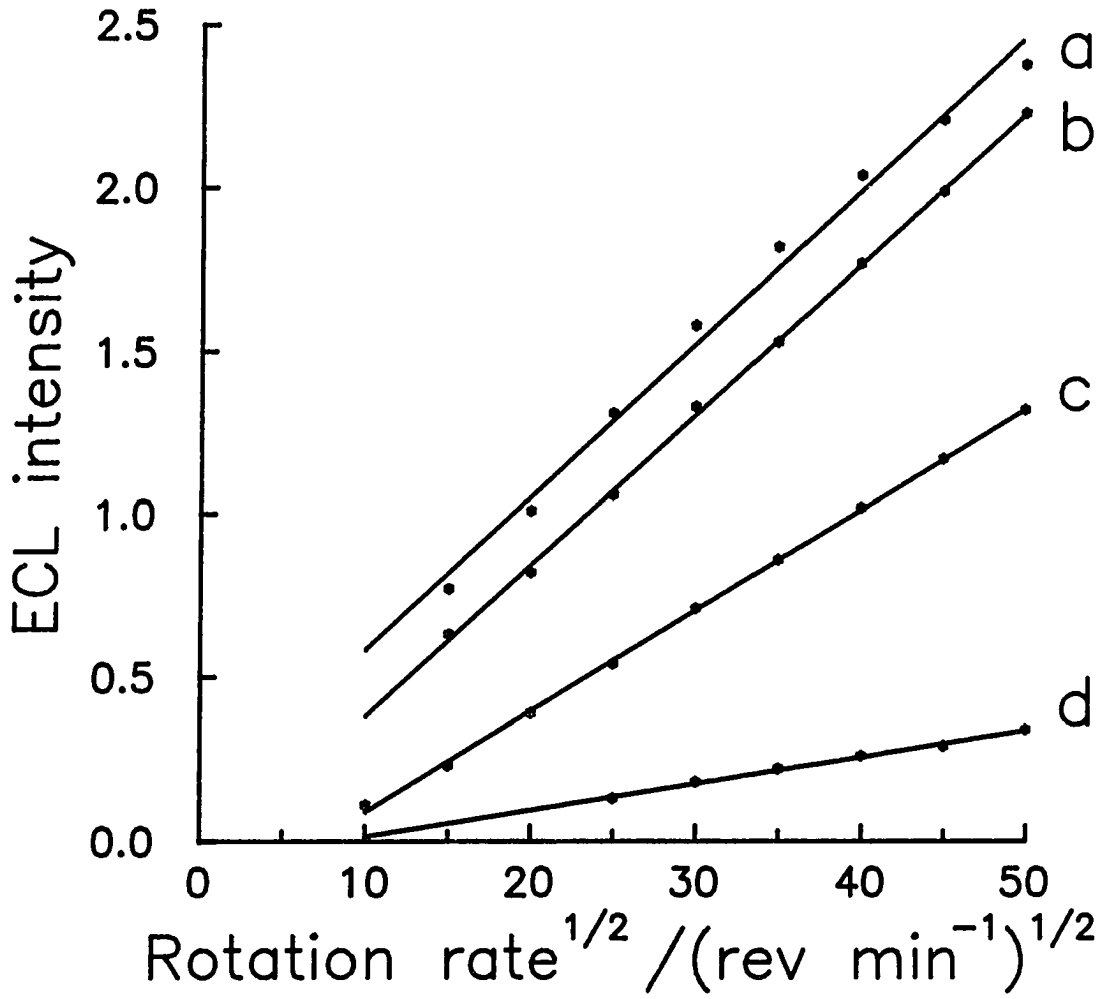

Figure 6. ECL intensity as a function of rotation rate$^{1/2}$.

Conditions: same as Figure 5.

Curves: (a) Au, (b) PbO_2, (c) 1% Bi-doped PbO_2, (d) glassy carbon.

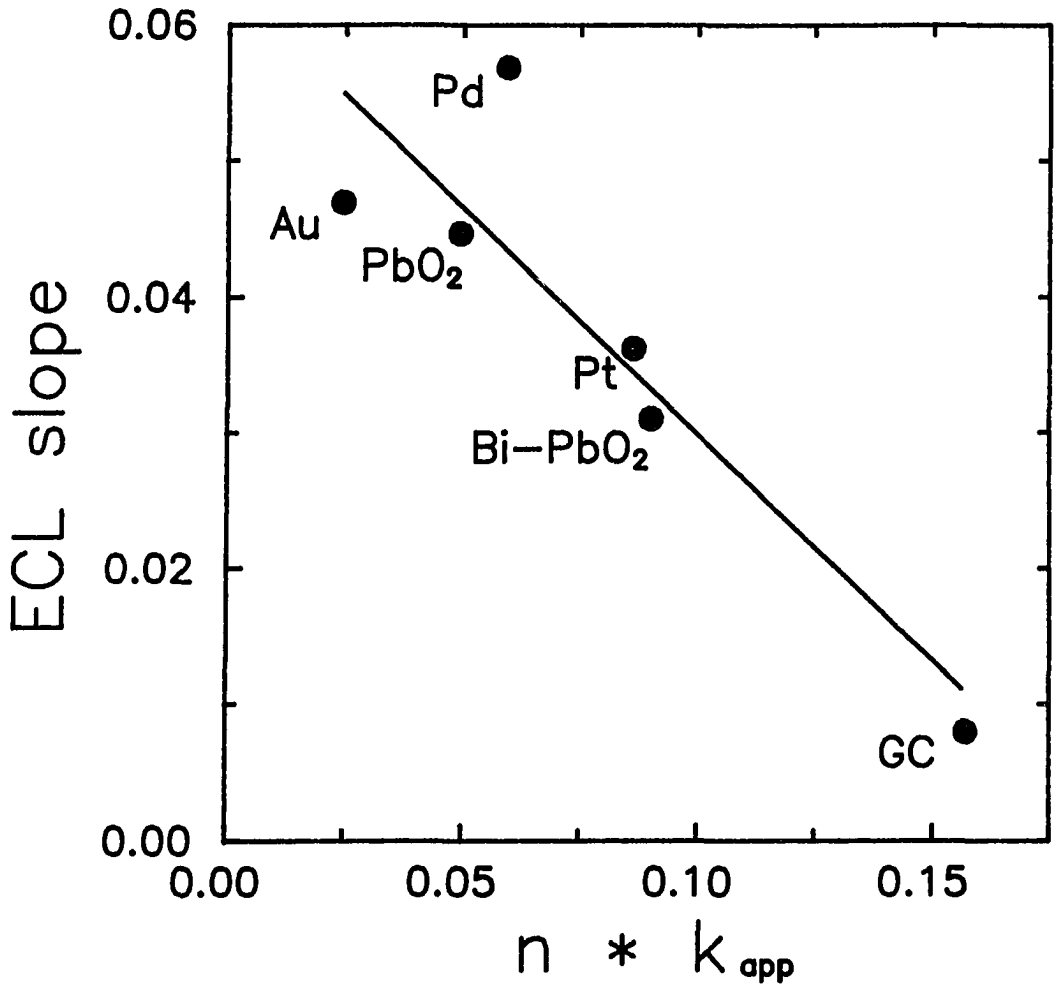

Figure 7. ECL slope as a function of nk_{app} for various electrode materials.

that I_{ECL} is not a reliable indication of the local current density when $E_{applied} >> E_{1/2}$. In fact, the assumption that the bright spots correspond to the active sites would be reliable only when $E_{applied}$ is greater than the $E_{1/2}$ at the active sites and less than $E_{1/2}$ at the "inactive" sites (6-8).

The inverse relationship between electrode activity and I_{ECL} is thought to arise because it is $L^{\cdot -}$ that subsequently reacts with dissolved O_2 in the chemiluminescent reaction. Hence, if LH^- is oxidized completely to AP^{-2} ($n = 4$ eq mol^{-1}), no ECL should be expected. Conversely, if LH^- is oxidized to $L^{\cdot -}$ ($n = 1$ eq mol^{-1}), maximum ECL is expected. These two competing reaction pathways for LH^- result in fractional values for $n < 4$ eq mol^{-1} for most electrode materials. Thus, when the oxygen-transfer anodic reaction of LH^- at the electrode surface is slow (small k_{app}), a larger fraction of $L^{\cdot -}$ escapes the electrode surface to undergo the chemiluminescent reaction. Several assumptions have been made in this simplified consideration. First, oxidation to AP^{-2} ($n = 4$) does not result in chemiluminescence, i.e., I_{ECL} in the absence of H_2O_2 or O_2 is negligible. This was confirmed for Au and GC, but direct production of AP^{-2} in the excited state at the electrode could explain the seemingly anomalous behavior at Pd (see Figure 7). Also, oxidation of more than the hydrazide group of LH^- would complicate interpretation of these results. For example, if the oxidation of the amine

group of LH^- was significant for certain electrode materials, higher values of n and k_{app} could result with no consequential decrease in I_{ECL}. Similarly, if a significant portion of an electrode surface was completely fouled so that n = 0 in these regions, the measured values of n and k_{app} would decrease along with I_{ECL}. For GC, no anodic current was observed for the oxidation of AP^{-2}, indicating that the amine group of LH^- probably was not oxidized at GC. However, an anodic wave was observed for AP^{-2} at Au, Pt, and Pd electrodes. For these three electrodes, the anodic current was not dependent on rotation rate, but was dependent on scan rate. This was indicative of a totally surface controlled reaction that is typical for amines on Au. For experiments performed at constant potential, the current for amine adsorption/oxidation would have decreased to negligible values by the time the anodic current and I_{ECL} were measured (> 25 sec). Also, because n < 4 eq mol^{-1} for these electrodes, it is unlikely that oxidation of the amine group was significant.

Experimental rate laws for ECL. The anodic current and I_{ECL} were measured simultaneously at the disk of the Au RRDE, as is illustrated in Figure 3. Values were obtained as a function of the concentration of LH^-, O_2, and H_2O_2 to determine the order of the reaction with respect to each reactant. The rotation rate of the electrode was 900 rev min^{-1}. The linear regression statistics for plots of $\log(I_{ECL})$

vs. $\log(C^b)$ are listed in Table 2. The slope of these plots corresponds to the order of the reaction. In the presence of O_2, the experimental rate law for the ECL reaction is described by Eq. [4]. The reaction orders with respect to LH^-

$$I_{ECL} \propto [\text{luminol}]^{1.44}[O_2]^{0.45} \qquad [4]$$

and O_2 are concluded to be 3/2 and 1/2, respectively. The rate law was quite different when H_2O_2 was the co-reactant (O_2 excluded), as given by Eq. [5]. In this case, the order of reaction is concluded to be unity for both LH^- and H_2O_2.

$$I_{ECL} \propto [\text{luminol}]^{1.01}[H_2O_2]^{0.98} \qquad [5]$$

In both cases, it was confirmed that the electrode current was first order with respect to LH^- in the ranges indicated in Table 2. The electrode current was also first order with respect to H_2O_2 when H_2O_2 was present in solution. It had not been expected that O_2 would have an effect on the electrode current, since O_2 was not electroactive at 0.55 V for the electrodes studied in alkaline solution. However, when the solution was saturated with O_2, the electrode current was ca. 15% larger than when equilibrated with lower partial pressures of O_2 (0.1% to 5.0%). This could be the result of the production of $O_2^{\cdot -}$ by the reaction of $L^{\cdot -}$ and O_2, which could then be oxidized at the electrode. Another possible explanation for the increased current at high O_2

Table 2. Linear regression statistics for plots of $\log(I_{ECL})$ *vs.* $\log(C^b)$.

Eq. of line: $Y = A + BX$

where $Y = \log(I_{ECL})$

and $X = \log(C^b)$

Reactant varied	[luminol]	[luminol]	$[O_2]$	$[H_2O_2]$
luminol	0.001-1 mM	0.010-0.5 mM	0.39 mM	0.39 mM
O_2	air satd.	0.0 %	0.1-5.0 %	0.0 %
$[H_2O_2]$	0.0	0.25 mM	0.0	0.02-0.2 mM
No. obs.	52	15	6	10
A^a	5.04 ± 0.06	3.70 ± 0.02	0.67 ± 0.03	3.83 ± 0.01
B^b	1.44 ± 0.01	1.01 ± 0.01	0.45 ± 0.02	0.98 ± 0.01
R^2	0.9975	0.9989	0.9922	0.9989

[a] Uncertainties indicate the standard error of Y.

[b] Uncertainties indicate the standard error of B.

concentrations is the reaction of two $O_2^{\cdot -}$ radicals to form O_2 and H_2O_2 with subsequent oxidation of H_2O_2.

The data for I_{ECL} as a function of LH^- concentration in the presence of O_2 (Curve a) and H_2O_2 (Curve b) are shown in Figure 8. Straight lines are superimposed on the plots with

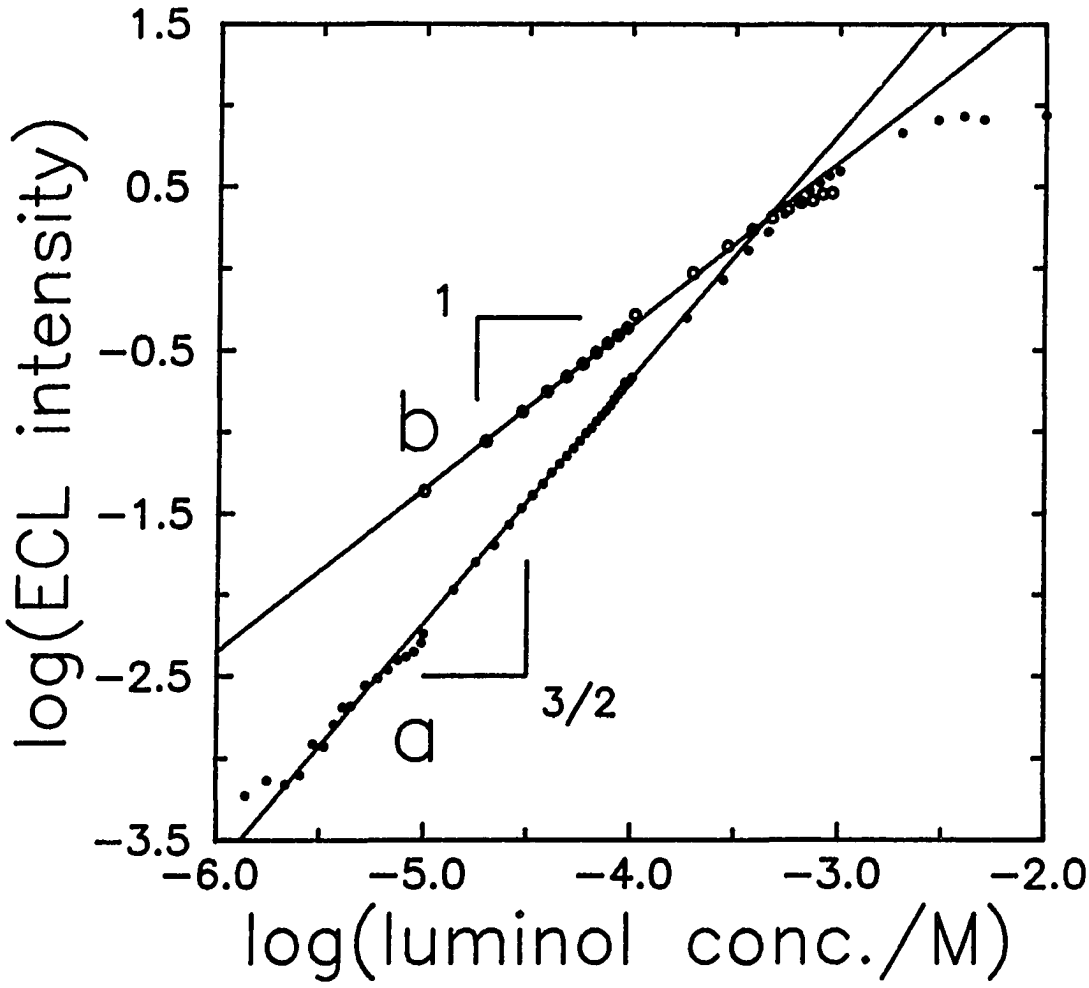

Figure 8. ECL intensity as a function of luminol concentration at a Au electrode.

Conditions: 900 rev min^{-1}, 0.1 M NaOH, 0.55 V.

Curves: (a) air saturated, (0.21 mM O_2)
(b) 0.25 mM H_2O_2, N_2 purged.

slopes of 3/2 and 1 for the presence of O_2 and H_2O_2, respectively. The I_{ECL} for the reaction in the presence of O_2 was comparable to the I_{ECL} with H_2O_2 in the solution. A zero order dependence was observed for > ca. 1.0 mM LH^- and 0.5 mM LH^- for the reaction in the presence of O_2 and H_2O_2, respectively. This behavior indicates that LH^- was no longer the limiting reagent at these high concentrations.

Spatial heterogeneity of PbO_2 electrodes activated by adsorbed Bi(V). ECL images were obtained for a pure PbO_2-film electrode before and after exposure to a solution containing ca. 20 uM Bi^{+3}. Spatial heterogeneity was apparent after exposure to Bi^{+3} (Figure 9) that was not evident in the micrographs for pure PbO_2. The dark areas appeared after the exposure to Bi^{+3} at 0.6 V. The three bright rings correspond to holes in the PbO_2 electrode that were evident under external illumination. It was unclear whether the dark spots corresponded to active sites on the electrode surface where the dark reaction (n = 4 eq mol^{-1}) dominated, or to totally inactive regions (i.e., n = 0 eq mol^{-1}). The I_{ECL} would be negligible in both cases, since the ECL reaction depends on the production of $L^{\cdot -}$ (n = 1 eq mol^{-1}). In either case, it is clear that the anodic adsorption of Bi^{+3} as Bi(V) did not result in uniform activation of the PbO_2 surface. Hence, it seems likely that Bi-adsorbed PbO_2 electrodes do not exhibit a uniform current density for LH^- oxidation.

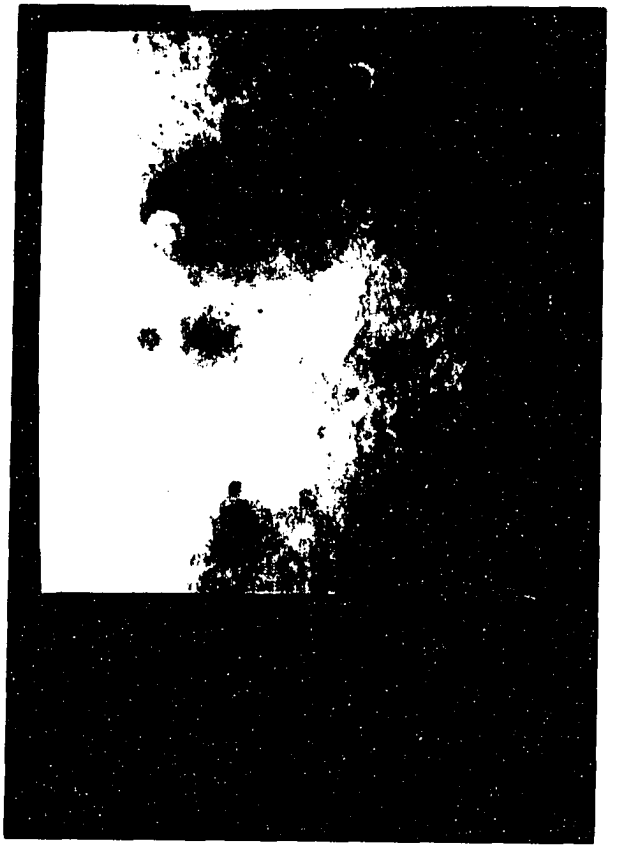

Figure 9. ECL micrograph of Bi-adsorbed PbO_2 electrode.

Conditions: 0.4 mM luminol, 50 mM borate buffer at pH = 10, 0.6 V, 100 sec photon count, 20 uM Bi^{3+} adsorbed at 0.6 V for < 5 min. The panel represents a viewing area 400 um on a side.

CONCLUSION

The mechanism given by Eqs. [6]-[12] is consistent with the experimental rate laws for the ECL reaction in the presence of O_2 and H_2O_2. The ECL mechanism is identical in both cases, except for the reactions that produce and deplete the superoxide ion, $O_2^{\cdot -}$, i.e., Eqs. [8] and [9] for H_2O_2 and Eqs. [10] and [12] for O_2.

Electrode reactions for luminol:

$$LH^- + OH^- \longrightarrow L^{\cdot -} + e^- + H_2O \qquad [6]$$

$$L^{\cdot -} + 4OH^- \longrightarrow AP^{-2} + N_2 + 3e^- + 2H_2O \qquad [7]$$

Electrode reactions for H_2O_2:

$$HO_2^- + OH^- \longrightarrow O_2^{\cdot -} + H_2O + e^- \qquad [8]$$

$$O_2^{\cdot -} \longrightarrow O_2 + e^- \qquad [9]$$

Solution reactions:

$$L^{\cdot -} + O_2 \longrightarrow O_2^{\cdot -} + L \qquad [10]$$

$$L^{\cdot -} + O_2^{\cdot -} \longrightarrow AP^{-2} + N_2 + \text{light} \qquad [11]$$

$$H_2O + O_2^{\cdot -} + O_2^{\cdot -} \longrightarrow O_2 + HO_2^- + OH^- \qquad [12]$$

Electrode reactions involving oxidation of LH^- are assumed to be the same whether the co-reactant is H_2O_2 or O_2. The first step in either mechanism corresponds to the one-electron oxidation of LH^- to $L^{\cdot -}$ (Eq. [6]). This radical can then undergo either the oxygen-transfer oxidation to AP^{-2} at the electrode surface in the dark reaction (Eq. [7]), or escape

into the solution to initiate the chemiluminescent reaction (Eq. [10]-[12]).

The steady-state concentration of $L^{\cdot -}$ is given by Eq. [13], assuming that the electrode reactions (Eq. [6]-[7])

$$[L^{\cdot -}] = (k_6/k_7)\,[LH^-]\,[OH^-]^{-3} \qquad [13]$$

dominate production and consumption of $L^{\cdot -}$. This is reasonable, considering that n varied in the range ca. 3 to 4. A value of n = 3 eq mol^{-1} would correspond to ca. 67 % of LH^- oxidized with n = 4 eq mol^{-1} and 33 % oxidized with n = 1 eq mol^{-1}. This corresponds to 67% of $L^{\cdot -}$ consumed by the electrode reaction in Eq. [7].

For the ECL reaction in the presence of H_2O_2, the expression for the steady-state concentration of $O_2^{\cdot -}$ is given by Eq. [14], again assuming the electrode reactions dominate the production and consumption of $O_2^{\cdot -}$.

$$[O_2^{\cdot -}] = (k_8/k_9)[HO_2^-][OH^-] \qquad [14]$$

The general expression for the ECL intensity is given by Eq. [15], which is essentially the rate of production of AP^{-2}

$$I_{ECL} = \chi k_{11}[L^{\cdot -}][O_2^{\cdot -}] \qquad [15]$$

in the excited state (AP^{-2*}) (Eq. [11]). In Eq. [15], χ is a proportionality constant that includes the quantum efficiency of chemiluminescence, and geometric and scaling factors

related to the photometric detection. This expression combined with Eq. [13] and Eq. [14] gives the theoretical rate law for ECL in the presence of H_2O_2 (Eq. [16]). This is in agreement with the experimental rate law determined at the Au disk electrode.

$$I_{ECL} = \propto k_{11}(k_6/k_7)(k_8/k_9)[LH^-][HO_2^-][OH^-]^{-2} \qquad [16]$$

For the ECL reaction in the presence of O_2, the steady-state concentration of $O_2^{\cdot -}$ is given by Eq. [17], which

$$[O_2^{\cdot -}] = (k_{10}/k_{12})^{1/2}[L^{\cdot -}]^{1/2}[O_2]^{1/2} \qquad [17]$$

assumes that the reaction of two superoxide ions dominates the consumption of $O_2^{\cdot -}$. The $O_2^{\cdot -}$ species is produced by the reaction of $L^{\cdot -}$ and O_2, which has been studied by pulse radiolysis (16). The other product of this reaction is 5-aminophthalazine-1,4-dione (L) which is produced by the 2-electron oxidation of LH^-. See Ref. (11) for structures of this and other intermediate products in the chemiluminescent reaction. Substitution of Eq. [17] and Eq. [13] into Eq. [15] gives the theoretical rate expression for I_{ECL} in the presence of O_2 (Eq. [18]). The 3/2 dependence on the LH^- concentration arises because of the inclusion of the quenching reaction

$$I_{ECL} = \propto k_{11}(k_{10}/k_{12})^{1/2}(k_6/k_7)^{3/2}[O_2]^{1/2}[LH^-]^{3/2}[OH^-]^{-9/2} \qquad [18]$$

between two superoxide radicals. If this reaction was omitted and the consumption of $O_2^{\cdot -}$ was dominated by Eq. [11], the rate law would be first order with respect to LH^-. Clearly, such a prediction is not consistent with the experimental evidence.

For both cases of ECL considered here, the rate expressions are consistent with the inverse relationship observed between I_{ECL} and electrode activity. Thus, as the oxygen-transfer rate constant (k_7) increases, I_{ECL} decreases. Actually, this relationship is more complicated since it is really the ratio k_6/k_7 that determines I_{ECL}. The situation is even more complicated when oxidation of H_2O_2 is the source of $O_2^{\cdot -}$. In that case, the electrode activity for the oxidation of H_2O_2 also influences I_{ECL}. Furthermore, the presence of LH^- interfered with the oxidation of H_2O_2 at many electrode materials.

Because of the inverse relationship between I_{ECL} and electrode activity, an unambiguous identification of active sites must involve consideration of the potential dependence of I_{ECL}. For example, it was reported that the ECL reaction occurred at less positive potentials at the most active sites at HOPG. The surrounding electrode surface was characterized by more positive values of $E_{1/2}$ for I_{ECL}, but the maximum I_{ECL} was significantly larger than that at the active sites (8). Our results help explain this observation. However, an

alternate scenario could be developed in which higher I_{ECL} would be observed because of increased flux to the active sites. For future interpretation of ECL data, it must be remembered that the absence of ECL corresponds both to regions for which n = 0 (i.e., no activity) and for which n = 4 (i.e., high activity). High ECL intensity corresponds to electrode regions of moderate activity (i.e., $1 \leq n << 4$).

ACKNOWLEDGMENTS

Ames Laboratory is operated for the U.S. Department of Energy by Iowa State University under Contract No. W-7405-ENG-82. D.C.J. and J.E.V. acknowledge financial support by the Director for Energy Research, Office of Basic Energy Sciences, U.S.D.O.E. R.C.E. acknowledges financial support by the National Science Foundation through grant CHE-8703018.

REFERENCES

1. Yeo, I.-H.; Johnson, D. C. J. Electrochem. Soc., 1987, 134, 1973-1977.
2. Yeo, I.-H.; Kim, S.; Jacobson, R.; Johnson, D. C. J. Electrochem. Soc., 1989, 136, 1395-1401.
3. Hsiao, Y.-L.; Johnson, D. C.; J. Electrochem. Soc., 1989, 136, 3704-3711.
4. Lacourse, W. R.; Hsiao, Y.-L.; Johnson, D. C.; Weber, W. H. J. Electrochem. Soc., 1989, 136, 3714-3719.
5. Feng, J.; Johnson, D. C. J. Electrochem. Soc., 1990, 137, 507-510.
6. Engstrom, R. C.; Pharr, C. M.; Koppang, M. D. J. Electroanal. Chem., 1987, 221, 251-255.
7. Engstrom, R. C.; Johnson, K. W.; DesJarlais, S. Anal. Chem., 1987, 59, 670-673.
8. Bowling, R. J.; McCreery, R. L.; Pharr, C. M.; Engstrom, R. C. Anal. Chem., 1989, 61, 2763-2766.
9. Chang, H.; Johnson, D. C. J. Electrochem. Soc. 1990, 137, 2452-2457.
10. Erdey, L.; Buzas, I.; Vigh, K. Talanta, 1966, 13, 463-469.
11. Lind, J.; Merenyi, G.; Eriksen, T. E. J. Am. Chem. Soc., 1983, 105, 7655-7661.
12. White, E. H.; Zafiriou, O.; Kagi, H. H.; Hill, J. H. M. J. Am. Chem. Soc., 1964, 86, 940-941.

13. White, E. H.; Bursey, M. M. J. Am. Chem. Soc., 1964, 86, 941-942.

14. Haapakka, K. E.; Kankare, J. J.; Anal. Chim. Acta, 1982, 138, 253-262.

15. Haapakka, K. E.; Kankare, J. J.; Anal. Chim. Acta, 1982, 138, 263-275.

16. Merenyi, G.; Lind, J.; Eriksen, T. E. J. Phys. Chem., 1984, 88, 2320-2323.

17. Levich, V. G., Physicochemical Hydrodynamics; Prentice Hall: Englewood Cliffs, NJ, 1962; p 75.

18. Epstein, B.; Kuwana, T. J. Electroanal. Chem., 1967, 15, 389-397.

19. Pratt, K. W. Anal. Chem., 1984, 56, 1967-1970.

20. Friedman, L.; Carpenter, P. G. J. Am. Chem. Soc., 1939, 61, 1745-1747.

SECTION IV.

ELECTROCATALYSIS OF ANODIC, OXYGEN-TRANSFER REACTIONS BY SIMULTANEOUS EVOLUTION OF O_2[1]

---

[1] submitted to J. Electrochem. Soc.

ABSTRACT

Difference voltammetry at rotated-disk electrodes was applied to a study of several anodic O-transfer reactions that appear to occur concurrently with O_2 evolution. This voltammetric technique was useful for extracting the rotation-dependent component of the total current from the large, rotation-independent current for O_2 evolution. Data for oxidation of I^- at Pt, Au, Pd, Ir, and glassy carbon electrodes show that the $E_{1/2}$ for IO_3^- production is directly related to the overpotential for O_2 evolution at the electrode materials. Data obtained at an Ir electrode for various reactions with widely varying E^o values reveal uniform $E_{1/2}$ values closely correlated with the potential for onset of O_2 evolution in both alkaline and acidic solutions. The results support the conclusion that the anodic discharge of H_2O is an integral part of these anodic O-transfer mechanisms.

INTRODUCTION

Virtually all anodic oxidations of organic compounds that involve the transfer of oxygen from H_2O in the solvent phase to the oxidation products are irreversible with half-wave potentials ($E_{1/2}$) that are much larger than predicted from the thermodynamic potentials (E^o) for the reactions. Most of these O-transfer reactions do not occur at appreciable rates throughout the region of positive potential at the common electrode materials, including noble metals, carbon, and pure lead dioxide. As a consequence, only a limited amount of voltammetric data is available for anodic reactions of organic compounds, especially aliphatic compounds (1). However, given the fact that oxidations of all organic compounds by O_2 to produce CO_2 and H^+ or H_2O are spontaneous, it is clear that the absence of voltammetric data is a consequence of kinetic rather than thermodyamic limitations.

Because the evolution of O_2 by anodic discharge of H_2O in aqueous media dictates the positive potential limit accessible at stable anode materials, the electrochemical oxidation of all organic molecules is theoretically possible. Hence, there are virtually unlimited possibilities for development of (i) electrochemical processes for the degradation of toxic organic chemical wastes as well as (ii) amperometric transducers for anodic detection. However, to achieve these possibilities, electrocatalysts must be discovered which significantly lower

the activation barrier for anodic O-transfer reactions, allowing them to proceed at reasonable rates at electrode potentials for which the rate of O_2 evolution is negligible in aqueous solvents.

The observed irreversibility for anodic O-transfer reactions of electrosynthetic interest appears to have led to the use of electrodes with large O_2-evolution overpotentials that allow application of larger positive values of electrode potentials. There is reason to question the basis of this tendency. The anodic evolution of O_2 is an example of an anodic O-transfer reaction and it is generally accepted that the first step in the mechanism is the discharge of H_2O to generate an adsorbed hydroxyl radical ($^{\cdot}OH_{ads}$) (2-5). It is reasonable to expect that the anodic discharge of H_2O is also a requirement of anodic O-transfer reactions (6-8). Thus, it is reasonable to expect that the potential required for onset of anodic O-transfer reactions is virtually coincident with that for onset of O_2 evolution. Evidence supporting this speculation has come from our laboratory for the oxidation of $As(OH)_3$ to $OAs(OH)_3$ (9) and I^- to IO_3^- (10) at oxide-covered Pt electrodes in acidic media. Furthermore, it has been demonstrated that PbO_2-film electrodes can be activated for various anodic O-transfer reactions by incorporation of various doping agents within the oxide films to generate

surface sites at which the O_2-evolution overpotential is apparently smaller than that of pure PbO_2 surface (11-13).

It is difficult to study anodic reactions that occur concurrently with O_2 evolution because of the large background current. In studies of the oxidation of $As(OH)_3$ (9) and I^- (10), square-wave hydrodynamically modulated voltammetry was applied at a Pt rotated disk electrode (RDE) to extract the rotation-dependent currents for the reactions of interest from the rotation-independent currents for evolution of O_2 and formation of surface oxide. In research described here, difference voltammetry (DV) was used to achieve the same purpose. In DV, the current-potential (i-E) response curves obtained for two rotation speeds at a RDE are subtracted to yield a difference response (Δi-E) in which evidence of O_2 evolution is absent. DV was applied to obtain $E_{1/2}$ values for various anodic O-transfer reactions, including the irreversible oxidation of I^- to IO_3^- at glassy carbon (GC), Au, Pd, Pt, and Ir electrodes in acidic media.

EXPERIMENTAL

Equipment. Voltammetric data were obtained using a RDE4 potentiostat and an ASR rotator (Pine Instrument Co.) interfaced with an IBM PC-XT computer. The interface consisted of a DAS-8PGA data acquisition board (MetraByte Corp.) and ASYST-2.0 software (Keithley/Asyst). The electrochemical cell was made of Pyrex with porous glass disks separating the working, reference, and counter electrode compartments. The reference electrode was a saturated calomel electrode (SCE; Fisher Scientific Co.), and all potentials are reported vs. the SCE. The counter electrode was a coiled Pt wire (ca. 7.6 cm^2). Rotated ring-disk electrodes (RRDE) were Model AFDT (R_1 = 0.383 cm, R_2 = 0.398 cm, R_3 = 0.422 cm; Pine Instrument Co.). Electrode materials were Au, Pt, Pd, and glassy carbon (GC). Also, an Ir rotated disk electrode (RDE, 0.46 cm^2) and a second GC RDE (0.196 cm^2) were used.

Reagents. Solutions were prepared by dissolving the following Reagent Grade chemicals in solutions of the various supporting electrolytes: KI, $VOSO_4 \cdot H_2O$, $MnSO_4 \cdot H_2O$, Tl_2SO_4, glucose, and dimethylsulfoxide (DMSO) from Fisher Scientific Co.; KNO_2 from Baker Chemical Co.; and $CrK(SO_4)_2 \cdot 12H_2O$ from Aldrich Chemical Co. Water was purified in a Milli-Q system (Millipore) after passage through two D-45 deionizing cartridges (Culligan).

Procedures. Electrodes were polished with successively finer grades of alumina (1.0, 0.3, and 0.05 um) in H_2O on microcloth (Buehler Limited), and then rinsed with deionized H_2O. The electrode potential was cycled in solutions of supporting electrolyte between the potential limits indicated until the residual i-E curves were reproducible. Voltammetric (i-E) data were obtained at ambient room temperature ($23 \pm 2^{o}C$).

Measurement of overpotentials. Difference voltammetric curves (Δi-E) were produced by computer subtraction of the i-E curves obtained at two rotation rates. Overpotential values for oxidation of I^- to IO_3^- were calculated by subtraction of $E^{o'}$ = 0.785 V vs. SCE at pH 1 (14) from $E_{1/2}$ values taken from Δi-E curves for the negative potential scan. The O_2-overpotentials were calculated by subtraction of $E^{o'}$ = 0.93 V vs. SCE for the O_2/H_2O redox couple at pH 1 (14) from the E values on the residual i-E curves at which the current density for O_2 evolution was 4.3 mA cm^{-2} during the negative scan.

RESULTS AND DISCUSSION

Oxidation of iodide at Au. Iodide was selected as a model reactant for a variety of reasons. At least two anodic reactions are available for I^- in acidic media. The oxidation of I^- to I_2 is a relatively simple and reversible electron-transfer process (n = 1 eq mol^{-1}). The oxidation of I^- to IO_3^- (n = 6 eq mol^{-1}) is more complex, requiring the transfer of three oxygen atoms, and is likely to be highly sensitive to those catalytic aspects of the electrode which control the O-transfer mechanism. Whereas the anodic response of I^- has been studied most thoroughly at Pt electrodes (10,15-17), preliminary tests demonstrated that I^- is oxidized at all electrode materials available for this research.

A typical i-E curve for I^- at a Au RDE in 0.1 M H_2SO_4 is shown in Fig. 1 (Curve b) in comparison to the residual response (Curve a). The residual response is characteristic of Au electrodes in acidic media. An anodic wave is observed during the positive scan ($E_{1/2}$ = 1.07 V) for the formation of oxide on the electrode surface. Evolution of O_2 occurs with an exponential dependence on E in the region E > ca. 1.6 V. Cathodic dissolution of the surface oxide produces a peak signal (E_{peak} = 0.77 V) during the negative scan and the presence of dissolved O_2 is made apparent by the cathodic wave ($E_{1/2}$ = 0.03 V).

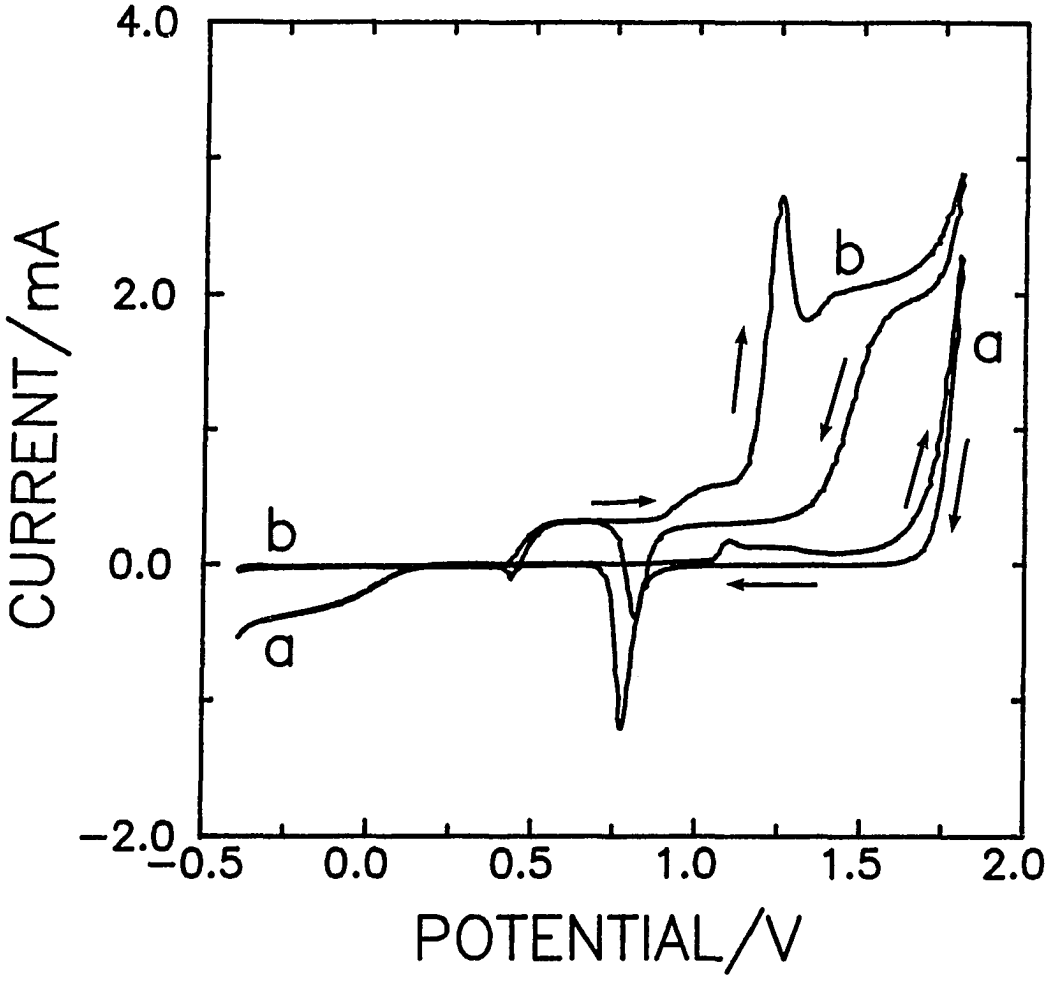

Figure 1. Voltammetric response (i-E) for I^- at a Au disk electrode in air-saturated 0.1 M H_2SO_4.

Rotation rate: 2500 rev min^{-1} (94.2 rad sec^{-1});
Scan rate: 100 mV sec^{-1}; Scan range: -0.4 to 1.81 V;

Curves: (a) residual, (b) 0.5 mM I^-.

The electrochemical behavior of I^- at Au (Fig. 1, Curve b) is relatively complex, with more than one oxidation product, depending on the applied potential and scan direction. The anodic wave for oxidation of I^- to I_2 ($E_{1/2}$ = 0.49 V) yields a current plateau during the positive scan (E = ca. 0.5 - 0.9 V) which is limited by the rate of mass transport of I^-. A second anodic wave ($E_{1/2}$ = 0.96 V) observed during the positive scan is tentatively identified as resulting from production of IO^- (n = 2 eq mol^{-1}), based on the observation that the current plateau is ca. twice that for I_2 production (n = 1 eq mol^{-1}). More conclusive evidence for this identification is presented later based on data obtained with a RRDE. The anodic peak at 1.25 V during the positive scan is the result of oxidation of adsorbed I^o and some I^- to IO_3^- by a process catalyzed by the formation of surface oxide on the Au electrode. The peak current was determined to depend both on the scan rate and the rotation rate of the electrode, which is similar to the behavior observed at Pt (10). Oxidation of I^- to IO_3^- occurs by a mass transport-limited process at E > ca. 1.3 V during the positive scan and a distinct wave with $E_{1/2}$ = 1.47 V is observed during the negative scan. Evolution of O_2 occurs for E > ca. 1.6 V.

The production of IO_3^- for E > ca. 1.3 V at the disk of the Au-Au RRDE was confirmed by examination of voltammetric data obtained at the ring electrode. The i_r-E_r curves were

recorded for constant E_d values increased by 100-mV increments over the potential range shown in Fig. 1. The $E_{1/2}$ values for the cathodic reaction at the ring electrode of the species generated at the disk electrode for E_d > ca. 1.3 V were identical to the $E_{1/2}$ value for IO_3^- observed using the ring electrode only in a solution containing IO_3^-.

Confirmation of the production of IO^- on the Au electrode at ca. 1.2 V (positive scan) was not possible by comparison of i_r-E_r curves obtained at the RRDE to voltammetric data for a solution of IO^- because HIO rapidly disproportionates to I_2 and IO_3^- in acidic solution (15). However, the presence of IO^- was tentatively confirmed from cyclic voltammetric data obtained at the stationary Au disk electrode as shown in Fig. 2. For a positive scan limit of 1.1 V (Curve a), two pairs of current peaks are observed. The first pair (Peaks 1&1') have a peak separation (ΔE_{peak}) of ca. 70 mV and correspond to the I_2-I^- redox couple. The second pair (Peaks 2&2'), corresponding to the reaction in question, has ΔE_{peak} = ca. 40 mV, which is nearly the reversible value for a 2-electron process (18). The $E^{o'}$ value estimated for this redox couple is 0.94 V which is considered to be in satisfactory agreement with the value of 1.01 V for the IO^--I^- couple (17). For a positive scan limit of 1.2 V (Curve b), some IO_3^- is produced (Wave 3) and, therefore, the cathodic signal at ca. -0.20 V (Peak 3') during the negative scan is attributed to reduction

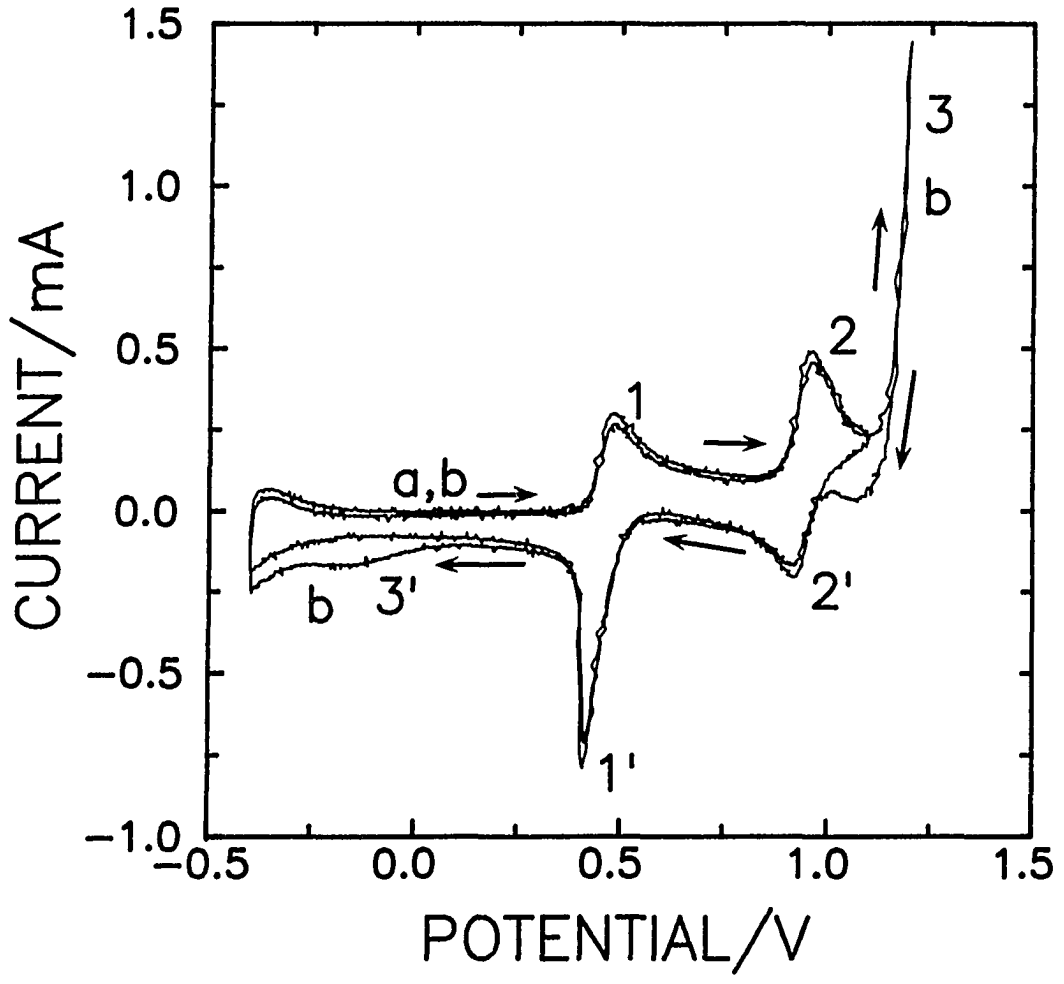

Figure 2. Cyclic voltammetric response (i-E) for 0.5 mM I^- at a stationary Au disk electrode in air-saturated 0.1 M H_2SO_4.

Scan rate: 1.0 V sec^{-1};

Scan range: (a) -0.4 to 1.1 V,
(b) -0.4 to 1.2 V.

of IO_3^-. This conclusion is in agreement with voltammetric data obtained for a solution of IO_3^-.

Difference voltammetry was used to investigate the oxidation of I^- at the Au electrode in the potential region where O_2 is evolved and the results are illustrated by the Δi-E data in Fig. 3. It is the assumption of difference voltammetry that the Δi-E curve does not contain contributions from rotation-independent faradaic process, i.e., the formation and stripping of surface oxide and O_2 evolution. However, it is apparent in Fig. 3 that the Δi signal decreases for increasing E in the region of O_2 evolution (E > 1.5 V). This decrease was consistently observed in the Δi-E curves obtained for all electrode materials tested. The residual Δi-E curves indicated no change in Δi in the potential regions of O_2 evolution.

The Au-Au RRDE was applied in the collection mode to determine if the decrease in Δi for E > 1.5 V is a result of a change in the rate of IO_3^- production or some other factor. As observed in Figs. 1 & 3, the presence of I^- completely eliminates the cathodic detection of dissolved O_2. This is a consequence of interference by strongly adsorbed I^o in the O_2-reduction mechanism. Hence, for E_r = -0.3 V, the ring electrode can detect IO_3^-, IO^- and I_2 from the disk electrode without interference from O_2 generated at E_d > 1.5 V. The i_r-E_d curve is shown in Fig. 4. Of greatest significance is the

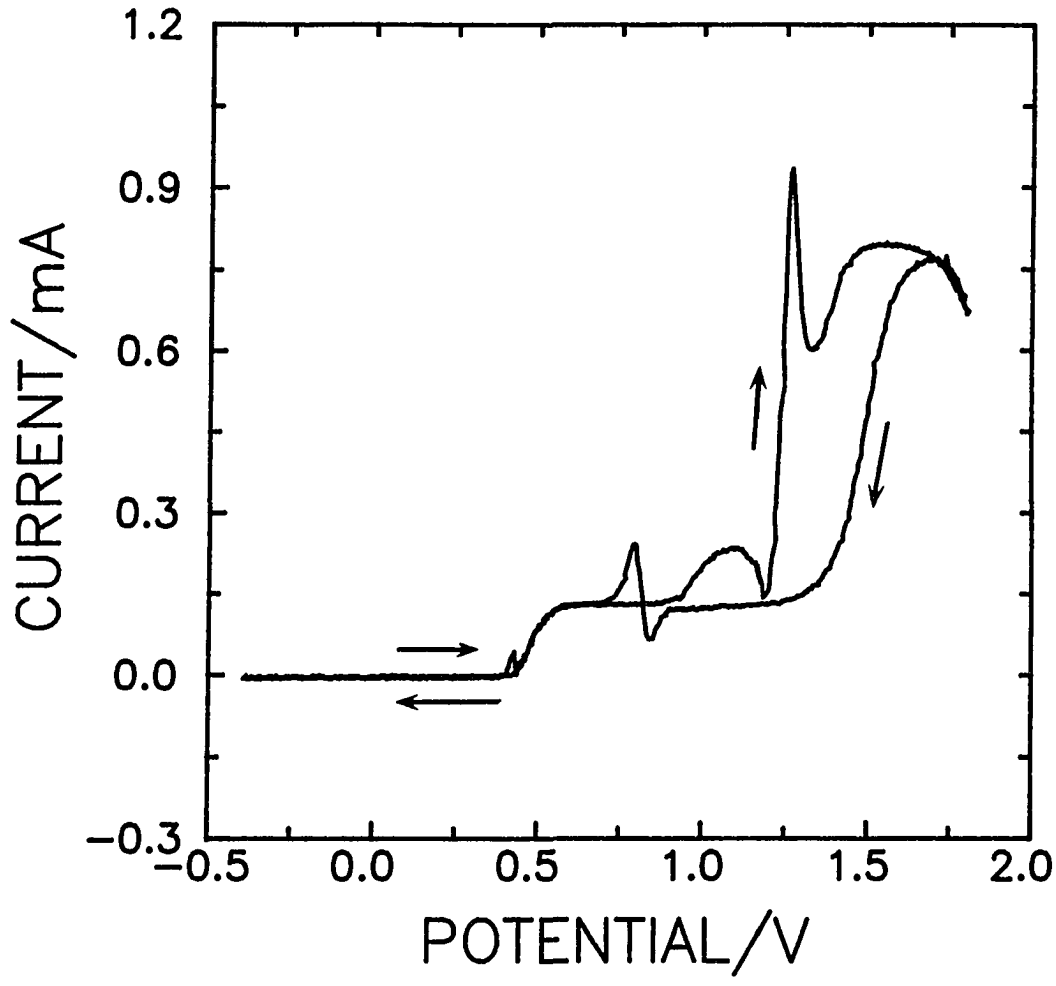

Figure 3. Difference voltammetric response (Δi-E) for 0.5 mM I^- at a Au disk electrode in 0.1 M H_2SO_4.

Rotation rates: 2500 and 900 rev min^{-1};
Scan rate: 100 mV sec^{-1}; Scan range: -0.4 to 1.81 V.

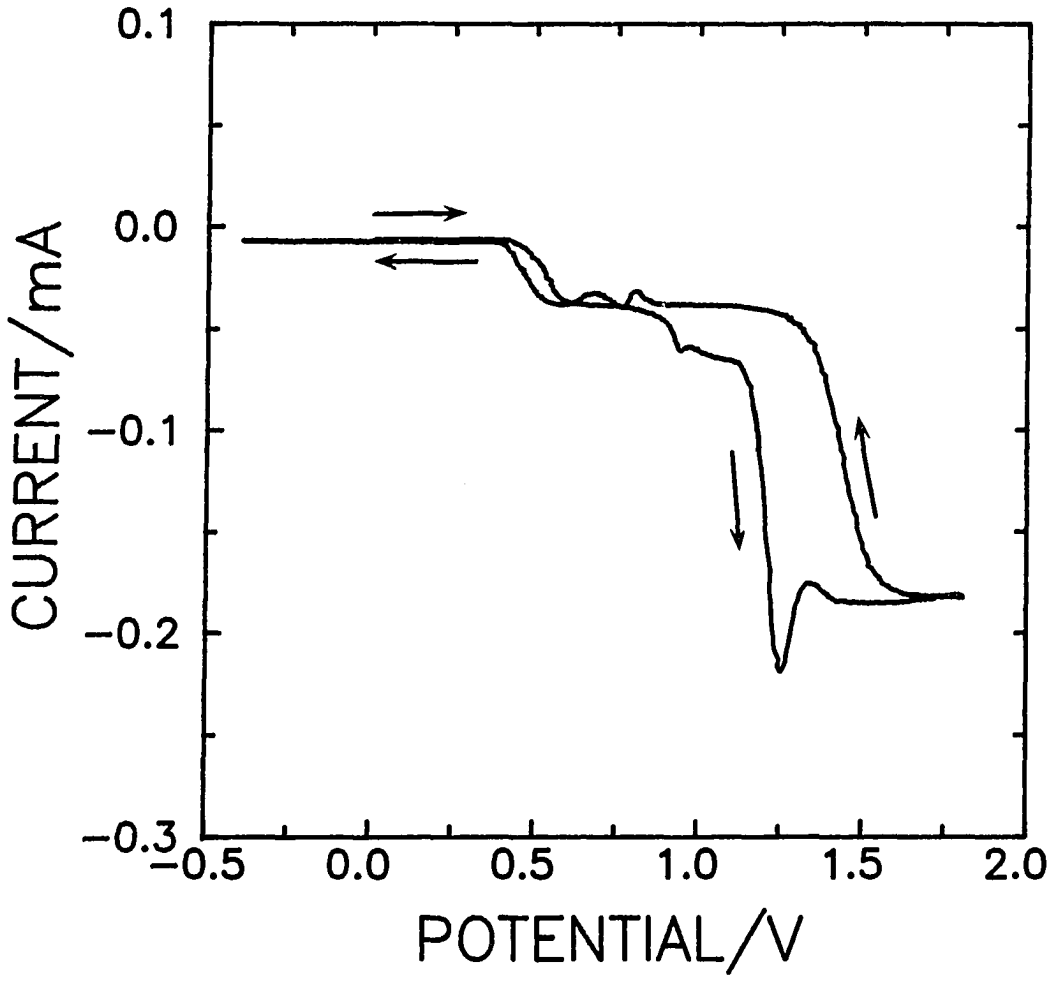

Figure 4. Ring current vs. disk potential (i_r-E_d) for 0.5 mM I^- at a Au-Au ring-disk electrode in air-saturated 0.1 M H_2SO_4.

Rotation rate: 900 rev min^{-1}; Ring potential: -0.3 V; Scan rate: 100 mV sec^{-1}; Scan range: -0.4 to 1.81 V.

observation that i_r is maintained at a constant value for E_d > 1.5 V. This is evidence that IO_3^- production does not decrease with increasing O_2 production. Hence, we conclude that the decrease in Δi for E > 1.5 V (Fig. 3) is the result of a variation of the rate of O_2 evolution with change in rotation rate as a consequence of the presence of I^-. This could be an indirect consequence of the coupling of the mechanism of IO_3^- production with that for O_2 evolution.

Voltammetric data were obtained also for the Pt-Pt RRDE in the collection mode. The i_r-E_d data were similar to those shown in Fig. 4 for the Au-Au RRDE. In essence, the rate of IO_3^- production at the Pt disk electrode does not decrease from a plateau value with the increase in O_2 evolution. It is also worthy of note that there was no evidence in the i-E data for Pt of a distinct wave for production of IO^-.

Oxidation of iodide at an oxide-covered Pt electrode. It is apparent from the Δi-E curve in Fig. 4 that $E_{1/2}$ values for IO_3^- production are not equivalent for the positive and negative scans at the Au electrode. A similar phenomenon was observed at the Pt electrode and was studied as a function of the negative scan limit. Representative Δi-E curves are shown in Fig. 5. For a negative limit of -0.2 V (Curve a) the difference in $E_{1/2}$ values for IO_3^- production is ca. 0.29 mV. This result is similar to that for oxidation of I^- to IO_3^- at a Pt electrode obtained by square-wave hydrodynamically

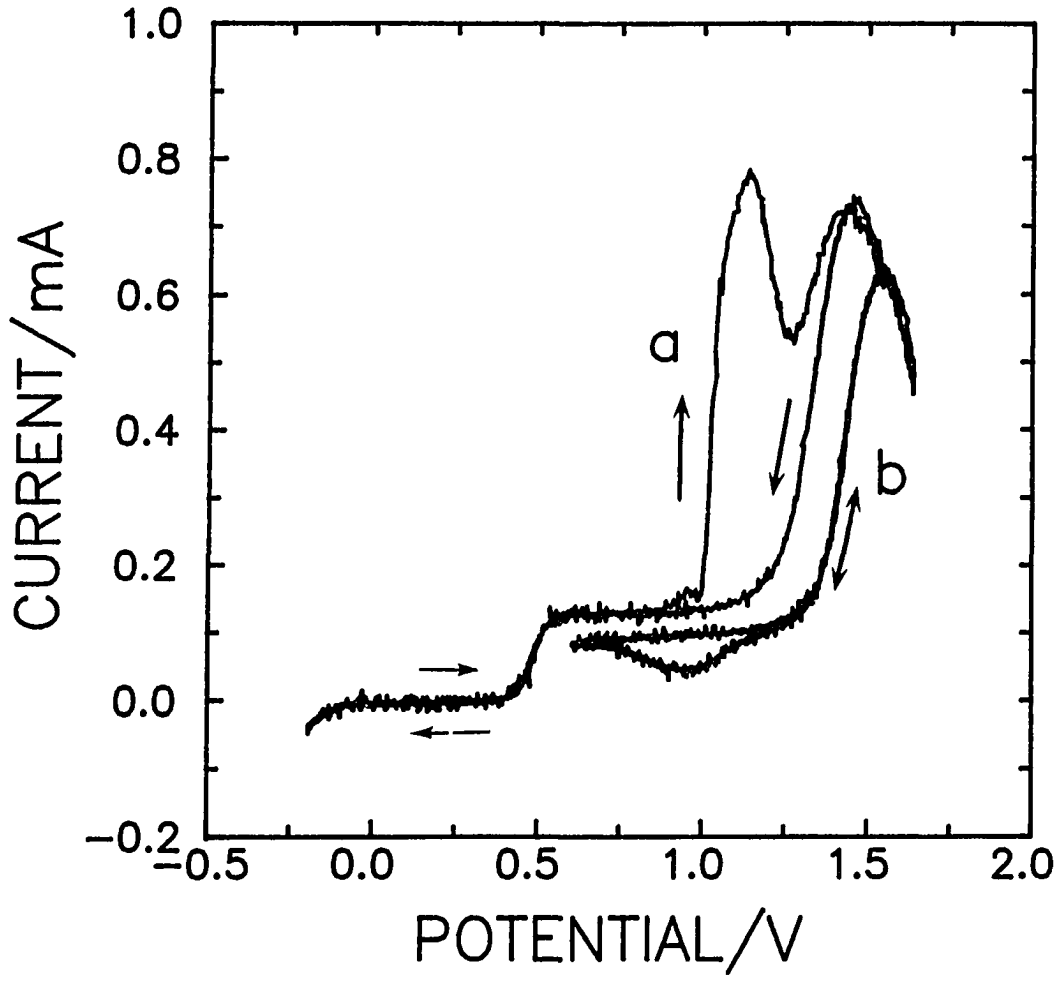

Figure 5. Difference voltammetric response (Δi_d-E_d) for 0.5 mM I^- at a Pt disk electrode in air-saturated 0.1 M H_2SO_4.

Rotation rates: 2500 and 900 rev min^{-1};
Scan rate: 100 mV sec^{-1};

Scan range: (a) -0.2 V to 1.55 V, (b) 0.6 V to 1.65 V.

modulated voltammetry (10). The $E_{1/2}$ values for IO_3^- production are independent of scan direction for a negative scan limit of 0.6 V (Curve b) for which the surface oxide is not removed by cathodic dissolution during the negative scan. These $E_{1/2}$ values (Curve b) also are shifted significantly more positive than the value observed on the negative scan of Curve a. It was apparent also from the i-E curves not shown that the overpotential of O_2 evolution is shifted to more positive potentials at an oxide-covered Pt electrode under the conditions of Curve b in Fig. 5. These results are concluded to be a consequence of the greater surface coverage and increased inertness of the oxide layer present after the potential has been scanned several times without cathodic dissolution of the oxide. It is also apparent in Fig. 5 that the plateau current for oxidation of I^- to I_2 is decreased in Curve b, as compared to Curve a, which is evidence for the decrease in active surface area for this electron-transfer process.

Oxidation of iodide at an Ir electrode. Typical voltammetric data for the oxidation of I^- at an Ir electrode are shown in Fig. 6. These i-E curves are very easy to interpret because there is no evidence for IO^- production, as observed for Au, and there are no peak signals resulting from IO_3^- production catalyzed by the formation of oxide during the positive scan, as observed for Au and Pt. Furthermore, the

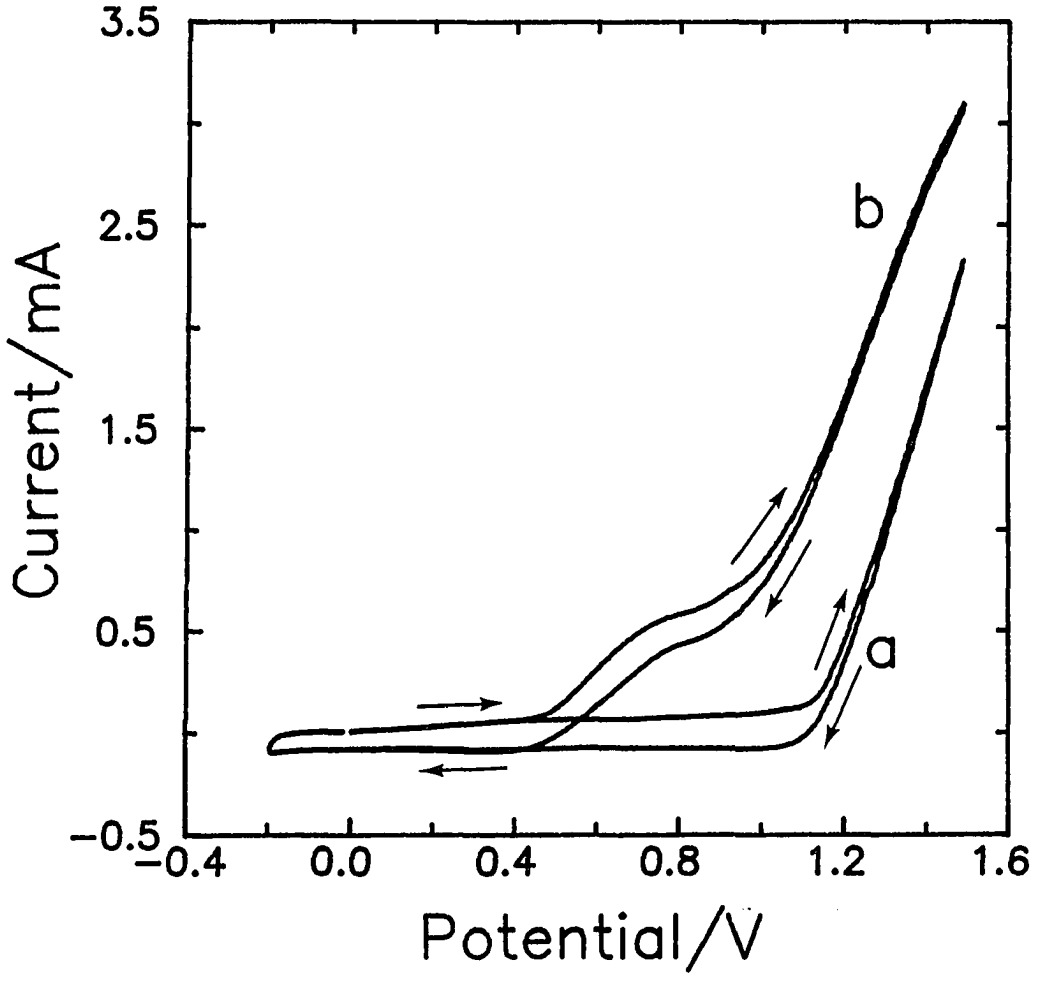

Figure 6. Voltammetric response (i_d-E_d) of I^- at an Ir disk electrode in deaerated 0.1 M $HClO_4$.

Rotation rate: 2500 rev min^{-1}; Scan rate: 100 mV sec^{-1}; Scan range: -0.2 V to 1.5 V;

Curves: (a) residual, (b) 0.5 mM I^-.

i-E curves are virtually superimposed for the positive and negative scans.

It is apparent from the i-E curves in Fig. 6 that a distinct wave for IO_3^- production is not easily resolved visually from the current for O_2 evolution. However, a discreet wave for IO_3^- production ($E_{1/2}$ = ca. 1.27 V) is readily detected in the Δi-E curves obtained by difference voltammetry and typical results are shown in Fig. 7.

Variation of $E_{1/2}$ for IO_3^- production with O_2 overpotential. Overpotentials (η) for oxidation of I^- to IO_3^- were determined from Δi-E curves obtained by difference voltammetry at GC, Au, Pt, Pd, and Ir electrodes in 0.1 M H_2SO_4, 0.1 M $HClO_4$ and 0.1 M HNO_3. All data were evaluated for the negative scan to eliminate erroneous results from oxide catalyzed IO_3^- production at the Au and Pt electrodes. The results are listed in Table 1 and plotted in Fig. 8 as a function of the overpotential for O_2 evolution obtained from the residual i-E curves.

Linear regression analysis of the data shown in Fig. 8 yields a slope of 0.55$\pm$0.07 (90% confidence) with an intercept of 0.19$\pm$0.06 V and a regression coefficient (r) of 0.964. The near-unity value for r is strong evidence that the anodic discharge of H_2O leading to production of O_2 is a requisite process in the oxidation of I^- to IO_3^-. The intercept of the plot in Fig. 8 is interpreted to correspond to the

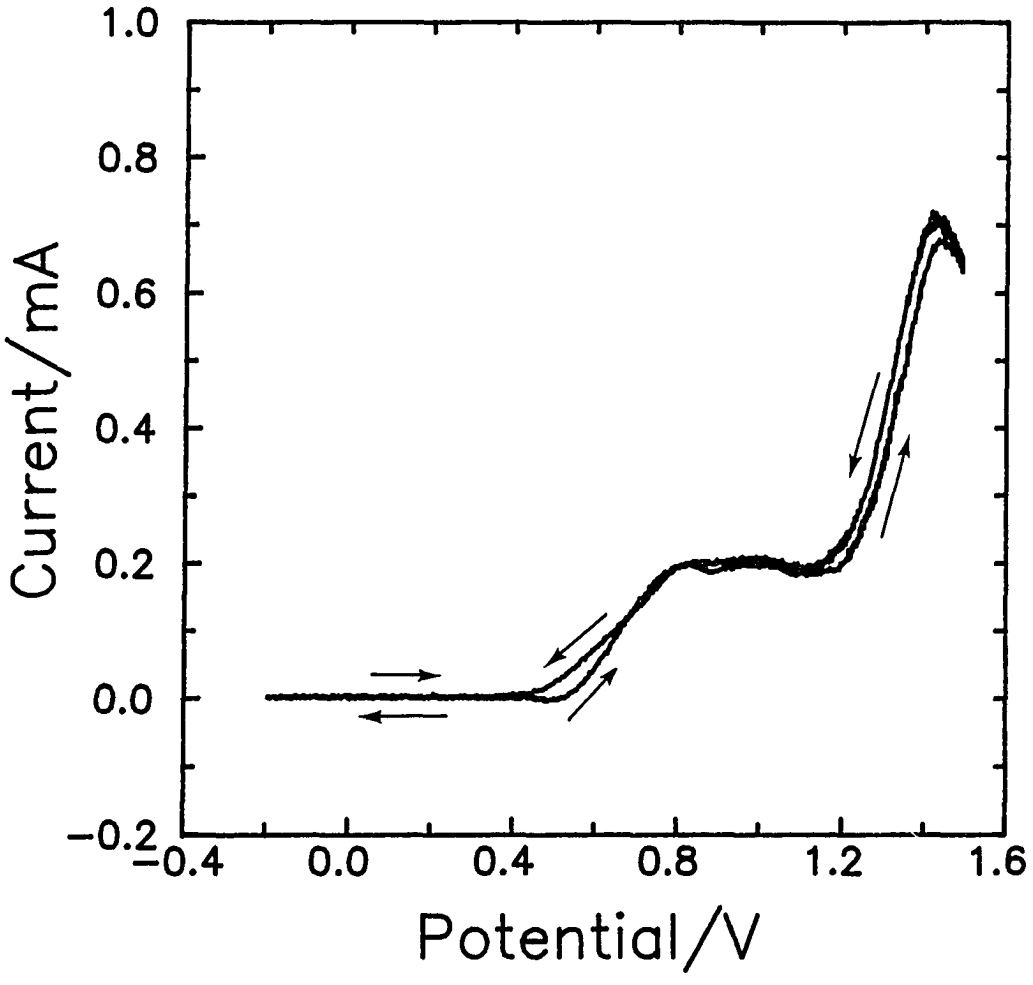

Figure 7. Difference voltammetric response (Δi-E) of 0.5 mM I^- at an Ir disk electrode in 0.1 M $HClO_4$.

Scan rate: 100 mV sec^{-1}; Scan range: -0.2 V to 1.5 V; Rotation rates: 2500 and 900 rev min^{-1}.

Table 1. Overpotentials for O_2 evolution and IO_3^- production, and values of $E_{1/2}$ for I_2 production.

Electrode ($0.46\ cm^2$)	Solution	η/V[a] $I^- \longrightarrow IO_3^-$	η/V[b] $H_2O \longrightarrow O_2$	$E_{1/2}$/V $I^- \longrightarrow I_2$
GC	0.1 M H_2SO_4	0.84	1.34	0.68
GC	0.1 M $HClO_4$	1.07	1.42	0.57
GC	0.1 M HNO_3	0.95	1.47	1.0
Au	0.1 M H_2SO_4	0.71	0.89	0.49
Au	0.1 M $HClO_4$	0.74	1.06	0.51
Au	0.1 M HNO_3	0.70	0.88	0.49
Pt	0.1 M H_2SO_4	0.53	0.61	0.48
Pt	0.1 M $HClO_4$	0.68	0.82	0.50
Pt	0.1 M HNO_3	0.55	0.62	0.48
Pd	0.1 M H_2SO_4	0.53	0.54	0.50
Pd	0.1 M $HClO_4$	0.60	0.69	0.55
Pd	0.1 M HNO_3	0.51	0.55	0.52
Ir	0.1 M H_2SO_4	0.35	0.36	0.50
Ir	0.1 M $HClO_4$	0.51	0.52	0.66
Ir	0.1 M HNO_3	0.27	0.33	0.50
GC2[c]	0.1 M H_2SO_4	0.69	0.98	0.47
GC2[c]	0.1 M $HClO_4$	0.72	1.08	0.96
GC2[c]	0.1 M HNO_3	0.72	0.95	0.59

a $\eta = E_{1/2} - 0.785$ V
b $\eta = E$ @ 4.3 $mA/cm^2 - 0.93$ V
c Area = 0.196 cm^2

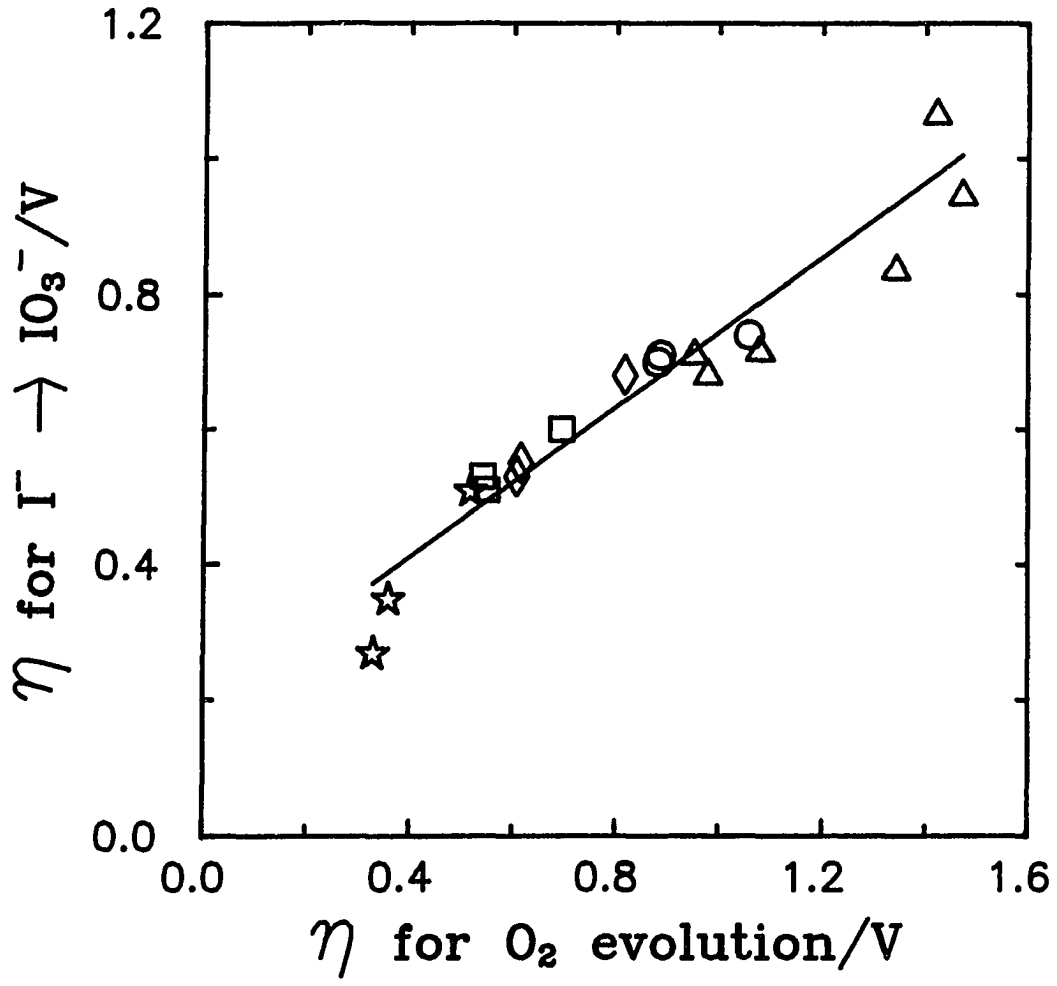

8. Correlation of overpotential for IO_3^- production with overpotential for O_2 evolution in 0.1 M H_2SO_4, 0.1 M $HClO_4$ and 0.1 M HNO_3.

Electrodes: (triangles) glassy carbon, (circles) Au, (diamonds) Pt, (squares) Pd, (stars) Ir.

hypothetical overpotential for IO_3^- production observed if the O_2-evolution reaction is reversible.

Also given in Table 1 are values of $E_{1/2}$ for oxidation of I^- to I_2. The $E_{1/2}$ values for I_2 production are virtually constant for the electrodes tested. In marked contrast, the $E_{1/2}$ value for IO_3^- production is clearly a sensitive function of electrode material and appears to be correlated with the overpotential for O_2 evolution at the various electrode surfaces. The overpotential data for the two GC electrodes are significantly different, indicating a remarkable difference in the catalytic nature of the respective surfaces. Nevertheless, data for both electrodes correlated well with those from the metal electrodes. These results demonstrate clearly that there is a significant difference in the role of the electrode surface in the simple electron-transfer mechanism for I_2 production and the more complex O-transfer mechanism for IO_3^- production.

Other O-transfer reactions at an Ir RDE. The oxidation of I^- to IO_3^- is interesting because of the convincing evidence that this O-transfer reaction can be catalyzed by a mechanism coupled with the O_2-evolution reaction at several electrode materials. The generality of this coupling mechanism was tested further for other anodic O-transfer processes with widely varying $E^{o'}$ values. The electrode chosen was Ir because this material exhibits the smallest O_2-

evolution overpotential of the materials available. The technique applied was difference voltammetry.

The $E_{1/2}$ values determined from Δi-E data are summarized in Table 2 for 0.1 M H_2SO_4 and 0.1 M NaOH. It is readily apparent that the $E_{1/2}$ values for a specified media are virtually identical and independent of the $E^{o'}$ values for the redox couples involved. Furthermore, the $E_{1/2}$ values are in the vicinity of the onset of O_2-evolution at the Ir electrode surface for the two media used. These results support the conclusion that these O-transfer reactions occur by mechanisms that are coupled with the O_2-evolution process at the electrode surface.

Table 2. Half-wave potentials at Ir in alkaline and acidic solution.

Reactant	Product	$E^{o'}/V$[a]	$E_{1/2}/V$
		0.1M H_2SO_4	
H_2O	O_2	0.93	1.29[b]
I^-	IO_3^-	0.79	1.14
dimethylsulfoxide	dimethylsulfone	-0.07	1.08
VO^{+2}	$V(OH)_4^+$	0.64	1.01
Mn^{+2}	$MnO_2(s)$	0.86	1.14
HNO_2	NO_3^-	0.60	1.14
		Avg.:	1.13±0.09
		0.1M NaOH	
H_2O	O_2	0.22	0.61[b]
I^-	IO_3^-	0.08	0.50
dimethylsulfoxide	dimethylsulfone	-0.78	0.53
glucose	gluconic acid	-0.91[c]	0.50
$Cr(OH)_3$	CrO_4^{-2}	-0.35	0.35
		Avg.:	0.50±0.09

[a] Calculated from data in Ref. (14).

[b] Evolution of O_2 at 4.3 mA cm^{-2}.

[c] Calculated from Ref. (1), p. 511.

CONCLUSIONS

The anodic discharge of H_2O, as the first step in the formation of O_2, is believed to produce adsorbed hydroxyl radicals ($^{\cdot}OH_{ads}$), as shown by Eqn. [1] (2-5). Hence, the

$$3H_2O \longrightarrow 3[^{\cdot}OH]_{ads} + 3H^+ + 3e^- \qquad [1]$$

results described for anodic O-transfer reactions can be explained by anodic mechanisms that are coupled to the O_2-evolution process <u>via</u> the $^{\cdot}OH_{ads}$ species. This is illustrated in Eqns. [2] - [4] for the step-wise oxidation of I^- to IO_3^-. Mechanisms similar to that shown for I^- oxidation are applicable for all species that undergo anodic O-transfer reactions.

$$I^- + {}^{\cdot}OH_{ads} \longrightarrow IO^- + H^+ + e^- \qquad [2]$$

$$IO^- + {}^{\cdot}OH_{ads} \longrightarrow IO_2^- + H^+ + e^- \qquad [3]$$

$$IO_2^- + {}^{\cdot}OH_{ads} \longrightarrow IO_3^- + H^+ + e^- \qquad [4]$$

The species designated as $^{\cdot}OH_{ads}$ is also formed as the first step in the anodic formation of surface oxides on noble-metal electrodes and production of some IO^- (at Au electrodes) and IO_3^- (at Au and Pt electrodes) is observed with oxide formation during the positive potential scans. There is no evidence for the production of IO^- or IO_2^- simultaneously with evolution of O_2. However, this is not an indication of the

failure of the proposed mechanism but an indication of the rapidity of the O-transfer steps.

Based on these conclusions, it is expected that the slope of the plot in Fig. 8 will be 1.0 instead of the observed value of ca. 0.5. Essentially, the observed slope indicates that, as the O_2-overpotential increases, the oxidation of I^- to IO_3^- becomes increasingly capable of competing with the O_2-evolution process for the $\cdot OH_{ads}$ species generated by the anodic discharge of H_2O. This might be the result of an increasing lifetime for this intermediate oxygen species in the O_2-evolution mechanism as the overpotential is increased.

It is predicted from these results that the typical strategy of choosing an electrode material with a large O_2-evolution overpotential for conducting anodic O-transfer reactions can result in higher current efficiency. A future publication will describe the use of composite electrodes containing a small percentage of noble-metal particles for improving the current efficiency of anodic O-transfer reactions that are catalyzed by O_2 evolution.

ACKNOWLEDGMENTS

Ames Laboratory is operated for the U.S. Department of Energy by Iowa State University under Contract No. W-7405-ENG-82. J.E.V. is grateful to Phillips Petroleum Corporation for providing a fellowship for the academic year 1990-1991. Special thanks to Rich Kniseley for performing initial voltammetric experiments on iodide.

REFERENCES

1. Clark, W. M. Oxidation-Reduction Potentials of Organic Systems; The Williams & Wilkins Co.: Baltimore, 1960.
2. Hoare, J. P. The Electrochemistry of Oxygen; Wiley: New York, 1968; p 87.
3. Bockris, J. O'M. J. Chem. Phys. 1956, 24, 817-827.
4. Trasatti, S. J. Electroanal. Chem. 1980, 111, 125-131.
5. Ruetschi, P.; Delahay, P. J. Chem. Phys. 1955, 23, 556-560.
6. Conway, B. E. Electrodes of Conductive Metallic Oxides, Pt. B; S. Trasatti, Ed.; Elsevier: New York, 1981; Chapter 9, p 453.
7. Gilman, S. J. Phys. Chem. 1963, 67, 1898-1905.
8. Gilman, S. J. Phys. Chem. 1964, 68, 70-80.
9. Cabelka, T. D.; Austin, D. S.; Johnson, D. C. J. Electrochem. Soc. 1984, 131, 1595-1602.
10. Austin, D. S.; Johnson, D. C.; Hines, T. G.; Berti, E. T. Anal. Chem. 1983, 55, 2222-2226.
11. Yeo, I-H.; Kim, S.; Jacobson, R.; Johnson, D. C. J. Electrochem. Soc. 1989, 136, 1395-1401.
12. Chang, H.; Johnson, D. C. J. Electrochem. Soc. 1989, 136, 17-22.
13. Chang, H.; Johnson, D. C. J. Electrochem. Soc. 1990, 137, 2452-2457.

14. Milazzo, G.; Caroli, S. Tables of Standard Electrode Potentials; Wiley: New York, 1978.

15. Johnson, D. C. J. Electrochem. Soc. 1972, 119, 331-339.

16. Hubbard, A. T.; Osteryoung, R. A.; Anson, F. C. Anal. Chem. 1966, 38, 692-697.

17. Desideri, P.G.; Lepri, L.; Heimler, D. Encyclopedia of Electrochemistry of the Elements; A.J. Bard, Ed.; Marcel Dekker: New York, 1973; Vol. 1, Ch. 3.

18. Bard, A. J.; Faulkner, L. R. Electrochemical Methods; John Wiley & Sons: New York, 1980; p 229.

SECTION V.

ELECTROCATALYSIS OF ANODIC, OXYGEN-TRANSFER REACTIONS AT KEL-F COMPOSITE ELECTRODES: THE EFFECT OF CONVECTION AT MICROELECTRODE ENSEMBLES

ABSTRACT

The higher rates of mass-transport to microelectrode ensemble electrodes resulted in an enhanced anodic response for O-transfer reactions with respect to the background current for evolution of O_2 at Kel-F composite electrodes. The $E_{1/2}$ for the O-transfer oxidation of I^- to IO_3^- was related to the O_2-evolution overpotential at Ru and graphite composite electrodes. The current density enhancement factor was studied as a function of fractional active area at these microelectrode ensembles, and the largest enhancement was observed for composite electrodes with 3% active area. The rotation rate dependence of the attenuation factor (ρ) was studied as a function of fractional active area. The attenuation factor was independent of rotation rate for composite electrodes with a relatively high fractional active area (i.e. 25%) and the rotation rate dependence of the current was equivalent to the response predicted by the Levich equation for a uniformly active electrode with a smaller geometric area. At composite electrodes with a relatively low fractional active area (i.e. 2%), the value of ρ was a function of rotation rate and significant non-linearity was observed for plots of current vs. the square root of rotation rate (i-$w^{1/2}$) and for plots of inverse current vs. the inverse square root of rotation rate (i^{-1}-$w^{-1/2}$).

INTRODUCTION

Many anodic O-transfer reactions are believed to be catalyzed by adsorbed hydroxyl radicals ($^{\cdot}OH_{ads}$) produced by anodic discharge of H_2O (Eqn. [1]) as the first step in the O_2-evolution reaction (Eqn. [2]) (1-7). This mechanism often

$$H_2O \longrightarrow {}^{\cdot}OH_{ads} + H^+ + e^- \qquad [1]$$

$$H_2O + {}^{\cdot}OH_{ads} \longrightarrow O_2 + 3H^+ + 3e^- \qquad [2]$$

$$R + {}^{\cdot}OH_{ads} \longrightarrow RO + H^+ + e^- \qquad [3]$$

results in a large anodic current due to simultaneous evolution of O_2 which interferes with the anodic current for the O-transfer reaction under study (Eqn. [3]). The analytical signal for the O-transfer reaction can be extracted using square-wave hydrodynamically modulated voltammetry (2,3) or difference voltammetry (1). Alternately, many O-transfer reactions have been catalyzed by doping PbO_2 with species that decrease the overpotential for O_2 evolution (4-7). In research described here, microelectrode ensembles were used to enhance the current for the O-transfer reaction with respect to the current for O_2 evolution.

The current response at microelectrode ensembles can be described by the ratio of the current observed at the microelectrode ensemble to the current observed at a solid electrode with an equal geometric area. This ratio was originally introduced to describe the current response of

partially blocked electrodes and, therefore, is termed an attenuation factor (ρ, Eqn. [4]) (8-12).

$$\rho = i_{ensemble}/i_{solid} \quad ; \; 0 \leq \rho \leq 1 \qquad [4]$$

The enhancement in signal-to-background (S/B) current density is given by Eqn. [5], which is based on the assumption that the background current density is proportional to the fractional active area of the electrode ($1 - \theta$). Thus, the

$$\text{S/B enhancement} = \rho/(1 - \theta) \qquad [5]$$

maximum enhancement in current density occurs for $\rho = 1$, which corresponds to total diffusion-layer overlap in chronoamperometry, i.e. diffusion to the geometric area of the microelectrode ensemble (13-16). Under these conditions, a microelectrode ensemble with 10% active area exhibits a S/B enhancement of 10.

Composite electrodes fabricated from mixtures of graphite and/or noble metals and Kel-F polymer were applied to the study of anodic O-transfer reactions which occur concurrently with O_2 evolution. Kel-F composite electrodes function as microelectrode ensembles (17) and have been used advantageously for voltammetry (18-20) and as flow-through electrochemical detectors (21-25). The S/B current enhancement with respect to O_2 evolution is discussed here for Kel-F composites applied to O-transfer reactions catalyzed by

O_2 evolution. Also, the rotation-rate dependence of ρ was investigated as a function of fractional active area $(1 - \theta)$.

EXPERIMENTAL

Equipment and procedures. The electrochemical system and procedures have been described previously (1).

Reagents and materials. Potassium ferrocyanide, potassium iodide, and glucose were reagent grade from Fisher Scientific Co. Water was purified in a Milli-Q system (Millipore) after passing through two D-45 deionizing tanks (Culligan). The Kel-F-81 powder (polychlorotrifluoroethylene) was graciously donated by 3M Company. Graphite powder (1 um) was obtained from Ultra Carbon Corporation. Powdered noble metals, including 325 mesh Ru and 2-5 um spherical Au were from Aesar.

Fabrication of composite electrodes. The procedure for fabrication of composite electrodes from mixtures of Kel-F, graphite, and noble metals has been described (18, 20). This procedure was followed as closely as possible with existing equipment. The appropriate amounts of Kel-F, graphite, and/or noble metal were mixed simply by shaking until the mixture was uniform. The mass fraction of each component for a three component mixture can be calculated from the desired volume fraction using a simple equation where

$$f_{mass,A} = f_{vol,A}D_A/(f_{vol,A}D_A + f_{vol,B}D_B + f_{vol,C}D_C) \quad [6]$$

$f_{mass,A}$ is the mass fraction of component A, $f_{vol,A}$ is the volume fraction of component A, and D_A is the density of

component A. The resulting mixture was then compressed at > 15000 psi for several seconds in a 13 mm pellet die using a laboratory press. The die was then removed from the press and heated to greater than 250 C as quickly as possible (< 25 min) using heating tape and a Thermolyne hot plate. The die was transferred back to the press and again > 15000 psi of pressure was applied continuously until the mixture had cooled to less than 100 C. A 1/8-inch diameter hole was drilled approximately 0.5 cm into the center of one side of the resulting pellet, and a stainless steel shaft was inserted so the composite electrode could be used as a rotated-disk electrode. The composite RDE was inserted in a Teflon shroud and sanded on 600 grit sandpaper until there were no cracks or gaps between the edge of the electrode and the Teflon shroud. The electrodes were then polished with 1-um, 0.3-um, and 0.05-um alumina in H_2O on Nylon (Buehler Ltd.).

Kelgraf electrodes consisting of 25, 20, 15, 10, 5, and 3 percent graphite by volume in Kel-F all had a resistance < 10 ohms. A 2% Kelgraf electrode had a resistance of < 150 ohms. Au composite electrodes were 5% Au in 10% Kelgraf, 3% Au in 10% Kelgraf, 2% Au in 10% Kelgraf, 1% Au in 5% Kelgraf, 0.6% Au in 10% Kelgraf, and 15% Au. Additional noble metal composites were 1% Ru in 5% Kelgraf and 15% Ru. Solid glassy carbon and Au rotated-disk electrodes (area = 0.46 cm^2) were used for comparison to the composite electrodes.

RESULTS AND DISCUSSION

Oxidation of iodide at graphite and Ru composite electrodes. Previous results (1) demonstrated that the $E_{1/2}$ for the O-transfer oxidation of I^- to IO_3^- is directly related to the O_2-evolution overpotential at Pt, Au, Pd, Ir, and glassy carbon electrodes. This same study showed that the $E_{1/2}$ for the electron-transfer oxidation of I^- to I_2 is largely independent of electrode material. This research is extended here to other electrode materials using Kel-F composite electrodes.

Voltammetric curves are shown in Figure 1 for the oxidation of I^- at two 5% Kelgraf (5% graphite by volume) composite electrodes, one of which also contains 1% Ru by volume. The oxidation of I^- to I_2 was essentially mass-transport limited with an $E_{1/2}$ = 0.48 V *vs.* SCE at both graphite and Ru sites. The oxidation of I^- to I_2 at the Ru sites accounts for the slightly larger limiting current observed at the 1% Ru/5% Kelgraf electrode (Curve d) as compared to that observed at 5% Kelgraf (Curve b).

A second anodic wave was apparent from Fig. 1 at both composite electrodes which was tentatively identified as corresponding to the oxidation of I^- to IO_3^-. At the Ru composite, this anodic wave occurred at potentials 0.43 V less positive than at graphite. This is coincident with the much lower O_2-evolution overpotential observed at the Ru composite

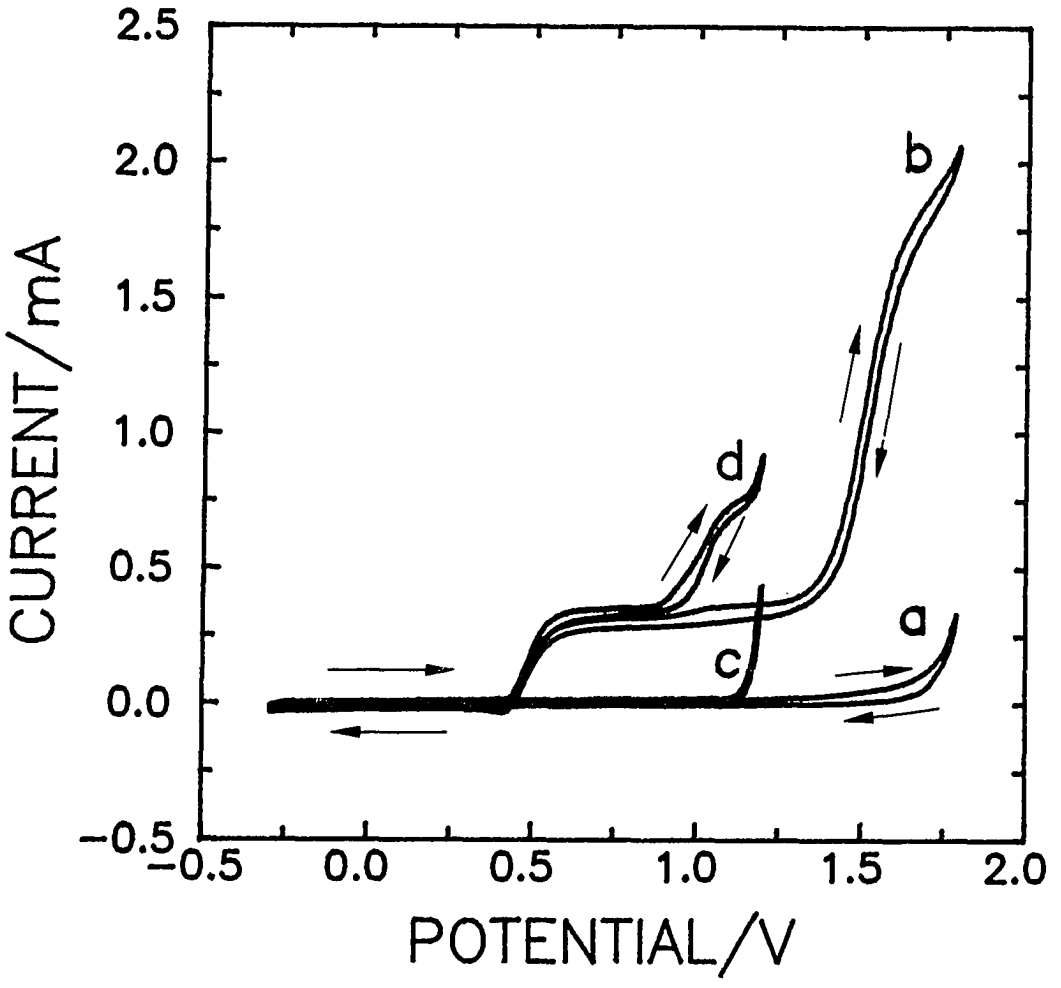

Figure 1. Voltammetric response (i-E) for I^- at 1% Ru composite electrode compared to 5% Kelgraf composite electrode.

Conditions: 100 mV sec^{-1}, 0.1 M H_2SO_4, 900 rev min^{-1}, O_2 removed.

Curves: (a) residual at 5% Kelgraf,
(b) 0.4 mM I^{-1} at 5% Kelgraf,
(c) residual at 1% Ru in 5% Kelgraf,
(d) 0.4 mM I^{-1} at 1% Ru in 5% Kelgraf.

(Curve c), as compared to that at 5% Kelgraf (Curve a). The oxidation of I^- to IO_3^- is apparently dependent on the O_2-evolution overpotential at Ru and graphite in a manner similar to that determined previously for other noble metal electrodes and glassy carbon (1).

The anodic wave for the oxidation of I^- to IO_3^- shown in Fig. 1 at 5% Kelgraf and at 1% Ru/5% Kelgraf was studied more thoroughly using difference voltammetry (data not shown). The i-E data at two concentrations (0.2mM and 0.4mM I^-) were subtracted to eliminate the contribution to the total current from the anodic current for O_2 evolution. At 5% Kelgraf, the oxidation of I^- to IO_3^- (n = 6 eq mol^{-1}) occurred with an $E_{1/2}$ = 1.47 V vs. SCE and a limiting current that was ca. 6 times the limiting current for the oxidation of I^- to I_2 (n = 1 eq mol^{-1}). The limiting current for the second anodic wave ($E_{1/2}$ = 1.04) at the Ru composite was approximately equal to that expected from the sum of the currents due to the oxidation of I^- to I_2 at the graphite sites and the oxidation of I^- to IO_3^- at the Ru sites.

These results confirm that the O-transfer oxidation of I^- to IO_3^- can be achieved at lower overpotentials using an electrode material with a low O_2-evolution overpotential such as Ru. The i-E curves in Fig. 1 also qualitatively confirm that this oxidation can be achieved at low overpotentials while maintaining a high current efficiency, whereas previous

results (1) demonstrated that the anodic current due to O_2 evolution severely decreases the current efficiency at solid electrodes with low O_2-evolution overpotentials, such as Ir. The anodic wave for the oxidation of I^- to IO_3^- at a 15% Ru composite (data not shown) was less clearly defined with respect to the background current due to O_2 evolution. This is concluded to be caused by a decreased current enhancement at higher fractional active areas, and was similar to the result reported for a solid Ir electrode (1).

Current density enhancement as a function of fractional active area at Kelgraf composite electrodes. The mass-transport limited oxidation of ferrocyanide was studied at glassy carbon and various Kelgraf composite electrodes to obtain quantitative data for the S/B current enhancement as a function of fractional active area. The limiting current as a function of the square root of rotation rate (i vs. $w^{1/2}$) is plotted in Figure 2 for glassy carbon and 25%, 15%, and 5% Kelgraf electrodes. The data have been normalized by the geometric area of the electrodes so that the glassy carbon electrode (Curve a) could be used for comparison ($\rho = 1$). The limiting current decreased systematically (Curves b-d) as the fractional active area was decreased. However, the decrease in limiting current was smaller than the decrease in fractional active area, resulting in a substantial S/B current advantage at the Kelgraf composite electrodes.

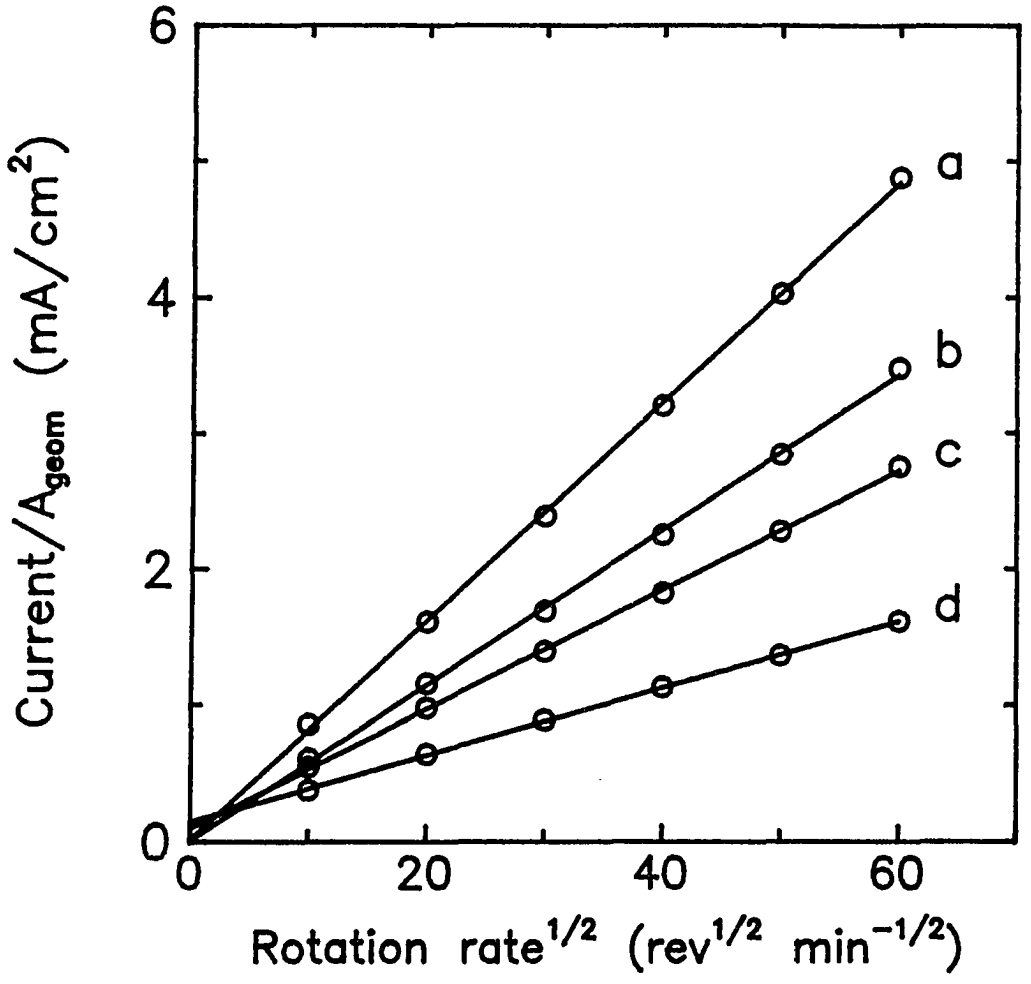

Figure 2. Current normalized by the geometric area as a function of rotation rate$^{1/2}$ at various Kelgraf composite electrodes compared to glassy carbon.

Conditions: 5.1 mM $K_4Fe(CN)_6$, 0.1 M KCl, 20 mV sec^{-1}.

Curves: (a) glassy carbon, (b) 25% Kelgraf, (c) 15% Kelgraf, (d) 5% Kelgraf.

The current density enhancement factor ($\rho/(1-\theta)$) and the attenuation factor (ρ) are summarized in Table 1 for 25%, 20%, 15%, 10%, 5%, 3%, and 2% Kelgraf composite electrodes at 3600 rev min^{-1}. The largest enhancement in current density (8.47) was obtained at the 3% Kelgraf electrode. This is also apparent from Figure 3, where the current normalized by the active area is plotted as a function of the square root of rotation rate. The glassy carbon data (Curve a) correspond to $\rho = 1$, and the larger current densities observed at the Kelgraf electrodes demonstrate the S/B current advantage at these electrodes as a function of rotation rate. The largest advantage at all rotation rates was observed at 3% Kelgraf. The current density at 5% Kelgraf was higher than that at 2% Kelgraf at high rotation rates. However, the 2% Kelgraf electrode exhibited a higher current density at low rotation rates. It is apparent that ρ varies as a function of rotation rate for Kelgraf electrodes with low fractional active area.

Rotation rate dependence of the response at Kelgraf composite electrodes. The data from Fig. 2 for GC and 25% Kelgraf are plotted as current^{-1} vs. rotation rate$^{-1/2}$ (i^{-1}-$w^{-1/2}$) in Fig. 4. The plot for GC (Curve a) is linear with a y-intercept $\simeq$ 0, and the current values are approximately equal to the values predicted by the Levich equation (26) for diffusion to an uniformly active RDE (ρ = 1). The i^{-1}-$w^{-1/2}$ plot for 25% Kelgraph (Curve b) is also

Table 1. Current density enhancement factor, $\rho/(1-\theta)$, as a function of fractional active area at Kelgraf composite electrodes.

Fractional active area $(1-\theta)$	i/A_{geom}[a] mA/cm^2	ρ	$\rho/(1-\theta)$
1.00[b]	4.88	1.00	1.00
0.25	3.48	0.71	2.85
0.20	3.17	0.65	3.25
0.15	2.75	0.56	3.76
0.10	2.17	0.45	4.45
0.05	1.61	0.33	6.60
0.03	1.24	0.25	8.47
0.02	0.57	0.12	5.85

[a] Data at 3600 rev min^{-1} from Fig. 2.

[b] Glassy carbon RDE (0.46 cm^2) was used for comparison.

approximately linear with a y-intercept $\simeq$ 0. However, the current values are less than the values predicted by the Levich equation by the factor ρ. For the 25% Kelgraf electrode, ρ was essentially independent of the rate of convection (rotation). This behavior was predicted by models which neglected radial diffusion (10,12) and appears to be

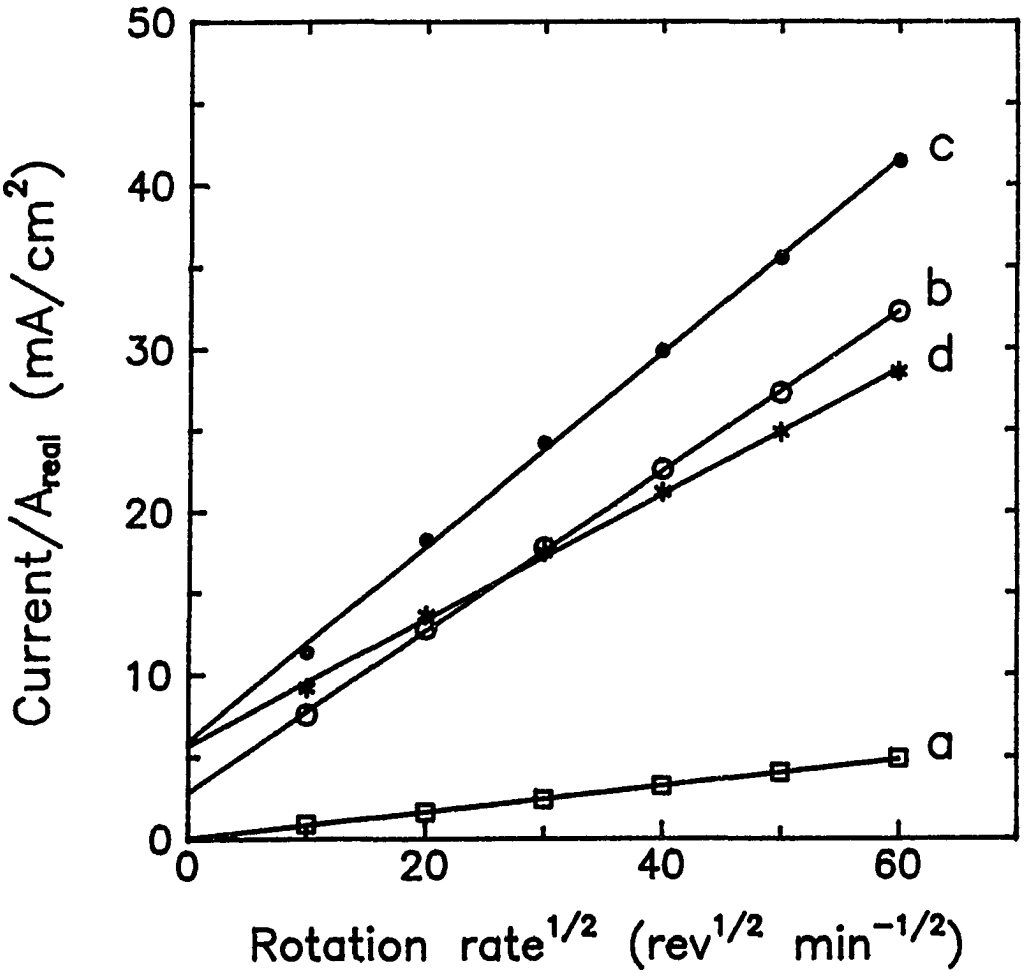

Figure 3. Current normalized by the active area as a function of rotation rate$^{1/2}$ at various Kelgraf composite electrodes compared to glassy carbon.

Conditions: same as Fig. 2

Curves: (a) glassy carbon, (b) 5% Kelgraf, (c) 3% Kelgraf, (d) 2% Kelgraf.

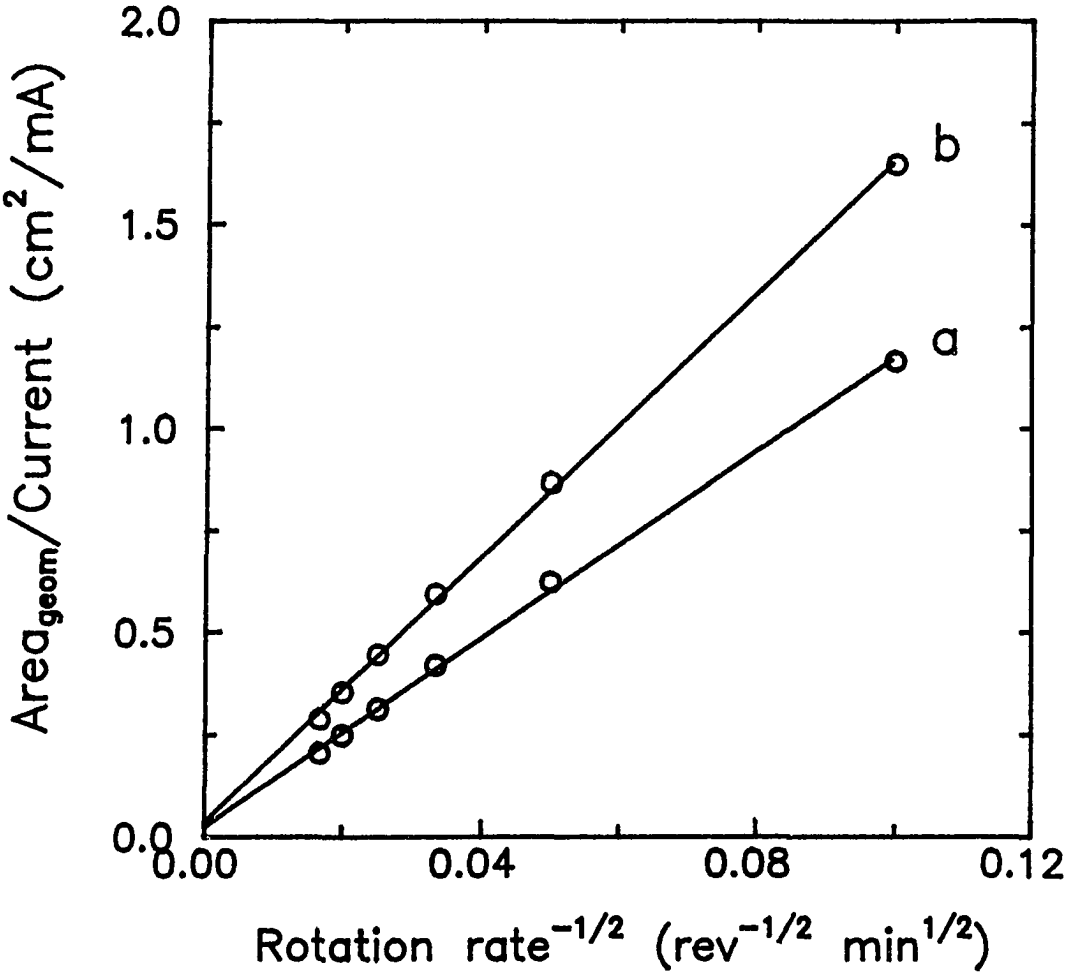

Figure 4. Current^{-1} as a function of rotation rate$^{-1/2}$ for a 25% Kelgraf electrode compared to a glassy carbon RDE.

Conditions: same as Fig. 2

Curves: (a) glassy carbon, (b) 25% Kelgraf.

appropriate for microelectrode-ensemble rotated-disk electrodes with relatively high fractional active areas.

In Figure 5, the i^{-1}-$w^{-1/2}$ data are plotted for 2% (Curve b) and 3% (Curve a) Kelgraf electrodes. Both curves show significant non-linearity, indicating that ρ is a function of rotation rate when the fractional active area of the microelectrode ensemble is low. Digital simulations which included terms for radial diffusion (11) demonstrated that ρ is a function of rotation rate and, therefore, the non-linearity of i^{-1}-$w^{-1/2}$ plots observed at 2% and 3% Kelgraf electrodes was probably due to the significance of radial diffusion at microelectrode ensembles with a low fractional active area.

Rotation rate dependence of the response at Au/Kelgraf composite electrodes. The rotation rate dependence of ρ was investigated at lower fractional active areas using Au/Kelgraf composite electrodes. Composite electrodes fabricated from Au and Kel-F were not conductive below ca. 10% Au by volume, so graphite was used to provide electrical connection to the Au sites for the very low fractional active areas used here. The oxidation of glucose was used as the model reaction since no anodic signal was observed for glucose oxidation at Kelgraf electrodes. However, the oxidation of glucose at Au results in a nearly mass-transport limited signal at low

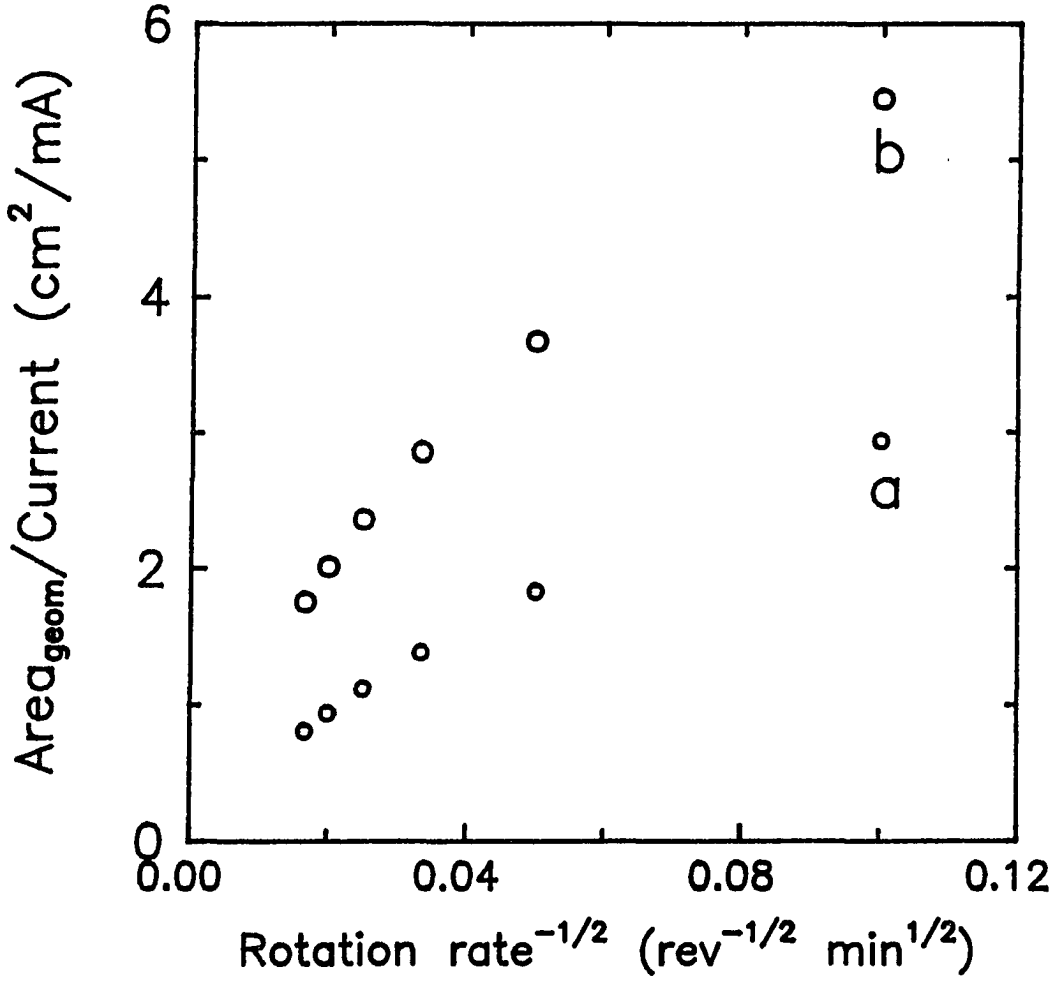

Figure 5. Current^{-1} as a function of rotation rate$^{-1/2}$ at Kelgraf composite electrodes.

Conditions: same as Fig. 2

Curves: (a) 3% Kelgraf, (b) 2% Kelgraf.

concentrations (27), so this reaction is ideal for studying mass-transport to Au sites in a Kelgraf matrix.

The peak current for the oxidation of the aldehyde portion of glucose was measured at E = -0.43 V at the solid Au RDE and at E = ca. -0.2 V at the Au/Kelgraf composite electrodes. These values were normalized by the active areas of the electrodes and are plotted as a function of the square root of the rotation rate in Figure 6. The data for a solid Au electrode (Curve a) is included for comparison to the Au/Kelgraf composites. The largest current densities were observed at the 3% Au composite electrode (Curves c), which is in agreement with the data previously discussed for ferrocyanide oxidation at Kelgraf electrodes. At the 0.6% Au composite electrode (Curve d), the anodic current for the oxidation of glucose was essentially independent of rotation rate, indicating that the Au active sites essentially behaved as isolated microelectrodes. This behavior is expected for active sites with large intersite separations. Although the current density was smaller than that observed at the 3% Au composite electrode, the 0.6% Au composite electrode still exhibited a significant S/B current enhancement when compared to the current density observed at the solid Au RDE. Composite electrodes which behave similarly to the 0.6% Au/10% Kelgraf electrode used here could be advantageous for flow-through electrochemical detection since they exhibit a large

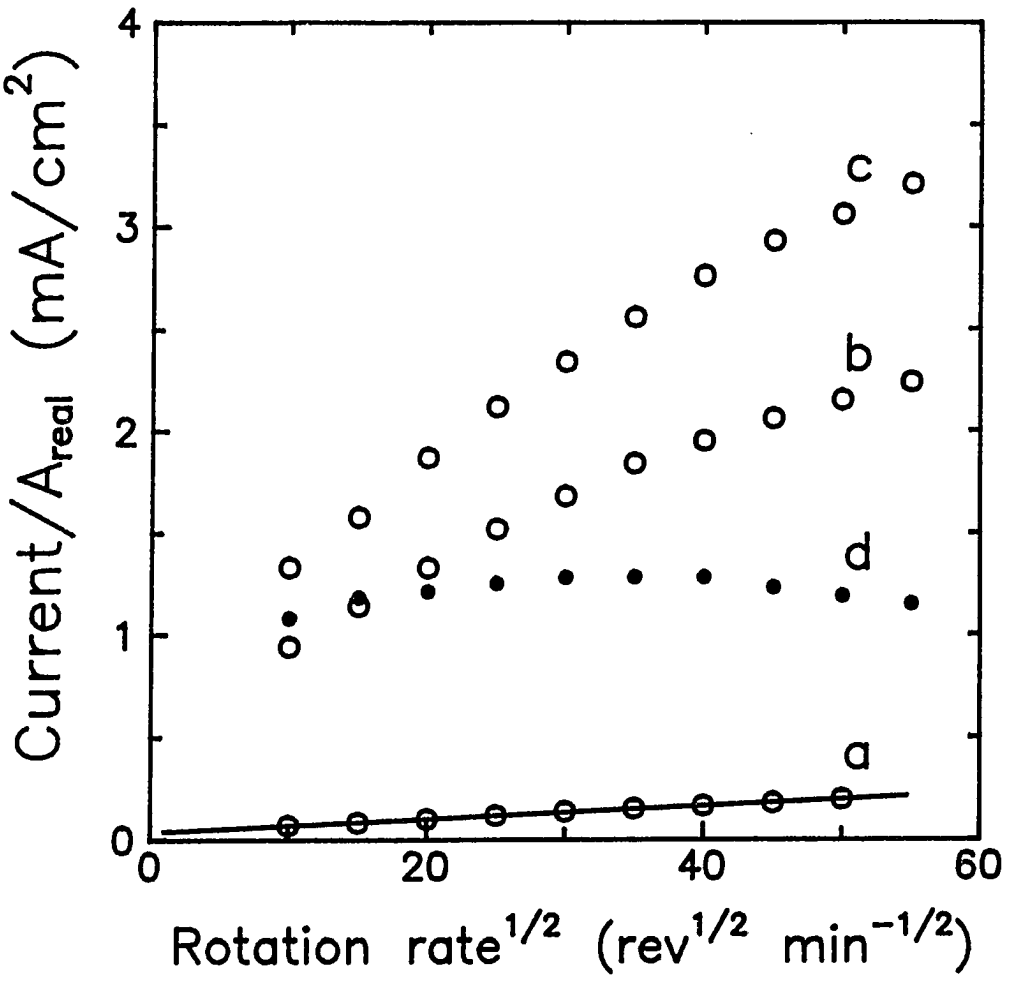

Figure 6. Effect of rotation rate$^{1/2}$ on the current at various Au/Kelgraph composite electrodes compared to a solid Au RDE. Data is normalized by the active area.

Conditions: 0.5 mM glucose, 0.1 M NaOH, 100 mV sec^{-1}, O_2 removed.

Curves: (a) solid Au, (b) 5% Au in 10% Kelgraph, (c) 3% Au in 10% Kelgraph, (d) 0.6% Au in 10% Kelgraph.

sensitivity to concentration changes, while being relatively insensitive to convection (rotation rate or flow rate).

Current density enhancement for the production of iodate with respect to the background current due to oxygen evolution. The values of the current density enhancement factor ($\rho/(1-\theta)$) listed in Table 1 for Kelgraf electrodes were calculated using the fractional active area based on the volume percent of graphite. However, the goals of this study include enhancing the current density for O-transfer oxidations with respect to the current for O_2 evolution. Therefore, the current density enhancement factor is calculated in Table 2 based on the background current due to O_2 evolution for the oxidation of I^- to IO_3^- at a 15% Au/Kel-F composite electrode. The enhancement factors calculated in this manner were much smaller than the enhancement factors calculated from the fractional active area. This is believed to be due to the porosity of the Kel-F composite electrodes, which results in a larger surface area than that estimated from the volume-percent of Au in the composite.

As demonstrated in Table 1 for ferrocyanide oxidation at Kelgraf electrodes, the enhancement factor is much larger at lower fractional active areas. However, the relatively low O_2-evolution overpotential at graphite (see Fig. 1) precluded the study of O-transfer reactions which occur concurrently with O_2 evolution at the Au/Kelgraf composites used in Fig. 6.

Table 2. Comparison of the current density enhancement factor at a 15% Au/Kel-F composite electrode calculated using the fractional active area (1-θ) and the background current for O_2 evolution.

	solid Au	15% Au/Kel-F
i/A_{geom} for O_2 evolution[a]	4.91 mA/cm^2	1.35 mA/cm^2
$\Delta i/A_{geom}$ from ΔC data[b]	2.54 mA/cm^2	0.93 mA/cm^2
$\Delta i/A_{geom}$ from $\Delta w^{1/2}$ data[c]	1.76 mA/cm^2	0.35 mA/cm^2
ρ from ΔC data	1.00	0.37
ρ from $\Delta w^{1/2}$ data	1.00	0.20
$\rho/(1-\theta)$ from ΔC data	1.00	2.47
$\rho/(1-\theta)$ from $\Delta w^{1/2}$ data	1.00	1.33
ρ/B from ΔC data[d]	1.00	1.35
ρ/B from $\Delta w^{1/2}$ data[d]	1.00	0.73

[a] At 1.8 V for potential limits = -0.3 to 1.8.

[b] i-E data for 1.0 mM I^- and 0.5 mM I^- at 900 rev min^{-1}.

[c] i-E data for 0.5 mM I^- at 2500 and 900 rev min^{-1}.

[d] Calculated from Δi for both solid Au and 15% KelAu normalized by the current for O_2 evolution.

CONCLUSIONS

The $E_{1/2}$ for the O-transfer oxidation of I^- to IO_3^- was demonstrated to be related to the O_2-evolution overpotential at Ru and graphite using Kel-F composite electrodes. These electrodes exhibited significantly larger current densities due to the enhanced rate of mass-transport to microelectrode ensembles. The maximum enhancement factor, defined as the attenuation factor (ρ) divided by the fractional active area ($1-\theta$), was observed for composite electrodes with 3% active area. This was confirmed at both graphite/Kel-F composite electrodes (Kelgraf) and at Au/Kelgraf composite electrodes.

The rotation rate dependence of the current was studied as function of fractional active area. At 25% Kelgraf electrodes, the response was similar to the response predicted by the Levich equation for a uniformly-active RDE of smaller geometric area, resulting in plots of i *vs.* $w^{1/2}$ and i^{-1} *vs.* $w^{-1/2}$ that were approximately linear with a y-intercept $\simeq$ 0. At 2% and 3% Kelgraf, extremely non-linear i-$w^{1/2}$ and i^{-1}-$w^{-1/2}$ plots were obtained, indicating that ρ was strongly dependent on the rotation rate. This was also confirmed at Au/Kelgraf composite electrodes. A composite electrode consisting of 0.6% Au and 10% graphite in Kel-F exhibited currents for glucose oxidation at the Au sites that were independent of the rate of rotation.

ACKNOWLEDGMENTS

Ames Laboratory is operated for the U.S. Department of Energy by Iowa State University under Contract No. W-7405-ENG-82. J.E.V. is grateful to Phillips Petroleum Corporation for providing a fellowship for the academic year 1990-1991. Thanks to Mary Simpson of 3M for donating the Kel-F-81 powder and to Bruce Tanner of ISU for the loan of the laboratory press. We also would like to acknowledge valuable discussions with Prof. Dennis Tallman of North Dakota State University.

REFERENCES

1. Section IV, this dissertation.
2. Cabelka, T. D.; Austin, D. S.; Johnson, D. C. J. Electrochem. Soc. 1984, 131, 1595-1602.
3. Austin, D. S.; Johnson, D. C.; Hines, T. G.; Berti, E. T. Anal. Chem. 1983, 55, 2222-2226.
4. Yeo, I-H.; Kim, S.; Jacobson, R.; Johnson, D. C. J. Electrochem. Soc. 1989, 136, 1395-1401.
5. Chang, H.; Johnson, D. C. J. Electrochem. Soc. 1989, 136, 17-22.
6. Chang, H.; Johnson, D. C. J. Electrochem. Soc. 1990, 137, 2452-2457.
7. LaCourse, W. R.; Hsiao, Y-L.; Johnson, D. C.; Weber, W. H. J. Electrochem. Soc. 1989, 136, 3714-3719.
8. Landsberg, R.; Thiele, R. Electrochim. Acta 1966, 11, 1243-1259.
9. Scheller, F.; Muller, S.; Landsberg, R.; Spitzer, H.-J. J. Electroanal. Chem. 1968, 19, 187-198.
10. Filinovsky, V. Yu. Electrochim. Acta 1980, 25, 309-314.
11. Levart, E. J. Electroanal. Chem. 1985, 187, 247-263.
12. Contamin, O.; Levart, E. J. Electroanal. Chem. 1982, 136, 259-270.
13. Gueshi, T.; Tokuda, K.; Matsuda, H. J. Electroanal. Chem. 1978, 89, 247-260.

14. Shoup, D.; Szabo, A. J. Electroanal. Chem. 1984, 160, 19-26.

15. Scharifker, B. R. J. Electroanal. Chem. 1988, 240, 61-76.

16. Weissharr, D. E.; Tallman, D. E. Anal. Chem. 1983, 55, 1146-1151.

17. Tallman, D. E.; Petersen, S. L. Electroanalysis 1990, 2, 499-510.

18. Anderson, J. E.; Tallman, D. E.; Chesney, D. J.; Anderson, J. L. Anal. Chem. 1978, 50, 1051-1056.

19. Petersen, S. L.; Tallman, D. E. Anal. Chem. 1988, 60, 82-85.

20. Petersen, S. L.; Tallman, D. E. Anal. Chem. 1990, 62, 459-465.

21. Anderson, J. L.; Chesney, D. J. Anal. Chem. 1980, 52, 2156-2161.

22. Chesney, D. J.; Anderson, J. L.; Weissharr, D. E.; Tallman, D. E. Anal. Chim. Acta, 1981, 124, 321-331.

23. Weissharr, D. E.; Tallman, D. E.; Anderson, J. L. Anal. Chem. 1981, 53, 1809-1813.

24. Tallman, D. E.; Weissharr, D. E. J. Liq. Chrom. 1983, 6, 2157-2172.

25. Anderson, J. L.; Whiten, K. K.; Brewster, J. D.; Ou, T.-Y.; Nonidez, W. K. Anal. Chem. 1985, 57, 1366-1373.

26. Levich, V. G. Physicochemical Hydrodynamics; Prentice Hall: Englewood Cliffs, NJ, 1962; p 75.

27. Larew, L. A.; Johnson, D. C. J. Electroanal. Chem., 1989, 262, 167-182.

SECTION VI.

GENERAL SUMMARY

Several aspects of anodic, oxygen-transfer reactions were studied. Substantial evidence was presented that adsorption of the reactant is necessary at Au electrodes when the electrochemical reaction involves oxygen-transfer from H_2O to the oxidation products. The anodic current for an oxygen-transfer oxidation was eliminated when a more strongly adsorbed compound was also present in the solution. The limiting current was unchanged for an oxidation that did not involve oxygen-transfer, i.e., the oxidation of hydrazine. An adsorption hierarchy at Au electrodes was developed using these competitive adsorption studies. We conclude that adsorption of the reactant is necessary for many oxygen-transfer oxidations at Au electrodes, enabling the reactant and the adsorbed hydroxyl radicals to react at the electrode surface.

Strategies to make catalytic electrodes for oxygen-transfer reactions include doping a catalyst with a low overpotential for oxygen evolution into an inert matrix with a high overpotential for oxygen evolution. The electrogenerated chemiluminescence of luminol was investigated as a possible method for characterizing the spatial distribution of current density across nonuniform electrode surfaces such as doped electrodes. Studies at various electrode materials revealed that the ECL intensity was actually inversely related to the electrode activity, defined as n times k_{app}. A mechanism was

proposed which was consistent with this inverse relationship, and also was consistent with the experimentally determined rate laws. It was concluded that the oxidation of luminol to 3-aminophthalate ($n = 4$ eq mol^-) at the electrode surface corresponded to the dark reaction, whereas oxidation of luminol with $n = 1$ eq mol^- initiated the chemiluminescent reaction in solution.

Evidence was presented that the adsorbed hydroxyl radicals present at electrode surfaces during O_2 evolution can be involved in electrocatalytic mechanisms of oxygen-transfer reactions. For example, the $E_{1/2}$ for the irreversible oxidation of I^- to IO_3^- was demonstrated to be directly related to the overpotential for O_2 evolution at Pt, Pd, Au, Ir, and glassy carbon. Also, a large variety of oxygen-transfer reactions were catalyzed by O_2 evolution at an Ir electrode.

Composite electrodes fabricated from mixtures of KEL-F, graphite, and noble metals were used to study oxygen-transfer reactions that occurred simultaneously with O_2 evolution. These electrodes exhibit higher rates of mass-transport than solid (pure) electrodes and, therefore, the current density for oxygen-transfer reactions involving diffusion is enhanced with respect to the current density for O_2 evolution.

SECTION VII.

ACKNOWLEDGMENTS

My graduate school experience has been almost completely positive, and that is largely due to my advisor, Prof. Dennis Johnson. He has been patient, always cheerful and positive, and supportive in every way possible. He also has been a seemingly unlimited source of ideas and solutions. In short, he has been the ideal research advisor and has earned my respect and admiration.

I would also like to thank the members of this group with whom I have worked for the past years, especially Dr. Larry Larew. Next to Dr. Johnson, I learned the most from Larry, and he made me feel at home by constantly heckling and teasing me. Thanks to the other two people with whom I have shared lab space: Rich Roberts and Dave Dobberpuhl. Dave has borne the brunt since Larry left whenever I felt the need to babel about research. These friends, and many others, have contributed lots of ideas and help, along with many pranks to break the monotony that, at times, is part of doing research.

Family and friends have been a great source of support, encouragement, and relaxation during my time at Iowa State. I would especially like to express my gratitude and love to my mom (Mary Jo) and many brothers: Tom, Bill, Pete, Bob, and Jim.

I am grateful to Prof. Royce Engstrom for giving me the opportunity to work with him; my trip to Vermillion was exciting and a great learning experience. Also, Prof. Dennis

Tallman at North Dakota State University gave helpful advice about the KEL-F composite electrodes developed by his group.

Ames Laboratory has provided funding for most of my graduate career, and I am appreciative for the vast resources and help provided by the many people in Ames Lab and the Chemistry Department. I am also grateful to Phillips Petroleum for a fellowship for the academic year 1990-1991. Thanks also to Union Carbide for the very enjoyable opportunity to participate in the Kenan Analytical Award Symposium.